Investigating the role of Wnt/PCP proteins in axon growth and neuronal cytoskeleton regulation

Thesis submitted in accordance with the requirements of the University of Liverpool for the degree of Doctor in Philosophy by

Péter Kaltenecker

Supervisors:

Dr. Natalia Sánchez-Soriano

Dr. József Mihály

September 2019

Table of Contents

List of figures

List of tables

Abbreviations

GC – growth cone
MT – microtubule
F-actin – filamentous actin
DAAM – Dishevelled Associated Activator of Morphogenesis
Arp2/3 – actin-related protein 2/3
WASP – Wiskott-Aldrich syndrome protein
FH1-2 – formin homology domain 1-2
WH2 – WASP-Homology 2
Rho – Ras homologous (GTPase)
PCP – Planar Cell Polarity
Fz – Frizzled
Dsh – Dishevelled
DIX – Dishevelled/Axin
PDZ – PSD-95, DLG, ZO1
DEP – Dishevelled, EGL-10, Pleckstrin
Fmi – Flamingo / Stan – Starry night
Stbm – Strabismus / Vang – Van Gogh
Pk – Prickle
Dgo – Diego
UAS – Upstream Activating Sequence
VNC – ventral nerve cord
CNS – central nervous system
ISN – intersegmental nerve
ISNb – intersegmental nerve b
SNa – segmental nerve a
LN_vs – ventral lateral neurons
PDF – pigment dispersing factor
s-LN_vs – small ventral lateral neurons
l-LN_vs – large ventral lateral neurons
GFP – green fluorescent protein
EB1 – end-binding protein 1
LD – light-dark cycle
ZT – Zeitgeber time

Abstract

Investigating the role of Wnt/PCP proteins in axon growth and neuronal cytoskeleton regulation

The Wnt/Planar Cell Polarity (PCP) signalling is responsible for the establishment of planar polarity in epithelial tissues. Besides this function, it is also known to play multiple roles in neuronal development, however, the mechanism by which PCP signalling acts in these processes remained largely unclear. Neurons are highly polarised cells with extended neuronal protrusions in order to connect to target cells. The growth and maintenance of these protrusions crucially depend on the cytoskeleton. In recent years, many direct regulators of the neuronal cytoskeleton have been described, however it is still not completely understood how external or internal signals are conveyed to the neuronal cytoskeleton. The aim of this project was to study how core members of the PCP signalling module regulate the neuronal cytoskeleton, and to understand how they contribute to axon growth in *Drosophila melanogaster*.

To this end, we used primary embryonic cell cultures which provide powerful subcellular readouts to determine the state of the neuronal cytoskeleton; and we studied the embryonic and the adult nervous system in order to assess the *in vivo* relevance of our findings.

Our results showed that most PCP proteins are present both in the embryonic central and peripheral nervous system, and the loss of some of these components causes an early stall of the intersegmental nerve b (ISNb) in embryos. In addition, we found that the PCP proteins regulate axon growth and guidance in the ventral lateral neurons (LN_v), a group of neurons in the adult brain that are responsible for controlling the locomotor activity and sleeping behaviour of the flies, as the LN_v axons project ectopically in most of the PCP mutants. Accordingly, these pathfinding defects result in a strongly reduced LN_v function and lead to severe alterations, particularly in the sleep/wake transition, since the morning activity of the PCP mutant flies is disrupted and becomes associated with an increased amount of daytime sleep.

In accordance with these, we found that some PCP proteins affect axon growth in primary neuronal cell cultures as well. In addition, the lack of some of the PCP components alters the state of the actin and microtubule (MT) cytoskeleton in cultured neurons. In order to investigate the mechanism by which these PCP proteins can control the neuronal cytoskeleton and contribute to axon growth, we also studied DAAM (Dishevelled Associated Activator of Morphogenesis), a formin type of protein which has previously been linked to PCP signalling. Besides its known actin-regulatory function, we found that DAAM strongly affects the MT cytoskeleton as well, in ways similar to the PCP proteins. Moreover, the loss of DAAM causes a similar ISNb stalling phenotype than that of the PCP proteins in the embryo.

Together these findings suggest that the PCP proteins are necessary to properly regulate the neuronal cytoskeleton, presumably by controlling DAAM, and contribute to axon growth *in vivo* in the embryonic nervous system and in the adult brain. Beyond that, our studies also revealed a new physiological function of the Wnt/PCP pathway in controlling the sleeping behaviour of the adult flies.

1. Introduction

1. 1. Axon growth and the neuronal cytoskeleton

The formation of neuronal circuits during development is essential for proper functioning of the nervous system. Neurons are structurally and functionally highly polarised cells that extend slender neuronal protrusions, dendrites and axons, to reach their target cells and communicate with them. The dendritic compartment is responsible for receiving of the information whereas the axons are indispensable for transmission of the neuronal signals. Axonal growth is guided by the growth cone (GC), a highly dynamic fan-shaped structure, localised at the distal tip of the axon. GCs play a fundamental role in correct pathfinding by reacting to the attractive and repulsive guidance cues of their environment. Growth cone advance is critically dependent on the neuronal cytoskeleton that undergoes dynamic changes upon guidance signalling and plays an essential role in directed movement of the axon towards its appropriate targets.

1. 1. 1. Organisation of the neuronal cytoskeleton and its role in axon advance

The neuronal cytoskeleton comprises of two main components, the actin and the microtubule (MT) cytoskeleton. **Figure 1** shows the principal organisation of the neuronal cytoskeleton in the axon. Along the axonal shaft MTs are organised into parallel running discontinuous MT bundles which provide a strong structural scaffold for the axon. In addition, the MT tracks also serve as highways for axonal transport mechanisms, for example, during synapse formation they ensure the transport of

synaptic proteins from the soma to the GC [1]. The axon shaft also contains actin filaments, of which the most prominent are the regularly spaced cortical actin rings, formed by short actin filaments [2].

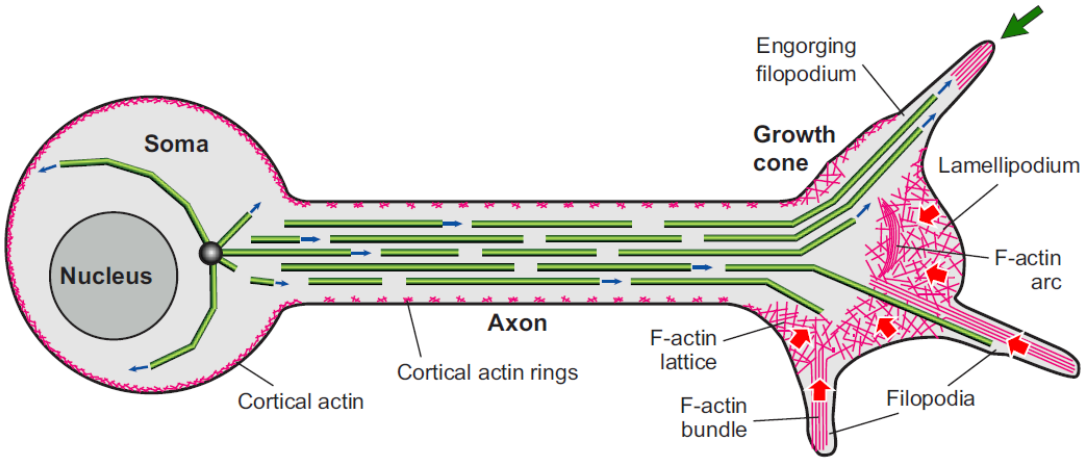

Figure 1. The principal organisation of the neuronal cytoskeleton
Bundles of MTs are shown in green in the axon and in the growth cone (GC). Along the axon, most MTs point distally with their plus ends [3] and are organised into a robust shaft. From the MT-rich central zone of the GC, individual splayed MTs can invade into filopodia and subsequently become stabilised in response to attractive signals (green arrow). In the peripheral zone, F-aktin (shown in pink) form parallel bundles in the filopodia which promotes MT extension. In contrast, in the lamellipodia F-actin is organised into a misaligned meshwork. Red arrows represent the retrograde flow of F-actin which pushes back most MTs into the central zone. In addition, circumferential F-actin arcs (transverse bundles of F-actin in the transition zone) also antagonise MT extension into the peripheral zone. (adapted from [4])

The GC can be subdivided into three main structural domains designated as the peripheral, central and transition zones. The peripheral zone of the GC often comprises of two different types of membranous protrusions, the finger-like filopodia and the veil-like lamellipodia. These structures are actin rich, filopodia contain parallel bundles of filamentous actin (F-actin), whereas a network of relatively short actin filaments can be found in lamellipodia. The tip of the axonal MT shaft forms the MT-

rich central zone of the GC, from where individual splayed MTs can invade into the actin-rich peripheral zone. The transition zone lies between these two regions in which the actin and MT cytoskeleton overlap and eventually interact with each other [5, 6].

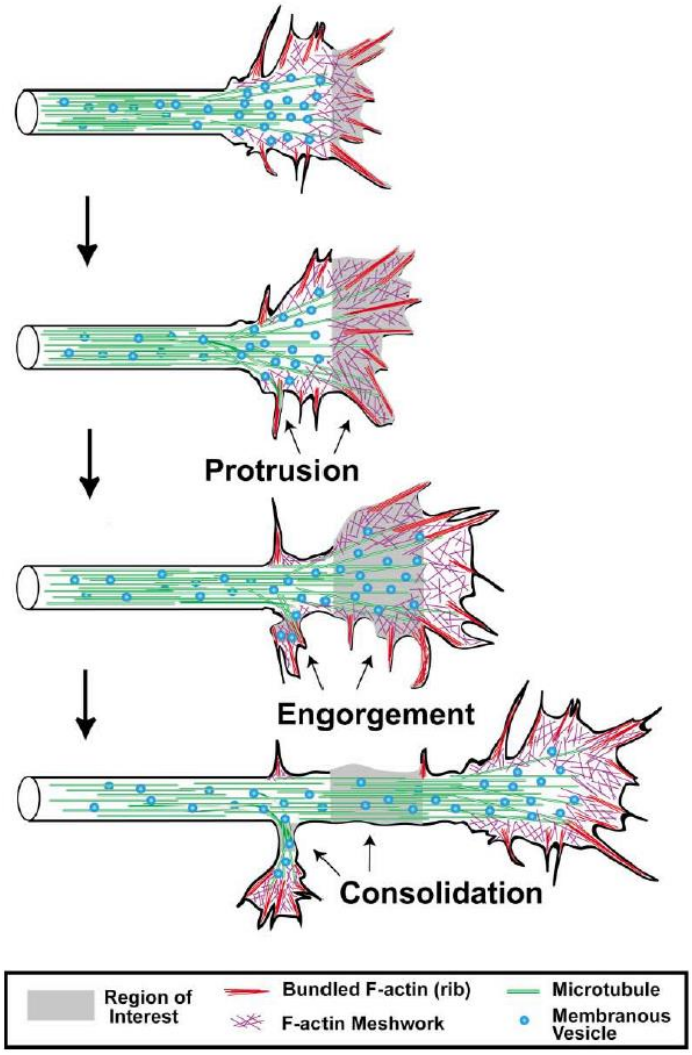

Figure 2. The stages of axon growth

Schematic figure showing the three stages of axon advance. In the first stage, new membrane protrusions of the GC emerge by the extension of filopodia and lamellipodia. During engorgement, MTs invade the new protrusions which subsequently become invested with membranous vesicles and organelles. In the final stage called consolidation, the proximal part of the GC shrinks leading to the formation of a new axon segment. (adapted from [5])

During axon growth, GCs sense the guidance cues through their filopodia and lamellipodia, and subsequently undergo dynamic changes in their shape by the continuous assembly and dis-assembly of the cytoskeletal components. In the process of GC advance there are three morphologically distinct stages of axon growth called protrusion, engorgement and consolidation (**Fig. 2**) [7]. Protrusion occurs at the leading edges of the GC by the elongation of filopodia and lamellipodia which is thought to be primarily driven by polymerisation of the actin filaments. During engorgement, MTs invade the newly formed protrusions which become filled with membranous vesicles and organelles, such as mitochondria and endoplasmic reticulum, likely through both Brownian motion and MT-driven transport. This is followed by the stage of consolidation, when the proximal side of the GC shrinks around the axonal MT bundle, during which the majority of the actin filaments depolymerise, resulting in the formation of a cylindrical axonal shaft [5]. The continuous repetition of these three stages leads to the elongation of the axon, until recognition of the target cell(s), followed by synapse formation.

In the process of axon growth MTs play an essential role in axon extension, whereas the actin cytoskeleton is thought to be primarily required for proper pathfinding. Many studies showed that the inhibition of actin polymerisation does not necessarily supress axon growth per se, but results in misdirected axon outgrowth both *in vivo* and in cultured neurons [8-14]. In contrast, the blocking of MT dynamics leads to axon growth inhibition [14-16]. These observations suggested that F-actin is particularly important for the dynamic shape changes and exploratory movements of the GC, whereas the MT cytoskeleton, besides providing a basic scaffold along the axon, is indispensable for axon elongation.

In addition, it has become clear that the dynamic interactions between the actin and MT cytoskeleton are crucial for GC advance. From the central zone of the GC, individual MTs can extend into the actin-rich lamellipodia and filopodia, and can explore the peripheral zone through dynamic polymerisation and depolymerisation

events (**Fig. 1**). Therefore, individual MTs interact with F-actin during this process in which their exploratory behaviour is influenced by the actin cytoskeleton. F-actin backflow both from filopodia and lamellipodia, and the formation of transverse actin bundles antagonise MT extension, whereas radial F-actin bundles can serve as tracks for MT elongation and promote MT extension into filopodia. Once external signals stabilise a filopodium against retraction, it captures individual MTs into a certain direction which then become stabilised and joined by other MTs from the central zone of the GC. Subsequently, it initiates engorgement and consolidation, and finally leads to the formation of a new axonal segment. [5, 6, 17-20]

1. 1. 2. The regulation of cytoskeletal dynamics during axon growth

The continuous change and rearrangement of the cytoskeletal elements is required for GC movements during axon growth, which cannot be achieved without the regulation of cytoskeletal dynamics. Both MTs and actin filaments are dynamic polymers that sometimes have to be in a stable form but at other times exist in an actively changing state, thus, the precise control of their dynamics during axon growth is essential.

MTs are polarised structures with a plus (+) and a minus (-) end. Their smallest units are the α- and β-tubulin monomers which form heterodimers and polymerise into protofilaments. The majority of MTs contain 13 protofilaments which arrange into hollow tubes to form MT polymers (**Fig. 3**). Most MTs point distally with their plus ends along the axon, and aim towards the periphery in the GC [3, 19-22]. *In vivo*, MTs show dynamic instability evident at their plus ends primarily: the event in which growth is followed by shrinkage is termed catastrophe, whereas the transition from shrinkage to growth is called rescue [23]. Actin filaments are also polarised polymers exhibiting a (+) end (a.k.a. barbed end) and a (-) end (a.k.a. pointed end). Compared to MTs,

actin filaments are more flexible and they are composed of globular actin monomers forming a double helical structure (**Fig. 3**). In GCs barbed end of the actin filaments usually faces towards the cell membrane [5, 19, 20, 24].

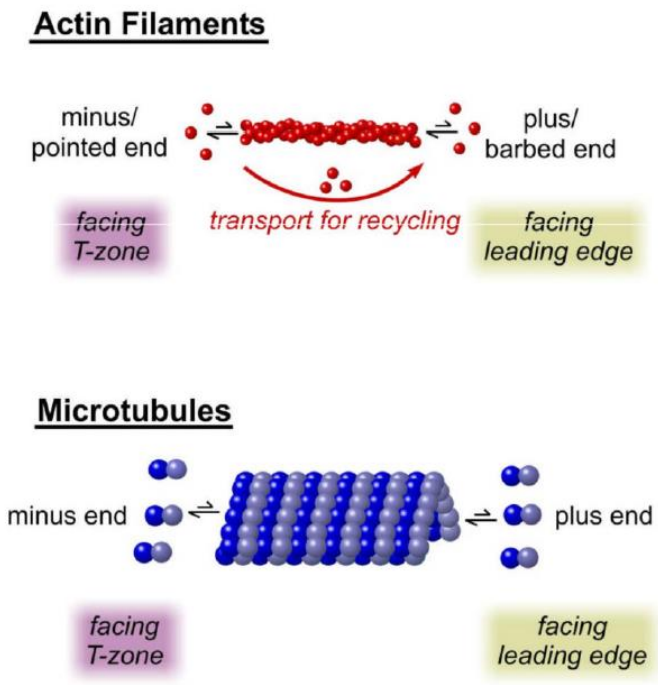

Figure 3. The dynamics of actin filaments and microtubules

Actin filaments are polarised polymers of globular actin monomers (red spheres), presenting a barbed and a pointed end. Actin monomers exists in two forms, such as ATP-actin and ADP-actin. ATP-actin association usually happens at the barbed end of actin filaments, it is followed by GTP hydrolysis, and GDP-actin dissociates from the pointed end. MTs are also polarised structures, with a plus and a minus end, and composed of protofilaments [made out of α- and β-tubulin heterodimers (blue and grey spheres)]. GTP-tubulin dimers are preferentially added to the plus end of MTs, similarly to actin GTP hydrolyse, and GDP-tubulin dimers can dissociate from the minus end. (adapted from [19])

The formation, stability and destruction of both MTs and actin filaments are well-controlled in the entire neuron and throughout the whole life of the cell. In order to maintain such structures like the shaft of MTs along the axon, or induce dynamic

cytoskeletal rearrangements during morphogenetic changes of the GC, MTs and actin filaments are regulated by a huge set of MT- and actin-associated proteins.

1. 1. 2. 1. Actin-binding proteins and MT-binding proteins as cytoskeleton regulators

The actin-binding proteins and MT-binding proteins regulate actin and MT dynamics at multiple levels. Both groups exhibit numerous members that form complex networks to provide a robust machinery for proper control in all conditions. Based on their function and their effect on actin or MTs, the members of these two groups can be divided into many categories: (1) some of them are nucleation factors that are required for the formation of new actin filaments or MTs; (2) others bind monomers or oligomers of actin or tubulin and control their availability for nucleation or polymerisation; (3) some others bind the plus end (or barbed end) of MTs or actin filaments and regulate several aspects of plus end dynamics; (4) whereas minus end (or pointed end) binding proteins affect the stability of the polymers; (5) in addition, proteins that bind along MTs and actin filaments are essential for protecting them against depolymerisation, for cross-linking, and for linking them to other cytoskeletal components; (6) furthermore, some others are known to sever or actively depolymerise MTs and actin filaments; (7) finally, motor proteins are involved in controlling filament contraction and movements, and cargo transport [4, 5, 25, 26]. **Table 1** lists many members of the above mentioned categories of actin- and MT-binding proteins.

Cytoskeleton regulator class	microtubule binding proteins	actin binding proteins
Nucleators	γ-tubulin ring complex (*γ Tub23C* and other components); doublecortin (*DCX-EMAP*)	Arp2/3 complex (*Arpc1, Arp3*, etc.); formins (*DAAM, Fhos, CG32138, dia*)
Plus-end-binding proteins	MAPFRE/EB (*eb1*); MT-plus-end-tracking proteins (+TIPs); doublecortin (*DCX-EMAP*); CKAP5/CHTOG/XMAP215 (*msps*)	ENAH/VASP (*ena*); formins (*DAAM, Fhos, CG32138, dia*); capping proteins (*cpa, cpb*); adducins (*hts*)
Mono- or oligomer-binding proteins	Stathmin/SCG10 (*stai*); DPYSL2/CRMP2 (*CRMP*); CKAP5/ CHTOG/XMAP215 (*msps*); doublecortin (*DCX-EMAP*); tub-specific chaperone E (*tbce*); CLASP (*chb*)	WASF/SCAR/WAVE (*SCAR*); WASL/N-WASP (*WASp*); APC (*Apc*); β4-thymosin/TMSB4X (*cib*); profilin (*chic*); twinfilin (*twf*)
Shaft stabilisers and cross-linkers	MAPT (*tau*); MAP2 (*tau*); MAP1B (*futsch*); MACF1; dystonin (*shot*)	Fascin (sn); α-actinin (*Actn*); plastin/fimbrin (*Fim*); filamin (*cher*); tropomyosin (*Tm1*); moesin, ezrin, radixin (*Moe*); α/β-spectrin (*α / β -Spec*); drebrin (*CG10083*); coronin (*coro, pod1*); MLLT4/Afadin-6 (*cno*); CTTN (*Cortactin*); PPP1R9A (*spinophilin*)
Minus-end stabilisers	γ-tubulin ring complex (*γ Tub23C* and other components); CAMSAP1 (*Patronin*)	Tropomodulin (*tmod*); Arp2/3 complex (*Arpc1, Arp66B*, etc.)
Plus-end motors	Type 1 kinesins (*Khc, Klc, Pat1*); type 2 kinesins (*Klp64D, Klp68D, Kif3C, Kap3*); type 3 kinesins (*unc-104, Khc-73*)	Myosin XVA (*Myo10A*); myosin VA (*didum*); myosin II (*zip, sqh*)
Minus-end motors	cytoplasmic dynein/dynactin (*Dhc64C, ctp, sw, Gl*, etc.); type 13 kinesins/KIF2C/MCAK (*Klp10A, Klp59C, Klp59D*)	Myosin VI (*jar*)
Severers, de-polymerisers	katanin (*Kat60*); spastin (*spas*); type 13 kinesins/KIF2C/ MCAK (*Klp10A, Klp59C, Klp59D*)	Cofilin (*tsr*); gelsolin (*Gel*)

Table 1. Examples of conserved MT- and actin-binding proteins in *Drosophila* and human

Some proteins are indicated in more than one categories since they fulfil multiple functions. *Drosophila* orthologs are shown in the brackets. (adapted from [4])

In this work we studied DAAM (Dishevelled Associated Activator of Morphogenesis) as a possible cytoskeleton regulator involved in controlling neuronal development. DAAM belongs to the formin protein family encoding conserved actin nucleation factors, therefore out of the numerous MT- and actin-binding proteins the group of actin nucleators are discussed in this section. The generation of new actin filaments and networks is indispensable for various cell biological processes. Nucleation is the first step of actin polymerisation which involves the assembly of two or three actin monomers into a complex, providing a nucleus for further

polymerisation. This process is kinetically unfavourable *in vivo*, therefore, cells require actin nucleation factors to catalyse the formation of new actin filaments.

Historically, the Arp2/3 (actin-related protein 2/3) complex was identified first as a major actin nucleator [27]. Instead of nucleating actin filaments *de novo*, this complex contributes to the generation of branched actin networks and it consists of seven highly conserved subunits: Arp2, Arp3, and five additional supporting units (ArpC1-5) [28-30]. The complex in itself is inactive, it exists in a conformation in which the two Arp2 and Arp3 subunits are localised too far from one another to start nucleation, and it requires the presence of nucleation-promoting factors to function properly [30, 31]. Members of the Wiskott-Aldrich syndrome protein (WASP) family are known as the main nucleation-promoting factors of the Arp2/3 complex. These WASP proteins are able to bind actin monomers through their conserved C-terminus, whereas their central amphipathic and acidic regions together can bind the Arp2/3 complex [32-34]. The binding of WASP proteins induces a conformational change by which the complex will be able to bind to an existing actin filament. Subsequently, the Arp2 and Arp3 subunits will form a specific structure to mimic an actin dimer which serves as a nucleation core for new filament assembly. In addition, the recruitment of actin monomers by the WASP proteins is also an essential element of this process, since the monomer binding activity of the Arp2/3 complex alone is very weak [35-37]. As a result of these, the new actin filament will rise from the side of a pre-existing filament at a 70˚ angle.

In contrast to the Arp2/3 complex, formins are *de novo* nucleation factors which catalyse the generation of linear actin filaments. There are several formins that has been identified in different model organisms (6 in *Drosophila melanogaster*, 15 in mammals) [38, 39], out of which the best-studied are the Diaphanous-related formins including Diaphanous, DAAM and FRL (formin-related protein). A common characteristic feature of all formin proteins is a highly conserved formin homology 2 (FH2) domain, which is localised in the C-terminal half of the protein [38, 40-42]. This

domain plays an essential role in actin nucleation, in addition, it also has the ability to bind the barbed end of actin filaments. Besides the FH2 domain, Diaphanous-related formins also contain several other homology domains that are involved in controlling their activity. The N-terminal region comprises of a GTPase-binding domain, a diaphanous inhibitory domain, a dimerization domain and a coiled-coil region, whereas the FH2 domain is flanked by a formin homology 1 (FH1) and a diaphanous autoinhibitory domain in the C-terminal region [43, 44]. The domain structure of a typical Diaphanous-related formin is shown in **Figure 4**. Basically, the association of the N-terminal diaphanous inhibitory domain and the C-terminal diaphanous autoinhibitory domain keeps formins in an inactive conformation [41, 45]. Due to small GTPase binding to the N-terminus, these two inhibitory domains disassociate, resulting in an active conformational state [41, 46-50]. In order to become active, formins also need to form homodimers in which the dimerization domain and the coiled-coil region are essential. After dimerization, the two FH2 domains create a ring-like structure which is thought to bind and stabilise spontaneously formed actin dimers or trimers, providing a nucleation core for filament assembly. Following this nucleation step, formins remain attached to the barbed end through their FH2 domains, which allows the processive elongation of the forming actin filament. On the one hand, their presence inhibits the binding of capping proteins [45, 51-54]. In addition, there is a prolin-rich region within the FH1 domain that acts as a binding site for Profilin, therefore this domain also has a very important role in filament elongation by recruiting Profilin-bound actin monomers for the elongation steps [55].

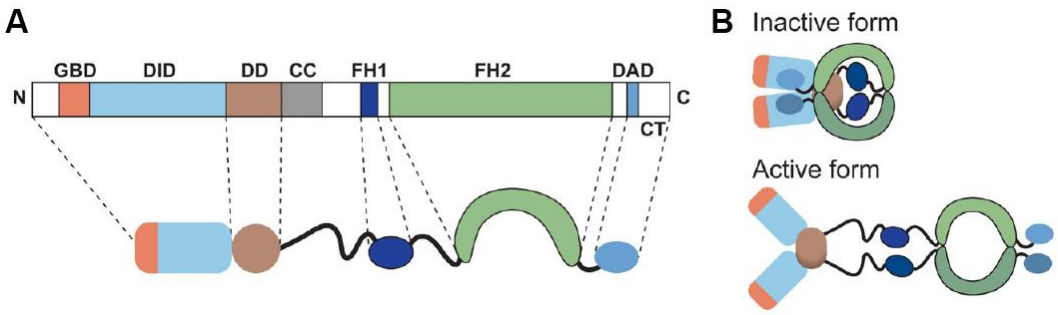

Figure 4. Domain architecture of Diaphanous-related formins, and the mechanism of activation

(**A**) The figure shows the structure of a typical Diaphanous-related formin which contains several conserved homology domains such as the GTPase-binding domain (GBD), the diaphanous inhibitory domain (DID), the dimerization domain (DD), the coiled-coil region (CC), the formin homology 1 (FH1) domain, the formin homology 2 (FH2) domain, the diaphanous autoinhibitory domain (DAD) and the C-terminal tail region (CT). The role of the certain domains is discussed in the text above. N, N-terminus; C, C-terminus. (**B**) By default, Diaphanous-related formins exist in an inactive autoinhibited state caused by the binding of the DID and DAD domains. Due to small GTPase binding to the GBD, these two inhibitory domains disassociate resulting in an opened active conformation of the protein. (adapted from [56])

Besides formins, several other factors have also been found to be responsible for *de novo* actin nucleation, such as Spire, Cordon-bleu, Leiomodin and junction-mediating regulatory protein, which are collectively called as tandem-monomer-binding actin nucleators [57-60]. The junction-mediating regulatory protein catalyses the formation of both linear actin filaments and branched actin networks, since it serves as a nucleation-promotion factor of the Arp2/3 complex as well [60], but other members of the group take part only in the nucleation of unbranched filaments [61, 62]. The common property of these nucleators is the presence of multiple WASP-Homology 2 (WH2) domains which are often found as tandem repeats in the protein and are able to bind actin monomers. The number of the WH2 domains varies between the different members. For example, Spire has four domains (the most in the group) [57] whereas the presence of three domains in the other members is already

sufficient for actin nucleation [58, 60]. Leiomodin has only one WH2 domain, however, it contains two other actin binding regions as well [59]. In this group, the mechanism of nucleation is based on the actin monomer recruiting ability of the tandem actin-binding domains which provide a polymerisation seed for actin filament assembly.

As it was described above, filopodia and lamellopodia are actin-rich structures of the GC in neurons: linear actin filaments are organised into parallel bundles along filopodia, whereas branched actin networks are typically localised in lamellopodia. According to this, it seems unambiguous that the different nucleation factors may act independently in the nucleation of filopodial and lamellopodial actin networks, however, several studies have suggested that formins and the Arp2/3 complex are necessary for actin filament assembly during the formation of filopodia and lamellopodia as well [36, 63]. Figure 5 demonstrates a model for filopodia generation in *Drosophila melanogaster*.

The example of the actin nucleation factors already shows that even the initial steps of actin filament generation involves many cytoskeleton regulators. Considering the huge number of MT- and actin-binding proteins, with many different functions, it is conceivable that the assembly and disassembly of cytoskeletal components is regulated by a complex and robust system in the cells. In the context of axon growth, it is well established that the dynamic rearrangement of the neuronal cytoskeleton is crucial in the process, however, it remained largely unclear how these changes are controlled at the cellular level. Despite the fact that many actin- and MT-binding proteins were already linked to the regulation of GC actin and MT dynamics, it is not exactly clear how these proteins are integrated into a complex regulatory system which is able to modify the state of the neuronal cytoskeleton in response to the external signals. Thus, unravelling those mechanisms that link guidance cues and cytoskeletal regulators into a functioning molecular machinery is a pivotal question.

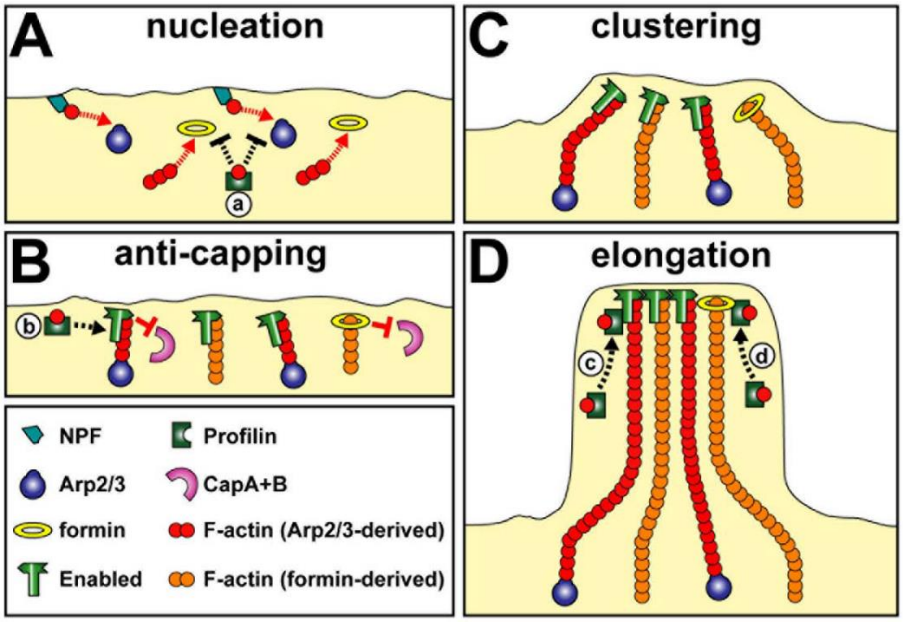

Figure 5. Filopodia generation model in *Drosophila* neurons

(**A**) The initial step of filopodia formation requires actin filament nucleation, however the assembly of new actin filaments can be initiated *de novo* or from the side of pre-existing filaments. In *Drosophila*, formins and Arp2/3 are well known nucleation factors (Arp2/3 is activated by nucleation-promoting factors, NPF). At this step, Profilin competes with the nucleation factors for the available actin monomers, therefore it suppresses actin nucleation. (**B**) After nucleation, actin polymerisation continues at the barbed end of the filaments. The presence of Enabled and formins at the filament barbed ends inhibits the binding of capping proteins (CapA+B) thus promotes elongation. (**C**) During elongation, Enabled contributes to the clustering of the filament barbed ends. In addition, the formin DAAM also promotes the formation of parallel F-actin bundles. (**D**) Enabled and DAAM are also involved in the processive elongation of actin filaments in the growing filopodium. At this stage, Profilin provides actin monomers for further elongation. (adapted from [64])

1. 1. 2. 2. Guidance cues and signalling pathways that control axon growth

GC movement during neuronal development is controlled by the extracellular environment. The translation of attractive and repulsive environmental guidance cues is crucial for axon advance: surface receptors of the GC sense the extracellular signals, and in turn, activate intracellular signalling pathways which lead to the dynamic rearrangement of the cytoskeletal components. Therefore, the identification

of these guidance cues and their downstream signalling pathways is crucial for understanding the molecular machinery of axon growth.

Due to extensive studies both in vertebrates and invertebrates, four major conserved families of axon guidance molecules were discovered in the 1990s, such as Netrins, Slits, Semaphorins and Ephrins [65-67]. Netrins and Slits are secreted signalling molecules, Ephrins are membrane-bound ligands, whereas the family of Semaphorins comprises of both secreted and membrane-bound forms. In addition, several families of transmembrane receptors were identified in relation to these signalling molecules: Netrins signal through the receptors Uncoordinated-5 and Deleted in colorectal carcinoma [68, 69], Slits through Roundabout family receptors [70] and Ephrins through the Eph family of receptor tyrosine kinases [71]. For the recognition of Semaphorins, multimeric receptor complexes are formed which include Plexin and several other components (such as Neuropilin, the neural cell adhesion molecule L1, and other receptor tyrosine kinases) [65, 72].

Netrins were first described as chemoattractants for vertebrate commissural axons [73, 74], however they can also function as repellents depending on the specific ligand-receptor context. Slits, Semaphorins and Ephrins are primarily known as repellents, controlling axon guidance in several different types of neurons, but also can act as attractive cues in some contexts [75]. One of the best characterised and understood developmental events is the midline crossing of commissural axons in which Netrins and Slits play a crucial role. In this process, Netrin functions as an attractant for commissural axons, whereas Slit acts as a repellent to prevent commissural axons from re-crossing, after crossing the midline (**Fig. 6**) [65, 76].

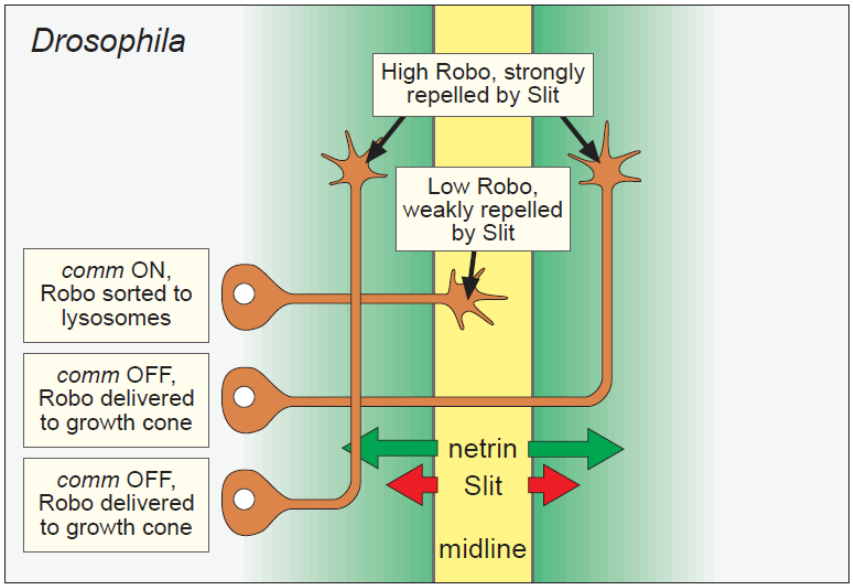

Figure 6. Midline crossing of commissural axons

During midline crossing, commissural axons grow towards the midline first, cross the midline and then continue growing on the contralateral side. Commissural axons are attracted to the midline by netrin before crossing, and are insensitive to the repellent Slit. However, the Slit receptor Roundabout (Robo) is expressed in commissural neurons by this time, it is targeted to lysosomal degradation by the intracellular sorting receptor Commissureless (Comm), instead of being delivered to the GC. After crossing the midline, Comm becomes inactivated allowing Robo to function in response to Slit, which prevents commissural axons from crossing the midline again. In addition, commissural axons also lose their sensitivity to netrin at this stage. (adapted from [65])

Beyond the fact that many guidance molecules and their receptors were proved to be involved in axon guidance, the Ras homologous (Rho)-family of small GTPases was found to be particularly important in transduction of the environmental signals. Rho GTPases, such as RhoA, Rac1 and Cdc42, are key players to integrate and link upstream directional signals and downstream cytoskeletal changes [77, 78]. Receptor activation by external signals first leads to the activation of Rho GTPase regulators. Some of these regulators activate Rho GTPases, like the guanine nucleotide exchange factors, whereas some others inactivate them, such as the GTPase activating proteins [77, 79]. Through complex interactions, Rho GTPases gather several upstream pathways and subsequently regulate downstream effector

molecules that control several aspects of cytoskeletal dynamics and provoke cytoskeletal rearrangements in many contexts (**Fig. 7**).

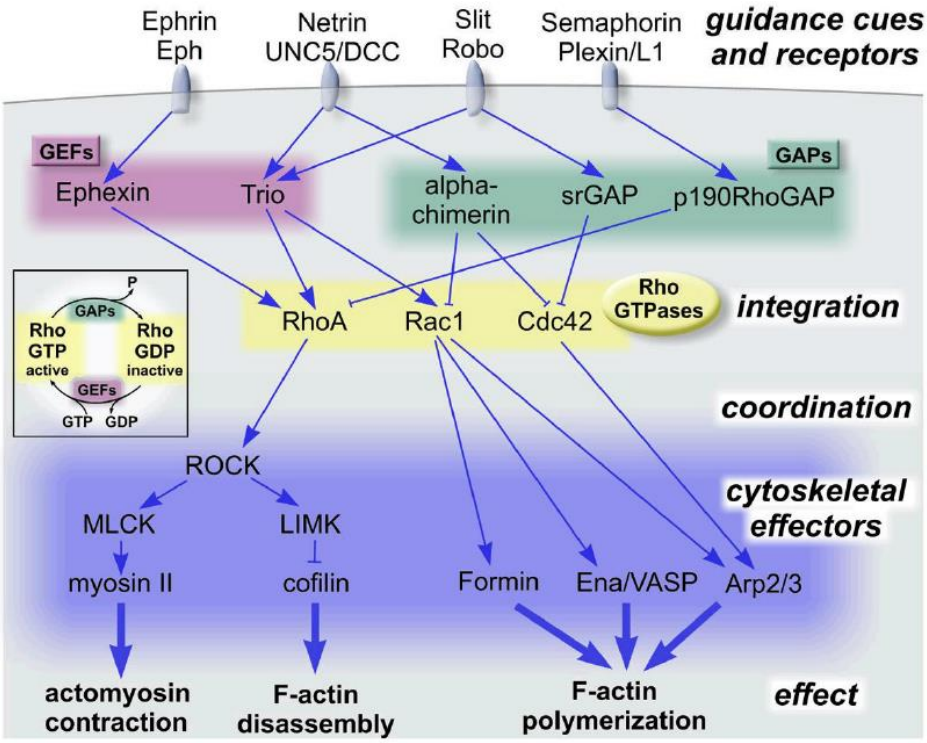

Figure 7. Rho GTPases as key signalling nodes

The figure shows how Rho-family GTPases integrate upstream guidance signals, through ligand-receptor binding and the subsequent activation of Rho GTPase regulators (GEFs, guanine nucleotide exchange factors; GAPs, GTPase activating proteins), and control effector molecules to provoke cytoskeletal changes during GC movements. The small box on the left shows the activation/inactivation cycle of Rho GTPases by GTPase activating proteins (GAPs, hydrolyse GTP to GDP) and guanine nucleotide exchange factors (GEFs, exchange GDP to GTP). Abbreviations of indicated cytoskeletal regulators: ROCK, Rho-associated protein kinase; MLCK, myosin light chain kinase; LIMK, LIM domain kinase; Ena/VASP, Enabled/vasodilator-stimulated phosphoprotein; Arp2/3, Actin-Related protein2/3. (adapted from [19])

As it is shown in **Figure 7**, guidance cues and receptors, Rho GTPase regulators, Rho GTPases and their downstream effectors form a robust and very intricate network, in which the same guidance cue can activate multiple GTPases through

complex interactions between Rho GTPases and their regulators. For instance, some of the Rho GTPase regulators are able to control several different GTPases, furthermore, a particular Rho GTPase might be a target of numerous regulators within the same cell. In addition, the same Rho GTPase can control different downstream effectors and influence various aspects of cytoskeletal dynamics in the GC [19, 80, 81].

Following the discovery of the major guidance molecules, another three families of signalling molecules were also implicated in axonal pathfinding. Notably, the Hedgehog, Decapentaplegic/Bone Morphogenic Protein/Transforming Growth Factor β and Wingless/Wnt families. The members of these families are secreted signal molecules which were previously identified as morphogens. Interestingly, these morphogens first control cell fate and tissue patterning during development, and then appear to be reused in latter developmental stages, for example to guide axons [75]. Some of these morphogens were found to provide guidance signals for several aspects of axon growth, such as midline crossing of commissural and retinal axons, and motor axon advance [82-88].

During the development of the vertebrate spinal cord, commissural neurons send axons ventrally towards the floor plate, where they cross the midline, and subsequently turn and continue growing to the anterior direction. During the initial phase of this process, Sonic hedgehog functions as a chemoattractant in the ventral midline of the spinal cord [82], whereas Bone Morphogenic Proteins are expressed in the roof plate and act as repellents [84, 85]. After crossing the midline, commissural axons are attracted by a Wnt4 gradient to turn and grow anteriorly [87], and repelled by a Sonic hedgehog gradient from the posterior pole [88]. **Figure 8** summarises the role of these morphogens in commissural axon development.

As exemplified above, many signal molecules have already been identified that guide axons, however, the exact mechanisms by which they control axon growth is still not completely understood. It would be crucial to elucidate how the combination

of external guidance signals is translated into cytoskeletal changes during GC movements and axon advance. For this, better understanding of the signalling mechanisms that link upstream guidance cues with their cytoskeletal effectors is crucial. In this work we focus on a non-canonical branch of Wnt signalling, referred as Planar Cell Polarity (PCP) signalling, since a growing number of evidence shows that this signalling module plays an essential role in the regulation of axon guidance and many other aspects of neuronal development.

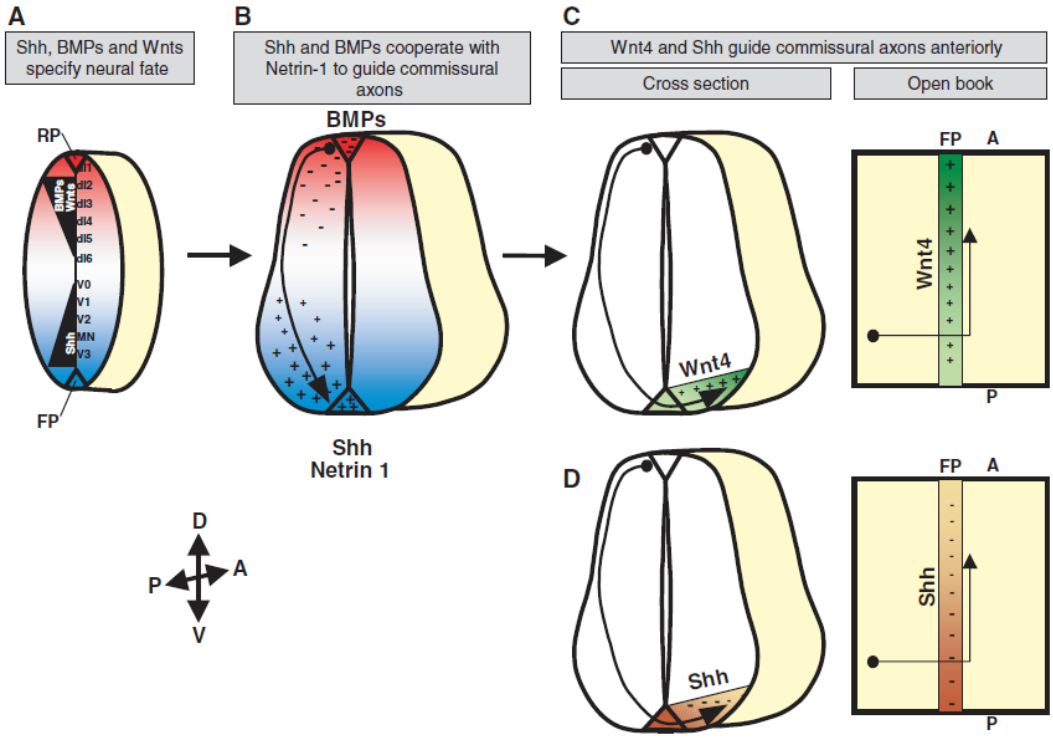

Figure 8. Morphogens guide commissural axons during spinal cord development

Schematic representation of the developing vertebrate spinal cord. (**A**) Concentration gradients of Bone Morphogenic Proteins (BMPs), Wnts (red) and Sonic hedgehog (Shh, blue) specify cell fate during the early development of the spinal cord. (**B**) Later, these morphogens serve as guidance signals during the growth of commissural axons, in which BMPs (red) repel commissural axons from the roof plate (RP) and Shh (blue), in combination with Netrin 1, attracts them to the floor plate (FP). After crossing the midline, (**C**) a Wnt4 gradient (green) attracts, whereas (**D**) a Shh gradient (orange) repels the anterior turn of commissural axons. D, dorsal; V, ventral; A, anterior; P, posterior. (adapted from [75])

1. 2. Wnt signalling

Wnts are highly conserved secreted glycoproteins that are well-known for their various functions in development including cell-fate determination, cell proliferation, migration, polarity establishment and neuronal development [89-92]. These proteins were designated by their firstly discovered members Wingless (*Drosophila*) and Int-1 (mice). The family of Wnt proteins comprises of 4 members in *Drosophila* and 19 members in vertebrates, which serve as ligand molecules for the Frizzled (Fz) family of seven-pass transmembrane receptors (six members in *Drosophila*; ten members in vertebrates) [93]. Upon Wnt binding to the Fz receptors three different signalling pathways might be activated: the canonical Wnt/β-catenin pathway, and the two non-canonical, Wnt/Ca^{2+} or Wnt/PCP pathways [94-98] (**Fig. 9**).

1. 2. 1. Wnt signalling pathways

Considering the high number of Wnts and Fz receptors, questions arise such as what gives the specificity for certain ligands and how the different Wnt signalling pathways become activated. Interestingly, some Wnts are known to be specific for certain pathways, whereas others appear to be involved in the activation of both canonical and non-canonical pathways. In addition to Fz receptors, other proteins have also been found to function as co-receptors in Wnt signalling, including the low density lipoprotein-related protein 5/6 [94, 99-101].

Downstream of Fz, Dishevelled (Dsh) is known to be a key component in the transduction of Wnt signals in all three Wnt signalling pathways. Dsh is thought to become activated in response to Wnt signalling, however, the definition of its active state is problematic. Several studies in different model organisms showed that this

process includes the phosphorylation of Dsh, as well as that of Dvl (the vertebrate ortholog of Dsh), but the role of this phosphorylation and the mechanism by which Dsh becomes phosphorylated is still not clear [102-105]. Dsh is a cytoplasmic protein and comprises of three highly conserved protein domains, the amino-terminal DIX (Dishevelled/Axin), the central PDZ (PSD-95, DLG, ZO1) and the carboxy-terminal DEP (Dishevelled, EGL-10, Pleckstrin) domains. The involvement of these domains in the canonical and non-canonical pathways is different which is crucial for the specific activation of distinct pathways. The DIX and PDZ domains are essential for Wnt/β-catenin signalling, whereas the non-canonical pathways utilise the PDZ and DEP domains [106, 107]. In addition, it has also been shown that upon Wnt activation Dsh translocates to the plasma membrane, which is crucial for activation of the pathway.

In the canonical pathway Wnts not only bind to the Fz receptor but also interact with the low density lipoprotein-related protein 5/6 co-receptor in vertebrates (Arrow in *Drosophila* [108]). In the absence of Wnt ligands, the proteasomal degradation of β-catenin is promoted by the Axin - Adenomatous polyposis coli - glycogen synthase kinase 3 multiprotein complex. Due to ligand binding, Dsh becomes activated and induces the stabilisation of β-catenin by preventing its phosphorylation by glycogen synthase kinase 3. It results in the cytoplasmic accumulation of β-catenin, which subsequently enters the nucleus and forms complexes with the T-cell factor/lymphoid enhancer-binding factor transcription factors to induce transcription of the Wnt-target genes [91, 109-111] (**Fig. 9 left panel**).

The non-canonical Wnt/Ca^{2+} signalling is known to be involved in the regulation of cell adhesion and cell movements. In this pathway the activated Fz receptor induces the activation of phospholipase C, with the contribution of Dsh and a heterotrimeric G-protein, which increases the intracellular level of inositol triphosphate. In response to the increased inositol triphosphate level, Ca^{2+} gets released from the endoplasmic

reticulum which subsequently activates protein kinase C and Ca^{2+}/calmodulin-dependent protein kinase II [96, 97, 112-114] (**Fig. 9 middle panel**).

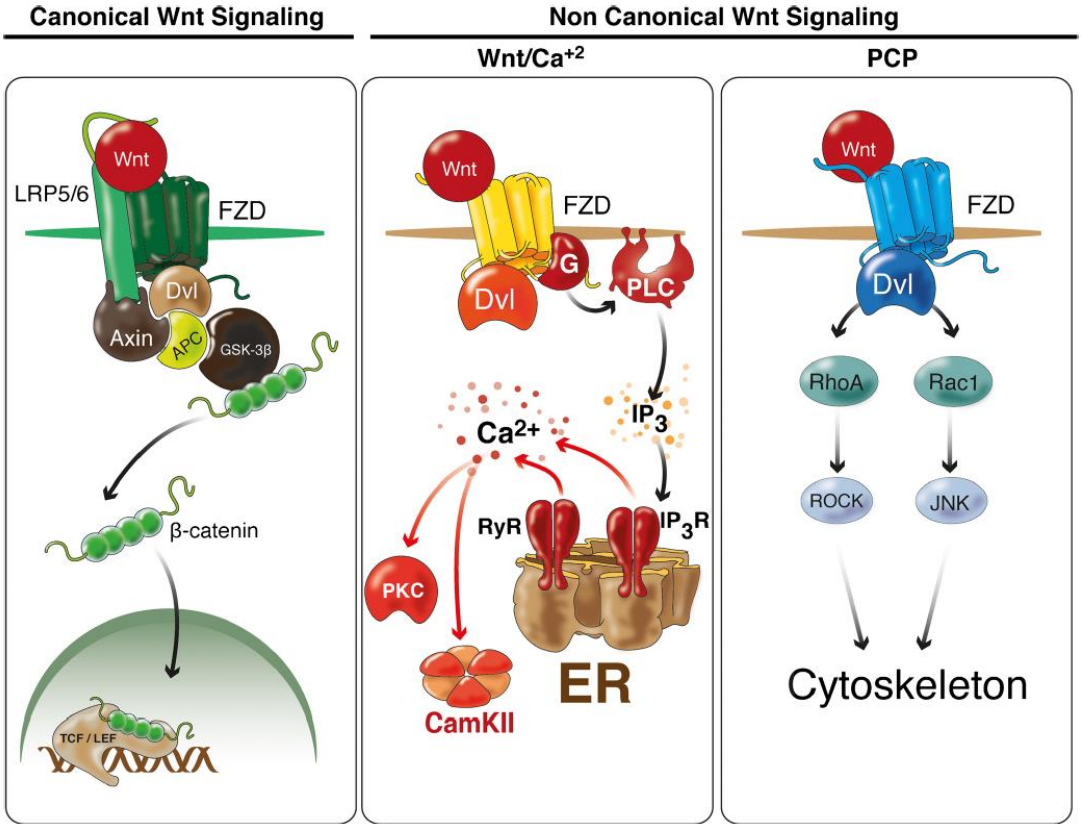

Figure 9. Wnt signalling pathways

Schematic figure showing the canonical and non-canonical Wnt signalling pathways. Wnt ligand binding to Frizzled (FZD, the vertebrate ortholog of Fz) receptors can activate three distinct pathways: the canonical Wnt/β-catenin, and the non-canonical Wnt/Ca^{2+} and Wnt/PCP pathways. As it is indicated in the figure, FZD and Dishevelled (Dvl, the vertebrate ortholog of Dsh) are key components and are involved in all three Wnt signalling pathways, however, each pathway employs a different set of downstream signalling components and controls distinct cellular processes (described in detail in the text). Abbreviations in the figure: LRP5/6, low density lipoprotein-related protein 5/6; APC, Adenomatous polyposis coli; GSK-3β, glycogen synthase kinase 3 β; TCF/LEF, T-cell factor/lymphoid enhancer-binding factor; G, G-protein; PLC, phospholipase C; RyR, Ryanodine receptor; PKC, protein kinase C; CamKII, Ca^{2+}/calmodulin-dependent protein kinase II; RhoA, Ras homolog family member A; ROCK, Rho-associated protein kinase; Rac1, Rac family small GTPase 1; JNK, c-Jun N-terminal kinase. (adapted from [115])

In the Wnt/PCP signalling pathway, Flamingo, Strabismus, Prickle and Diego, members of the core PCP protein family, form asymmetric multiprotein complexes with Fz and Dsh (detailed below in chapter 1. 2. 3.). Through complex interactions, these proteins are thought to modulate the activity of Dsh and thereby affect Wnt signal transduction. In this pathway Dsh activates the small GTPases Rho and Rac, which leads to the subsequent activation of Rho-associated protein kinase and c-Jun N-terminal kinase, ultimately affecting cytoskeleton remodelling [94, 96, 116-120] (**Fig. 9 right panel**).

Whereas the exact mechanisms of the context dependent regulation of Wnt signalling are largely unclear, recent studies clearly suggested that the Wnt/PCP pathway is important for multiple aspects of neural development, and it is a good candidate to be directly involved in cytoskeletal remodelling in the GCs [121-124]. Although in this work we focus on the role of Wnt/PCP signalling in neuronal development, traditionally it was known to be responsible for the formation of planar cell polarity, which will be discussed in the next section.

1. 2. 2. Planar cell polarity and the non-canonical Wnt/PCP signalling pathway

Polarisation of the cells is a crucial feature during development and formation of tissues, organs and organisms. For example, the establishment of apical-basal polarity in epithelial tissues is essential for particular functions, such as transport of fluids or directed secretion of specific agents and proteins. Besides apical-basal polarisation, most epithelial tissues represent a second polarity axis within the plane of the epithelia, which is called planar cell polarity or tissue polarity (for definitions see: [125-127]). PCP was discovered in insects and became very well-studied in *Drosophila melanogaster*, which highly contributed to the identification and characterisation of the most important genes that are involved in tissue polarisation.

Although several *Drosophila* tissues show planar polarity, the adult wing is arguably the best characterised model system to study PCP. During pupal life each wing cell produces an actin- and MT-rich protrusion, called a trichome, at the distal apical surface of the cell. In the adult wing each trichome is polarised along the proximal-distal axis and points distally. In contrast to this, in PCP mutants the trichomes often display abnormal orientation, and/or instead of a single trichome per cell, multiple trichomes are initiated ectopically at the centre of the cell [124] (**Fig. 10 A-B**).

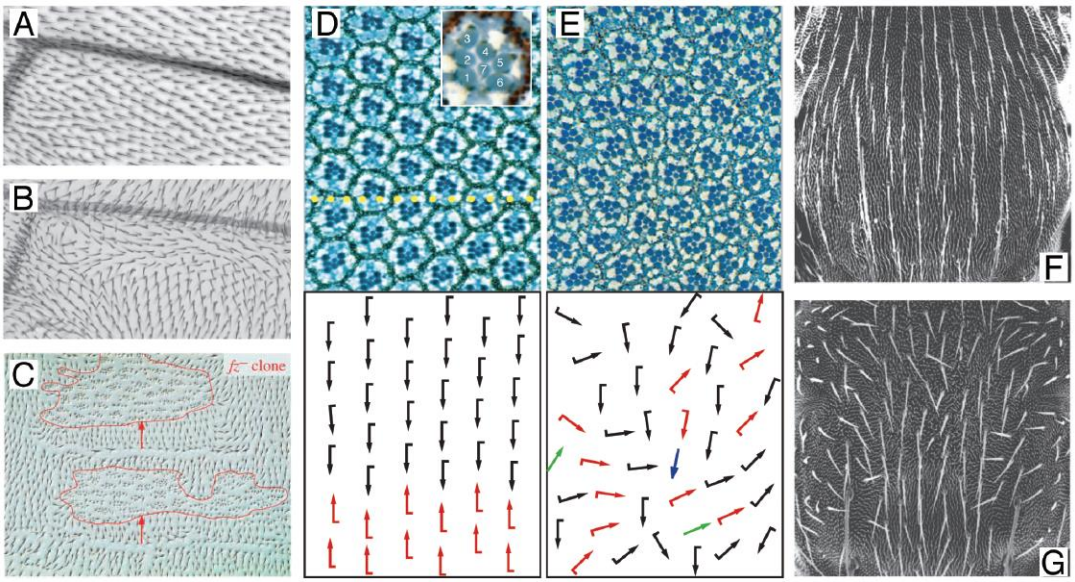

Figure 10. Typical PCP mutant phenotypes in *Drosophila*

(**A-B**) Enlarged view of a wild type (**A**) and a PCP mutant (**B**) adult wing. In the wild type trichomes point distally, whereas, trichomes display abnormal orientation in the PCP mutant wing. (**C**) Cuticular trichomes point to the opposite direction in the PCP mutant clones. (**D-E**) Representative images of wild type (**D**) and PCP mutant (**E**) adult eye sections showing the structure and the orientation of ommatidia. The yellow segmented line shows the equator, a dorso-ventral midline, which separates the eye into two hemispheres. Interestingly, the ommatidia of the dorsal and ventral hemispheres are mirror-symmetric to one another. In contrast to the wild type (**D**), PCP mutants (**E**) show an abnormal arrangement of ommatidia. (**F-G**) Scanning electron micrographs of the notum of adult flies. In wild type animals (**F**) all mechanosensory bristles point to the posterior direction, however, their orientation changes and the bristles become misaligned in PCP mutant flies (**G**). (adapted from [128])

Besides trichomes, the adult *Drosophila* cuticle is covered with mechanosensory bristles that are innervated and function as a simple sensory organ. Normally, these bristles point posteriorly, and changes in their orientation can be easily followed by studying the abdomen or the notum of the flies. The development of mechanosensory bristles depends on the asymmetrical division of the sensory organ precursor cells during pupal life, and the alignment of the axis of division with the anterior-posterior body axis is controlled by the PCP system. Thus, these bristles display a largely random orientation in PCP mutants [129-132] (**Fig. 10 F-G**).

In addition, the *Drosophila* compound eye, a complex and well-structured organ, has also been widely used to study planar polarity. The adult eye comprises around ~800 hundred unit eyes, also called ommatidia, each containing 8 photoreceptor cells and 12 accessory cells. Due to the asymmetric arrangement of the photoreceptor cells, each ommatidia displays an intrinsically asymmetric, chiral structure. In PCP mutants normal arrangement of the ommatidia is disrupted that is evident in abnormally oriented ommatidia, chirality reversals and/or in the appearance of symmetric ommatidia instead of the chiral structures [133-135] (**Fig. 10 D-E**).

Genetic analysis of the mutations affecting planar polarity in *Drosophila* and the subsequent identification of the most important genes involved in tissue polarisation revealed that Wnt/PCP signalling is fundamental in the establishment of PCP.

1. 2. 3. Wnt/PCP signalling and the formation of planar polarity in the epithelium

Six proteins were identified as the key components of the Wnt/PCP signalling pathway in *Drosophila* (known as core PCP proteins). Three of these are transmembrane proteins, whereas the others are intracellular. The seven-pass transmembrane protein Fz serves as the receptor in PCP signalling, as well as in canonical Wnt

signalling, and it binds Wnt ligands by its cysteine-rich extracellular domain [136, 137]. The other two transmembrane components are the atypical cadherin Flamingo (Fmi; also known as Starry night, Stan) [138], and the four-pass transmembrane protein Strabismus (Stbm; also known as Van Gogh, Vang) [139, 140]. Dsh is an intracellular protein which plays a crucial role in all canonical and non-canonical signalling pathways [119, 141]. The two other cytoplasmic components of the pathway are Prickle (Pk) and Diego (Dgo). Pk comprises of 3 LIM domains and 1 PET domain [142], whereas Dgo is an Ankyrin repeat protein [143]. **Table 2** summarises the core PCP genes, as well as their vertebrate orthologs, and the molecular features of their protein products.

In the *Drosophila* wing, PCP proteins interact with each other intracellularly to form asymmetrically localised protein complexes on the proximal and distal sides of the cells, which is essential for the establishment of tissue polarity. Besides this cell-autonomous function, the transmembrane proteins of the pathway, such as Fz, Stbm and Fmi, also have non-cell-autonomous functions and make asymmetric intercellular connections between neighbouring cells to form planar polarity along the tissue [125, 144, 145]. Interestingly, these cell-autonomous and non-cell-autonomous functions are necessary at different developmental phases: the interaction of PCP proteins between adjacent cells is important at the early pupal stage, whereas the formation of asymmetric intracellular protein complexes is necessary later during pupal life [144].

PCP gene	Tissues affected in Drosophila	Vertebrate orthologs	Molecular features
Core genes:			
frizzled (fz)	E, W, S, A	Fz3, 6 and 7	seven-pass transmembrane receptor, binds Wnt ligands, Dsh; recruits Dsh and Dgo to membrane
dishevelled (dsh)	all adult tissues	Dvl1–3, xDsh	cytoplasmic protein containing DIX, PDZ, DEP domains, recruited to membrane by Fz, binds Fz, Pk, Stbm and Dgo
flamingo (fmi)/ starry night (stan)	all adult tissues	Celsr 1–3	cadherin with seven-pass transmembrane receptor features, homophillic cell adhesions
diego (dgo)	E, W, T in GOF*	Inversin, Diversin	cytoplasmic Ankyrin repeat protein, recruited to membrane by Fz, binds Dsh, Stbm and Dgo. Diversin/Inversin in vertebrates
strabismus (stbm)/van gogh (Vang)	all adult tissues	Vangl1, 2	4-pass transmembrane protein, binds Pk, Dsh and Dgo, recruits Pk to membrane
prickle (pk)	all adult tissues	Pk1 – 4	cytoplasmic protein with 3 LIM domains and PET domain, recruited to membrane by Stbm, physically interacts with Dsh, Stbm and Dgo

Table 2. Summary of the core PCP genes and their vertebrate orthologs

Tissues affected in *Drosophila*: A, abdomen; E, eye; S, sensory organ precursor cells; T, thorax; W, wing; *other tissues not tested. The core PCP genes are highly conserved throughout the animal kingdom; their vertebrate orthologs are also shown in the table: Fz3, 6 and 7, Frizzled3, 6 and 7 (also known as FZD); Dvl1-3, Dishevelled1-3; xDsh, Xenopus Dishevelled; Celsr1-3, cadherin EGF LAG seven-pass G-type receptor 1-3; Diversin is also known as Ankrd6 (ankyrin repeat domain 6); Vangl1-2, Vang-like protein 1-2; Pk1-4, Prickle homologue 1-4. (modified table, from [128])

The surface of the *Drosophila* wing is covered by hexagonally shaped epithelial cells. According to the proximal-distal axis of the wing, the hinge of the wing is the proximal end whereas the apex is the distal end. All of the epithelial cells are polarised along this axis and exhibit a trichome on the distal apical surface of the cell. Asymmetric localisation of the PCP proteins is essential for trichome formation in the wing, however, this phenomenon is restricted to a short time period. During pupal development trichomes emerge from the wing cells at 32-36 hours after puparium formation. Before the establishment of trichomes, the core PCP proteins localise at

the apical-lateral membrane and show a uniform distribution at each side of the wing cells. This apical-lateral localisation is necessary for the proper function of PCP signalling, as targeted mislocalisation of the PCP proteins (e.g. Fz) to the basal membrane disrupts PCP function [146]. There is a period just before trichome formation, at 24-32 hours after puparium formation, in which the PCP proteins rearrange and form asymmetrically localised protein complexes at the proximal and distal cell edges (**Fig. 11**). Fz localises to the distal membrane and recruits Dsh and Dgo, whereas Stbm and Pk localises proximally. In contrast to these, Fmi can be found in both the proximal and the distal membranes (**Fig. 12**). The formation of these asymmetric complexes is critical for proper trichome initiation. Distal accumulation of the Fz-Dsh complex induces cytoskeleton activation through other effectors, which leads to the formation of actin- and MT-rich protrusions on the distal apical surface of the wing cells. At the same time, this process is inhibited on the proximal side by the Stbm-Pk complex [124, 147, 148].

During the formation of asymmetrical protein complexes each PCP component controls the localisation of the other components through complex interactions, however, their contribution is different. For instance, the absence of Fz, Stbm or Fmi prevents the apico-lateral localisation of the PCP proteins, whereas, loss of the cytoplasmic PCP proteins only affects the subcellular asymmetry of the PCP components between the proximal and distal sides of the cells [149] (**Fig. 11 D-E**). In addition, the transmembrane components of the PCP pathway are required to recruit the cytoplasmic Dsh, Dgo and Pk proteins to the membrane which leads to the formation of a proximal Stbm-Pk and a distal Fz-Dsh-Dgo complex (**Fig. 12**) [150]. Through their cytoplasmic components, these two complexes antagonise one another and prevent the formation of the other complex on the same side of the membrane.

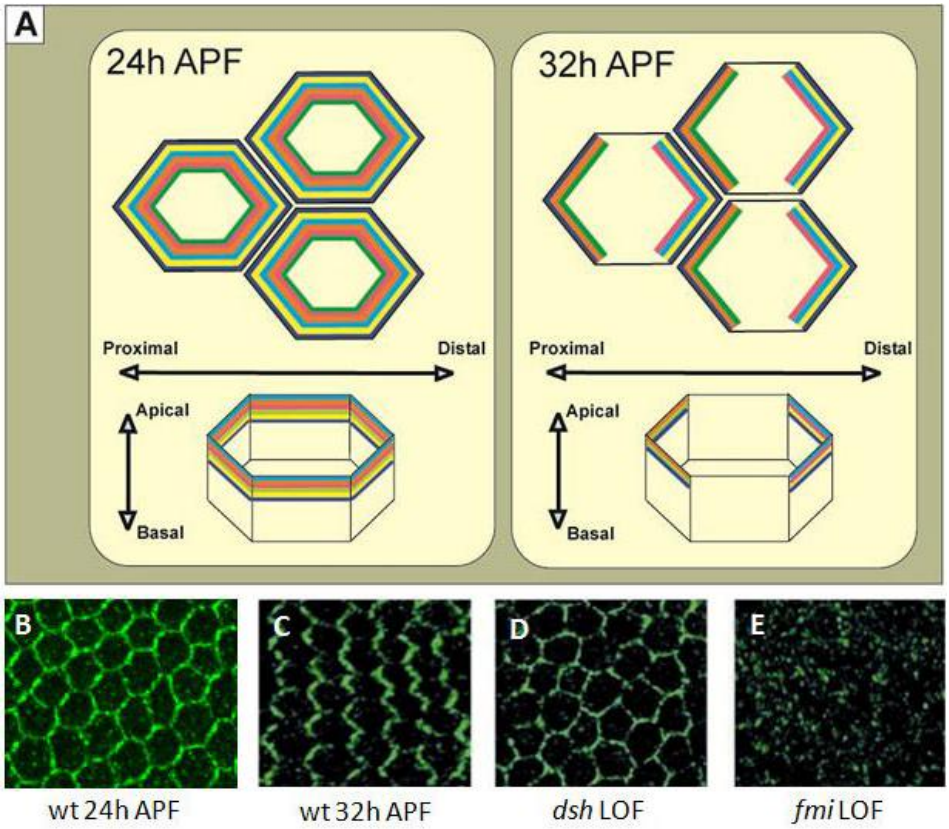

Figure 11. The formation of asymmetric protein complexes during wing cell development

(**A**) Schematic representation of wing cells at 24 hours and 32 hours after puparium formation (APF). At 24h APF, PCP proteins do not show polarised localisation at the apical-lateral membrane. In contrast, PCP proteins subsequently rearrange (32h APF) and form asymmetric protein complexes in the proximal and distal cell membranes. Each PCP protein is indicated by a different colour in the figure: Fmi, black; Stbm, orange; Pk, green; Fz, yellow; Dsh, blue; Dgo, pink. (**B**) The localisation of Fz in the pupal wing at 24h APF, which changes and becomes polarised at 32h APF (**C**). (**D**) The asymmetric localisation of Fz is disrupted in the dsh mutant wing (32h APF), whereas in the fmi mutant (**E**) even the apical-lateral localisation of Fz is prevented (32h APF). LOF, loss of function.

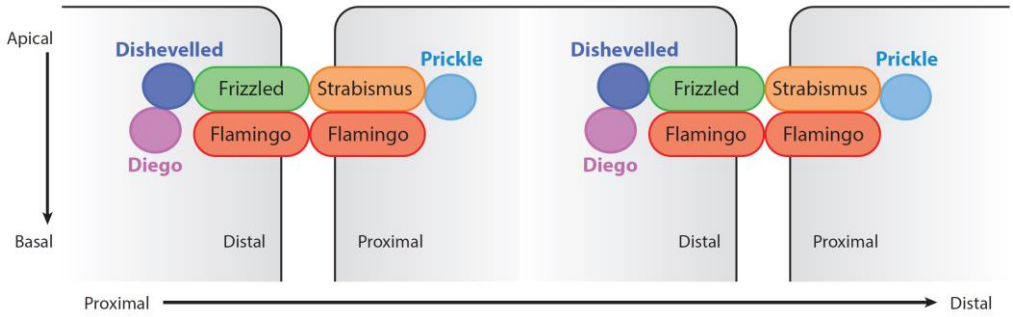

Figure 12. The asymmetric localisation of the core PCP proteins

Schematic representation of wing cells showing the asymmetric localisation of the core PCP proteins. (modified image, from [151]) Fz is localised in the distal, whereas Stbm is in the proximal membrane. These transmembrane proteins recruit the cytoplasmic PCP components and form the Fz-Dsh-Dgo (distal) and Stbm-Pk (proximal) protein complexes. In contrast, Fmi is localised in both membranes and forms homodimers between adjacent cells.

1. 2. 4. Role of the Wnt/PCP signalling in neuronal development

Traditionally, Wnt/PCP signalling was known to be responsible for the establishment of PCP in cells and tissues, however, a growing number of studies showed that members of this signalling pathway may have other functions. Besides *Drosophila*, studies expanded to vertebrate model organisms as well, and it became clear that the core PCP genes are highly conserved from invertebrates to vertebrates (for a review see [151]) (**Table 2**) and display many functional similarities. Importantly, these novel studies also revealed that, besides their basic function in tissue polarisation, the core PCP proteins are fundamental to several processes during nervous system development, such as neural tube closure, neuronal migration, axonal pathfinding and dendritic growth.

Relevance of the core PCP proteins in neural tube closure has been demonstrated in several model systems (e. g. Xenopus leavis, zebrafish and mice) [152-159], moreover, their involvement has been reported in human studies as well [160]. During neurulation, the neural plate narrows and elongates to make the neural groove, then

it folds and closes into the neural tube [153, 161]. **Figure 13** shows *Vangl2* and *Celsr1* mutant mice, representing a severe neural tube closure defect called craniorachischisis. Although the reduced function of PCP proteins leads to open neural tube formation in these cases, it is a result of impaired convergent extension during gastrulation, therefore this aberration is a consequence of defective tissue polarisation.

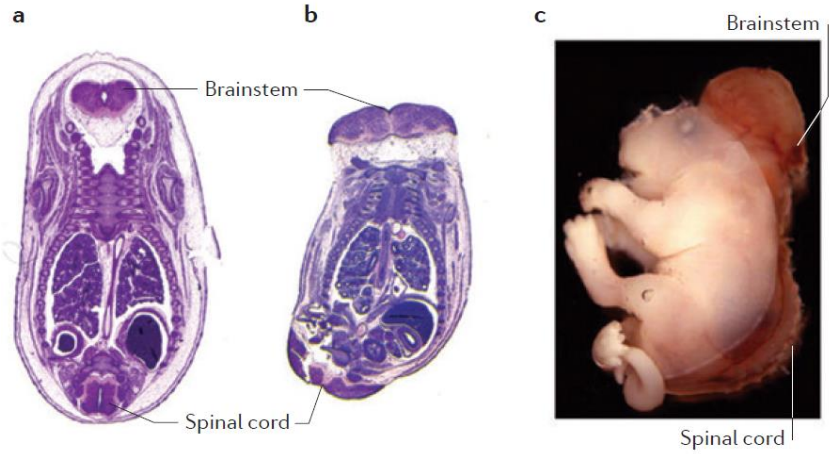

Figure 13. Neural tube defects in PCP mutant mice

The figure shows mouse embryos at embryonic day 14. In wild type embryos (**a**) the neural tube is properly formed, whereas, in PCP mutants (**b**, *Vangl2* mutant; **c**, *Celsr1* mutant) the process of neural tube closure is impaired, resulting in an open neural tube along the neural axis. (adapted from [162])

The rhombencephalon, a specific area of the brainstem, serves as the place of the migration of facial branchiomotor neurons during early development. These neurons are generated in rhombomer 4, around embryonic day 10 in mice, from which they migrate caudally through rhombomer 5 into rhombomer 6 to form the facial motor nucleus [163, 164]. This process is conserved from fish to mammals [165] and studies, both in zebrafish and mice, showed that the core PCP proteins control the

migration of facial branchiomotor neurons in a cell-autonomous and non-cell-autonomous manner as well [154, 166-170]. (**Fig. 14**)

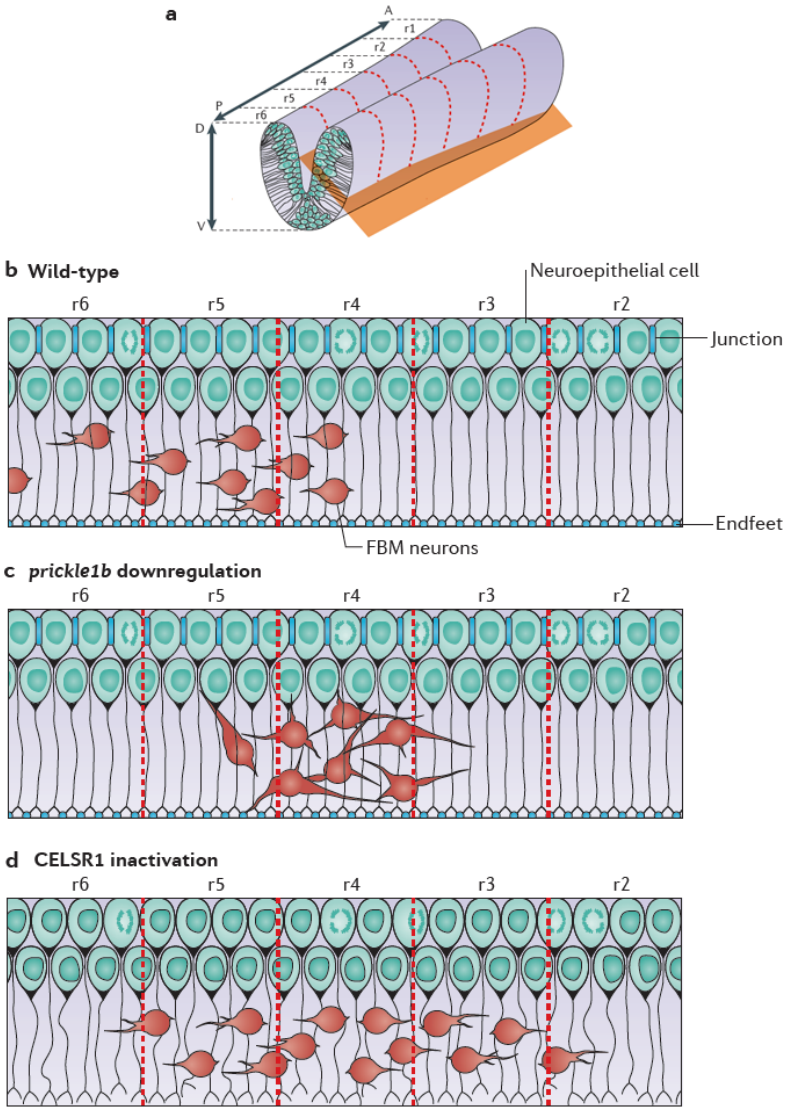

Figure 14. The role of the Wnt/PCP proteins in neuronal migration

(**a**) is a schematic representation of the developing rhombencephalon with its 6 rhombomers (r1-r6). Rhombomer 1 is localised anteriormost, up is dorsal in the figure. (**b-d**) show a particular section of the rhombencephalon (indicated in orange in **a**). In wild type animals (**b**) facial branchiomotor neurons (FBM) are generated in rhombomer 4 and migrate caudally to rhombomer 6, whereas, the migration of these neurons is disrupted in PCP mutants. For example, the downregulation of *prickle1b* in zebrafish (**c**) inhibits the caudal migration of facial branchiomotor neurons, thus, they accumulate centrally in the rhombomer. In addition, in *Celsr1* mutant mice (**d**), besides caudal migration, facial branchiomotor neurons also migrate rostrally. (adapted from [162])

In addition to these, the PCP proteins have been implicated in axon growth and guidance as well. Several studies, from *Drosophila* to mammals, showed that the core PCP proteins play a pivotal role in these processes, however their exact mechanisms have not been cleared in most cases. For instance, *fmi* controls axon-axon and axon-target interactions in the visual system of the fruit fly [171, 172]. In the *Drosophila* embryo, *fmi* interacts with *pk* to promote axon advance of the peripheral sensory neurons [173, 174]. In addition, Wnt/PCP proteins also regulate axonal branching of the *Drosophila* mushroom body neurons: PCP components, in cooperation with one another, are required for proper targeting and bifurcation of the mushroom body axons [175-177] (**Fig. 15**). There are some well-known mammalian examples for the involvement of the core PCP proteins in the regulation of axon guidance. For example, *Fz3* and *Celsr1* are essential for axonal pathfinding in the olfactory bulb (**Fig. 16 B-C**) and for the formation of reciprocal connections in the internal capsule (**Fig. 16 D-E**) [178-180]. Furthermore, *Fz3*, *Celsr3* and *Vangl2* are crucial for the anterior turn of commissural axons after midline crossing in the spinal cord (**Fig 16 F-H**) [87, 127, 181]. Very similarly to this, *Fz3a* and *Vangl2* are required for anterior pathfinding of the commissural primary ascending neurons, after midline crossing, in the zebrafish spinal cord [182].

Beyond axonal pathfinding, some PCP proteins were also found to be involved in dendritic development. In *Drosophila*, *fmi* is required for proper development of the sensory neuron dendrites [183, 184]. Furthermore, it was shown that *fmi* interacts with *stbm*, amongst other partners, in the mechanism of dendritic self-avoidance [185]. Interestingly, the mammalian homologues of *fmi* are also required for dendrite formation, however, *Celsr2* and *Celsr3* seem to have opposite functions. The downregulation of *Celsr2* leads to decreased dendrite length and reduced complexity of dendritic arborisations, whereas the silencing of *Celsr3* results in dendritic overgrowth [186].

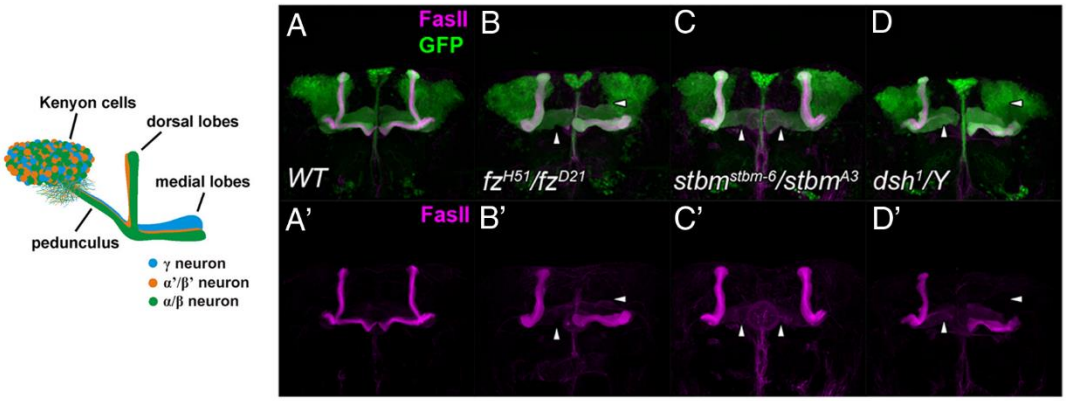

Figure 15. Phenotypes of PCP mutants in the *Drosophila* mushroom body

A schematic drawing of the mushroom body can be seen in the left (adapted from [177]), which comprises three types of Kenyon cells (KC), the γ (blue), α'/β' (orange) and the α/β (green) neurons. The cell bodies of KCs and their dendritic arborisation, called the calyx, is located in the dorsal brain, whereas their axons extend anterolaterally and form a massive fibre called the pedunculus. On the anterior side, the axons of γ KC cells run medially and form the γ lobe. In contrast, the α'/β' and α/β axons bifurcate to form the dorsal (α'/α) and medial (β'/β) lobes. (**A-D**) confocal microscopic images of wild type (**A**) and PCP mutant (**B-D**) adult brains. The whole mushroom body is visualised by expressing GFP (green), driven by a mushroom body-specific driver, and the lobes are visualised by FasII immunostaining (magenta). I contrast to the wild type, in *fz*, *stbm* and *dsh* mutants (**B-D**) the dorsal and/or medial lobes are lost or significantly reduced (white arrowheads). (adapted from [175])

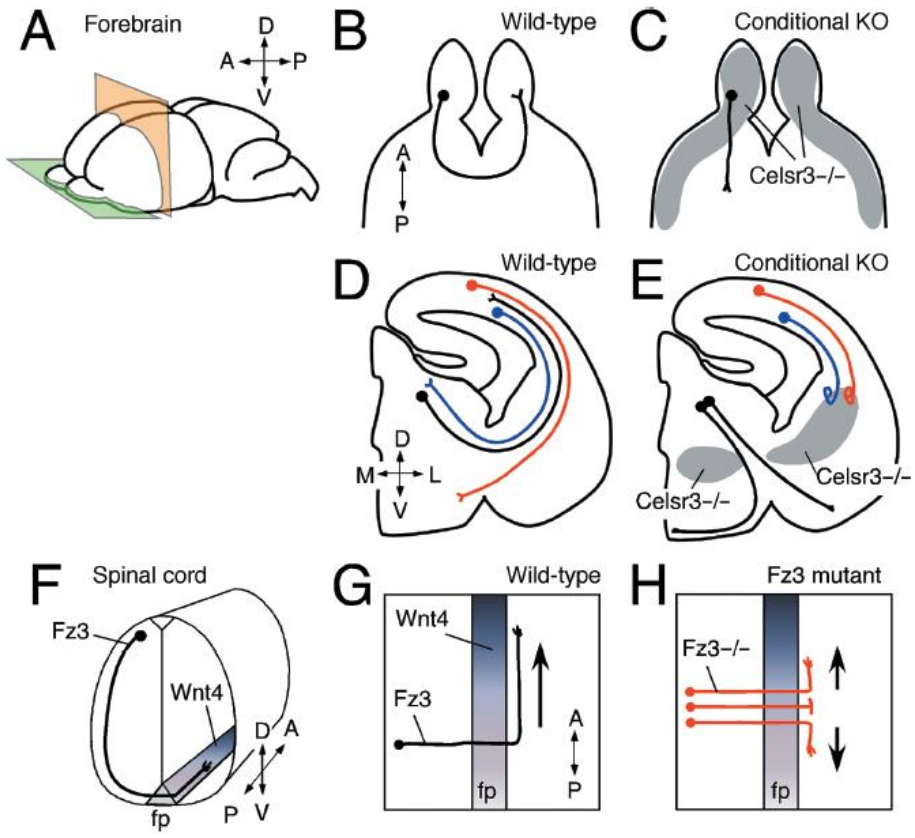

Figure 16. Axon guidance defects in PCP mutant mice

(**A-E**) Schematic representations of axonal tracts in the mouse forebrain. (**B-C**) Horizontal sections of the olfactory bulb (indicated in green in **A**). In the olfactory bulb, axons cross the midline and innervate the contralateral side normally (**B**). If *Celsr3* is inactivated specifically in the dorsal telencephalon (grey areas) olfactory bulb axons fail to project contralaterally (**C**). (**D-E**) Frontal sections of the forebrain (indicated in orange in **A**) showing the axons of thalamocortical (black), corticothalamic (blue) and subcerebral (red) neurons. Normally these neurons grow reciprocal projections in the internal capsule (**D**), but when the activity of *Celsr3* is reduced specifically in the striatum (grey areas) their axons fail to pass through the region and cannot make reciprocal connections (**E**). (**F-H**) Schematic drawings of the mouse spinal cord. In wild type mice, dorsal interneurons send commissural axons ventrally that cross the midline at the floor plate (fp), and then turn anteriorly (**F-G**). In *Fz3* mutant animals, this turn is randomised or commissural axons stall after crossing the floor plate (**H**). (adapted from [162])

Even though we see many examples for the involvement of the core PCP members in the regulation of neuronal development, the interpretation of these phenomena may not be straightforward. For instance, there can be situations in which PCP mutant phenotypes occur as a consequence of changes in planar polarity instead of being

specific for neuronal development, such as neural tube closure defects. Thus, to distinguish between the primary and secondary effects of Wnt/PCP signalling in these cases remained a critical concern. Furthermore, another key question is how Wnt/PCP signalling controls several aspects of neuronal development, particularly axon growth and guidance? What are the downstream members and effectors of this signalling pathway that regulate axonal advance during development, presumably by controlling the cytoskeletal changes?

To address some of these questions, *Drosophila melanogaster*, also known as the common fruit fly, serves as a great model organism. The simple but well-structured nervous system of *Drosophila* and the huge number of available genetic manipulation tools provide us with many possibilities to study the role of the core PCP components, as well as that of their possible effectors, in axon growth and guidance.

1. 3. The fruit fly, *Drosophila melanogaster*

1. 3. 1. A powerful tool for genetics

The first application of *Drosophila melanogaster* in laboratory experiments was more than a century ago by Tomas Hunt Morgan and it was also among the first organisms that were used for genetic analysis. Over the time, *Drosophila* helped to gain a significant knowledge in many different scientific fields – such as development, physiology, behaviour, etc. – by the systematic application of fly genetics and it became one of the most successful and widely used model organisms in live sciences. There are many advantages that make the fruit fly an ideal model organism; the most important ones are listed below:

- Work in *Drosophila* is low cost, considerably fast and handling of the experimental animals is easy. Several hundreds or even thousands of fly stocks can be kept and maintained in laboratory conditions to perform high-throughput experiments.
- The generation time of the fruit fly is short, it takes about 10 days at 25˚C (**Fig. 17**) and the whole lifespan is about 50 days, thus, several generations can be studied in a relatively short time.
- The fruit fly genome contains only four pairs of chromosomes, one pair of sex chromosomes (X and Y) and three pairs of autosomes (2, 3 and 4), of which the 4^{th} one is significantly smaller than the others.
- The whole genome sequence of *Drosophila* is known since 2000 [187] and it exhibits a high level of conservation. For example, about 60% of the human genes and about 75% of human disease genes are conserved in *Drosophila*

[188]. In addition, the genome displays lower redundancy than in higher level organisms which simplifies many experimental processes.

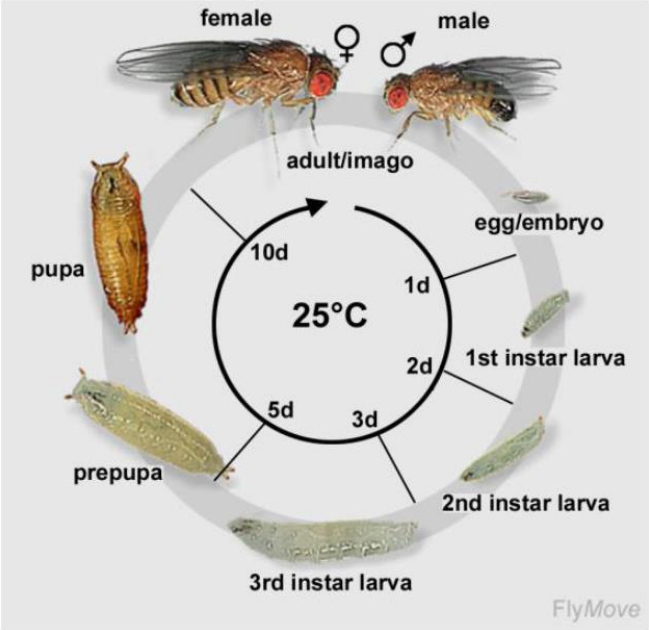

Figure 17. The life cycle of *Drosophila melanogaster*

Drosophila is a holometabolous insect, its development includes four life stages: egg, larva, pupa and imago. After fertilisation females lay eggs in which embryonic development lasts about one day at 25˚C. 1st instar larvae hatch from the embryo and moult into 2nd and 3rd instar larvae in the next 2 days. After 2 more days 3rd instar larvae form the pupa (prepupa and then the pupa). Metamorphosis happens during the pupal stages, which takes about 4-5 days, and after eclosoin adult flies emerge from the pupal case. (adapted from [189])

There are several genetic manipulation tools that make *Drosophila* a well-tractable model organism for genetic analysis. Amongst many of them, in this work we used the Gal4/*UAS* system in order to express a GFP-tagged protein specifically in cultured neurons *in vitro*. Gal4 is a transcription factor from yeast that serves as a transcriptional activator. There are no endogenous targets of Gal4 in the *Drosophila* genome, however, it specifically binds to the *UAS* (*Upstream Activating Sequence*) enhancer element. In an experimental situation one fly line carries Gal4 with a tissue-

or cell-specific promoter, while *UAS*, together with a certain gene of interest, is kept in another fly line. By crossing these lines, in the progeny Gal4 will activate the expression of the *UAS*-coupled gene at the tissue or cell that the promoter is specific for (**Fig. 18**). This very versatile system allows us to overexpress, misexpress or silence particular genes of interest at various cells or tissues at different developmental stages in the fly [190, 191]. In addition, the expression level of the Gal4/UAS system can be controlled by changes in the temperature or by using the Gal80 repressor. In this case a temperature-sensitive mutant of the yeast Gal80 ($Gal80^{ts}$) regulates the activity of Gal4 [192, 193].

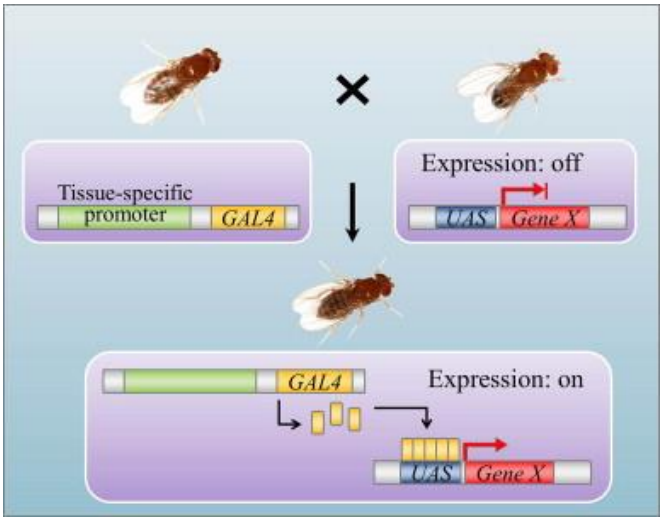

Figure 18. Schematic representation of the Gal4/UAS system

Parental fly lines carry either the Gal4 activator with a tissue- or cell-specific promoter or the *UAS* sequence with a particular gene of interest (*Gene X*). After crosses, these two components come together in the offspring: Gal4 specifically binds to *UAS*, and activates the expression of *Gene X* in a tissue- or cell-specific manner. (adapted from [194])

1. 3. 2. *Drosophila* as a model to study the nervous system and neuronal development

The nervous system of the fruit fly is complex and well-structured, however, in contrast to vertebrates where neuronal structures are usually represented by a large group of neurons, in *Drosophila* these structures are formed by a relatively low number of cellular elements. Therefore, changes in neuronal development or morphological alterations of the nervous system are well-traceable *in vivo*. Despite the fact that invertebrate and vertebrate neurons display organisational differences, their principal structures have been proposed to be homologous [195]. **Figure 19** shows a comparison of the invertebrate and vertebrate nervous systems.

There are two phases of *de novo* neurogenesis during development of which the first takes place in the embryo. Majority of the neurons formed during embryogenesis are maintained throughout development, however, many of them needs to be rearranged during metamorphosis. The second phase of neurogenesis starts during the larval life and becomes completed by the end of the pupal stage [196]. As a result of this, numerous developmental events can be examined throughout the whole life cycle of the flies; moreover, many different technics can be applied depending on the different stages of development. Together with these, the high number of genetic manipulation tools in *Drosophila* gives us the opportunity to search for mutations that cause morphological aberrations during neural development.

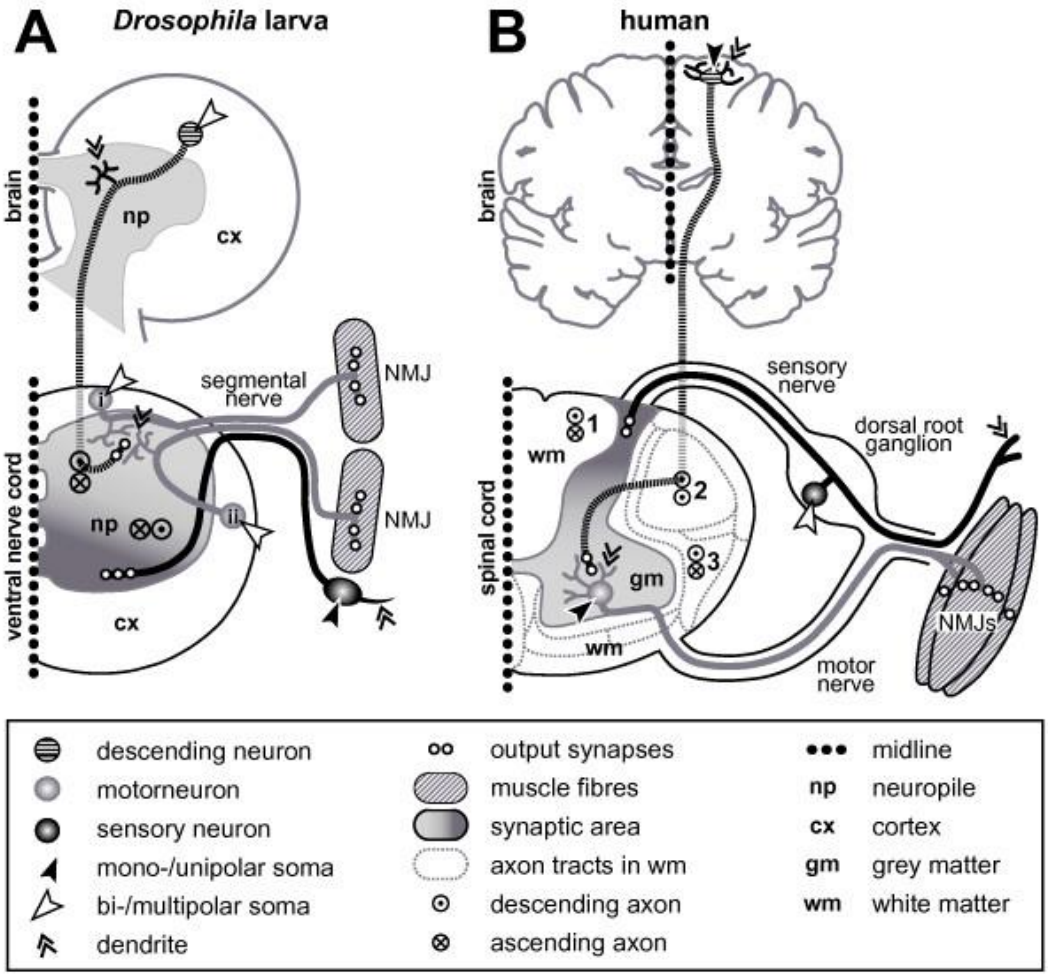

Figure 19. Comparison of the principal organisation of the invertebrate (*Drosophila*) and vertebrate (human) nervous systems

(**A**) shows half of the *Drosophila* larval brain and the ventral nerve cord (VNC), whereas, the adult human brain and the half of the spinal cord is presented in (**B**). Dotted lines indicate the midlines, symbols and abbreviations are described in the box above. Vertebrate sensory neurons are pseudo-unipolar and located within the dorsal root ganglia; after bifurcation of the neurites they grow both towards the central nervous system (CNS) and the periphery. In contrast, *Drosophila* sensory neurons are usually unipolar, located close to the sensory organs that they innervate and send axons towards the CNS. In *Drosophila*, the cell bodies of inter- and motoneurons are located in the cortex, outside the synaptic area (neuropile), whereas, cell bodies of comparable neurons of vertebrates are located in the synaptic area (gray matter). In vertebrates, ascending and descending axons project outside the synaptic area and form the white matter. In contrast, ascending and descending axons are located along the synaptic neuropile in *Drosophila*. (adapted from [197])

1. 3. 2. 1. The embryonic nervous system – a classic model for *in vivo* studies on axon growth and pathfinding

The *Drosophila* embryo is one of the most widely used and known *in vivo* systems to investigate axon growth and morphology. The embryonic nervous system can be divided into two parts: one is the central nervous system (CNS), that is composed of the ventral nerve cord (VNC) and the two brain lobes; whereas the other is the peripheral nervous system which comprises of the peripheral motor nerves and the sensory neurons. Extensive studies of the nervous system revealed that axonal projections display a stereotypical pattern in the embryo [198-202], out of which axonal tracts along the VNC (**Fig. 20 B**), peripheral motor nerves (**Fig. 21 A**) and axons of the peripheral sensory neurons are the typical subjects of morphological investigations. **Figure 20** shows the principal organisation of the embryonic CNS.

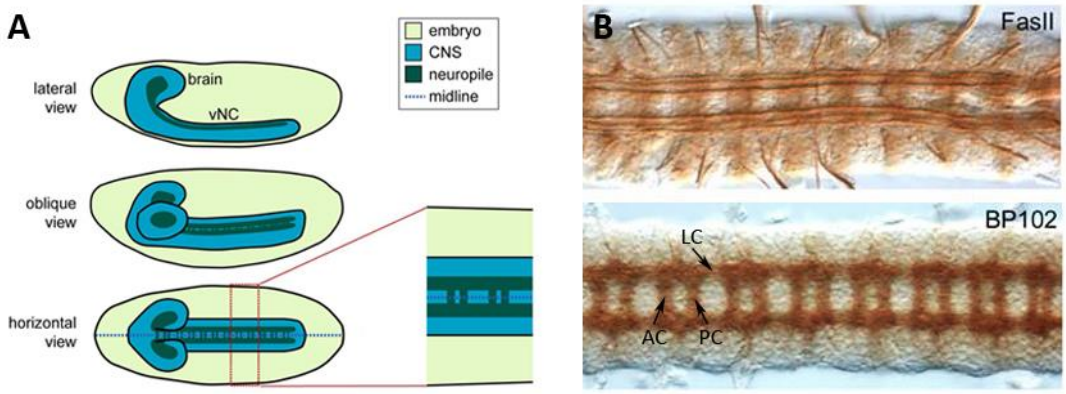

Figure 20. The embryonic central nervous system

(**A**) is a schematic representation of the CNS of a stage 16/17 embryo (modified image, from A. Prokop). The ventral nerve cord (VNC), together with the brain, is located at the midline of the embryo. The cortex of the VNC (blue) contains the cell bodies of the CNS neurons, whereas, axonal projections form the neuropile, a ladder-like structure along the VNC (dark green). (**B**) shows two typical antibody stainings to visualise axons in the VNC (modified image, from [203]). Fas II labels only a subpopulation of axonal fascicules in the embryonic nervous system: in the VNC it stains 3-3 parallel longitudinal tracts. BP102 labels all the axons of CNS neurons, showing the ladder-like structure of the neuropile composed of the

longitudinal connectives (LC) and the anterior and posterior commissures (AC and PC) in each segment.

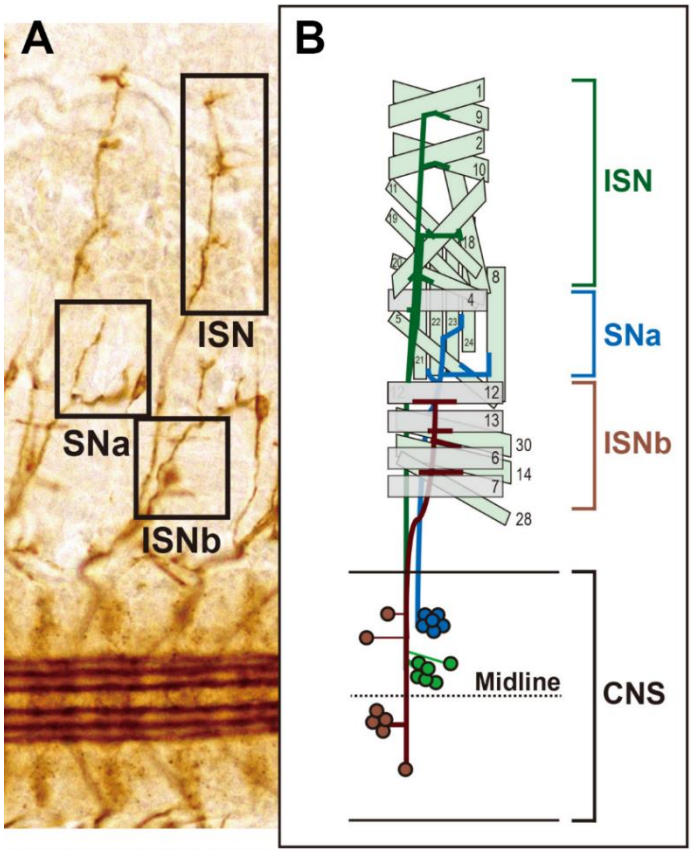

Figure 21. The organisation of the peripheral motor nerves

(**A**) The structure of the peripheral motor nerves is shown in a filleted preparation of a stage 16/17 embryo. Black rectangles indicate certain muscle fields that are innervated by the intersegmental nerve (ISN), the segmental nerve a (SNa) and the intersegmental nerve b (ISNb) motor nerves. In addition, longitudinal axon fascicles of the VNC (bottom) also can be seen in the image. (**B**) Schematic representation of the ISN, SNa and ISNb nerves. The axons of motor neurons form the peripheral motor nerves, while they leave the CNS, and innervate their target muscles along the whole hemisegment. Numbered quadrangles indicate the individual muscle fibers. (modified image, from [204])

In each hemisegment of the embryo muscle fibers are innervated by a particular motor nerve. These peripheral motor nerves display a complex but well-traceable structure in the embryo which can be easily visualised by FasII staining providing a

great model to observe alterations in axon growth and navigation. During embryonic development motor neurons first project into the synaptic neuropile to form dendrites at the dorsal region [197, 205]. From there, axons exit the neuropile and enter the peripheral branches of the motor nerves and grow towards their target muscles to form neuromuscular junctions. In this process each motor nerve innervates a specific muscle field of a hemisegment. The intersegmental nerve (ISN) navigate dorsally through the whole hemisegment to project to the dorsal and dorsolateral muscles, whereas the intersegmental nerve b (ISNb) separates from the main ISN bundle to form its own bundle and innervates the ventrolateral muscles. The segmental nerve a (SNa) also grows dorsally, passes the muscle field that is covered by the ISNb, and subsequently divide into two fascicles to innervate the lateral muscles (**Fig. 21**) [200, 206, 207].

Since axonal projections display precise stereotypical patterns in the embryonic VNC and in the peripheral motor nerves as well, both systems are suitable to study axon growth and pathfinding, and were used in this study. Morphological alterations of these axonal fascicles and nerves can be detected relatively easily, therefore the potential regulators of the guidance mechanisms during axonal advance can be identified.

1. 3. 2. 2. Ventral lateral neurons (LN_vs) in the adult brain, as an *in vivo* model to study axon growth

The adult *Drosophila* brain is a complex organ, consisting of a large number of neurons and different neuron types organised into a few dozens of higher neuronal structures. In order to study axon growth in the adult brain, we chose to investigate the ventral lateral neurons (LN_vs) which present a simple and stereotypical axonal pattern in the brain. LN_vs express the neuropeptide pigment-dispersing factor (PDF)

[208], and play an essential role in the regulation of the circadian clock and the locomotor activity of the adult flies [209-213]. The group of PDF-positive neurons is formed by a very small number of cells and can be divided into the two subgroups as small ventral lateral neurons (s-LN_vs) and large ventral lateral neurons (l-LN_vs) [214]. Both subgroups consist of 4-4 neurons in each hemisphere of the brain, although there is also a 5^{th} s-LN_v neuron which is PDF-negative.

The development of these neurons starts in the larva and finishes by the end of the pupal stage. During this process the axonal fascicle of the s-LN_vs projects dorsally, then turn towards the midline and form axonal terminals in the dorsal protocerebrum. Neurites of l-LN_vs bifurcate close to their origin and send fascicles to both the ipsilateral and the contralateral medullae. In order to reach the contralateral medulla, the l-LN_v neurites grow through the posterior optic tract (**Fig. 22**) [214, 215].

The small number of LN_vs and their simple and stereotypical axonal pattern allow us to study axon growth and guidance mechanisms at a high resolution. Furthermore, the morphology of LN_v axons can be visualised simply by immunostaining for the PDF neuropeptide, and thus, alterations in their axonal pattern can be detected accurately.

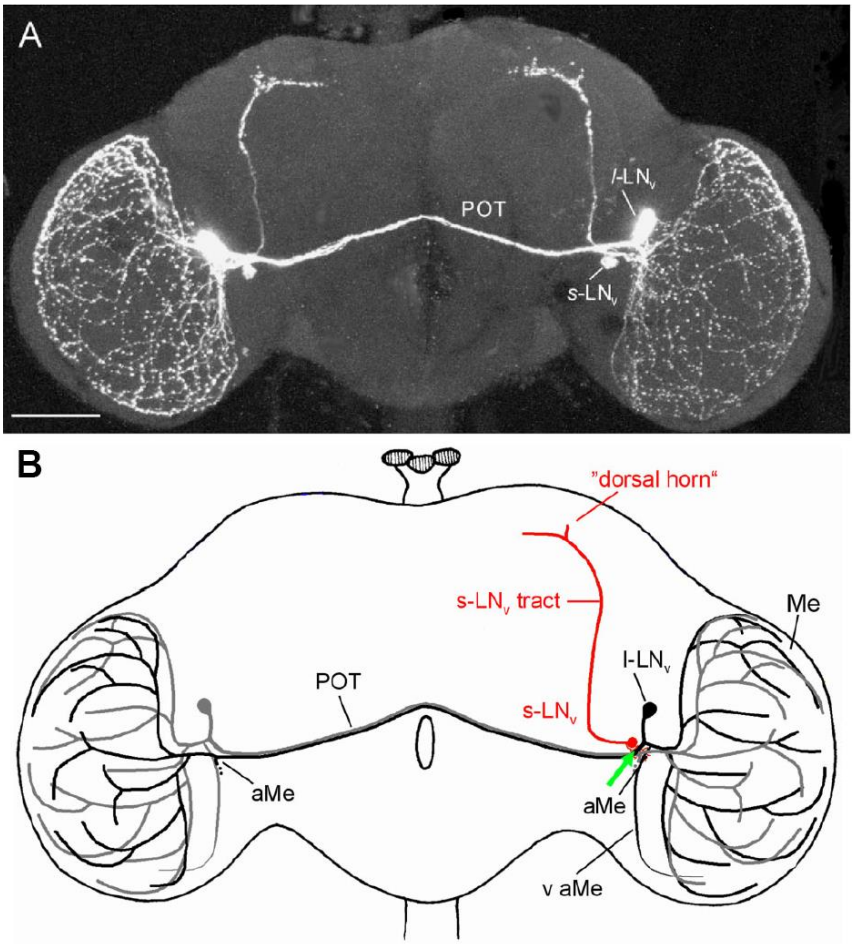

Figure 22. PDF-positive ventral lateral neurons in the adult brain

(**A**) shows both the small (s-LN$_v$) and the large (l-LN$_v$) ventral lateral neurons and their stereotypical axonal pattern in the adult *Drosophila* brain, visualised by anti-PDF immunostaining (adapted from [216]). (**B**) is a schematic representation of the LN$_v$ neurons (adapted from [215]). For simplicity, only 1 s-LN$_v$ neuron (red) and 1-1 l-LN$_v$ neurons (black and grey) from both hemispheres are presented. Following bifurcation, neurites of l-LN$_v$ neurons grow bi-directionally, one of them goes through the posterior optic tract (POT), to innervate both medullae (Me). Whereas, s-LN$_v$s project dorsally and form terminals in the dorsal protocerebrum. In addition, l-LN$_v$ neurons also have dendritic fascicles in the ipsilateral ventral accessory medulla (v aMe). The green arrow indicates a place in the accessory medulla (aMe) where the s-LN$_v$ and l-LN$_v$ neurons form putative synaptic connections between one another.

1. 3. 2. 3. Primary neuronal cell cultures from the *Drosophila* embryo

Drosophila primary neuronal cell cultures provide a great opportunity to study subcellular mechanisms of axonal growth. In this system, cytoskeletal elements including the dynamic properties of the actin and MT cytoskeleton, can be studied with high resolution, thus it allows us to investigate the role of potential cytoskeletal regulators downstream of the Wnt/PCP signalling pathway accurately.

Hanging-drop cultures of neuronal cells can be generated from stage 11 *Drosophila* embryos (detailed later in *Materials and methods*, chapter 3. 5.) in which several readouts are available to describe the state of the neuronal cytoskeleton [14, 217]. At standard temperature (26˚C) neurons can be studied in a broad time period in primary cell cultures. After 6 hours in culture, neurons are in an actively growing stage in which the dynamic changes of the actin and MT cytoskeleton are well detectable in the growth cone (GC), whereas in older cultures, for instance at 48h, neurons display a complex axonal arborisation and a mature morphology (**Fig. 23 A-C**) [14].

In cultured neurons many parameters of MTs and F-actin are quantifiable and serve as useful readouts. For example, the number, the length and the dynamics of filopodia provide information about F-actin dynamics, whereas the organisation of MTs in the GC reveals information about MT dynamics. GC morphology is another accessible readout which mainly represents the status of the actin-rich structures of the GC (**Fig. 23 D-G**). In addition, axon length reflects the growing capability of axons, mostly depending on MT dynamics [14].

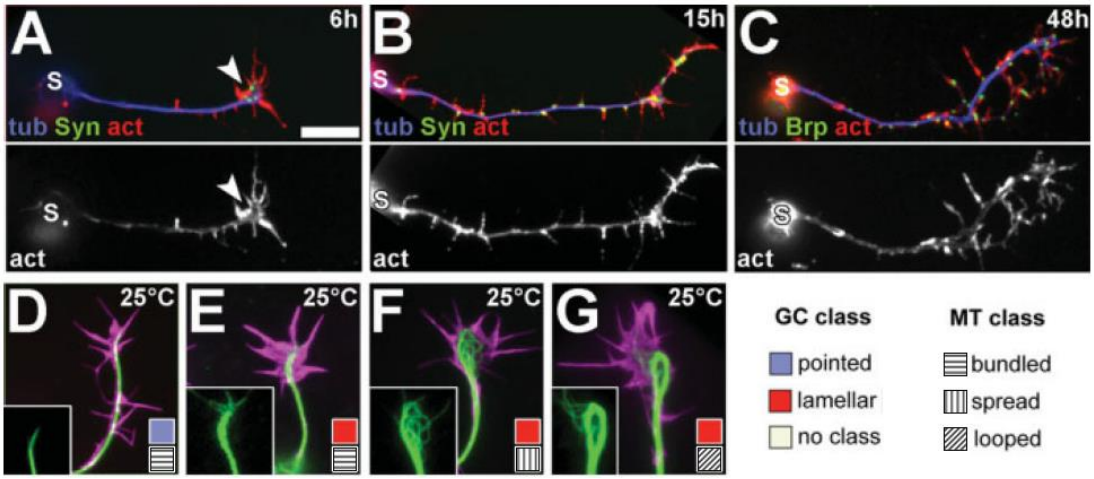

Figure 23. Neurons in *Drosophila* primary cell cultures

(**A-C**) Images of isolated single cultured neurons, grown at 25˚C for 6h, 15h and 48h. Neurons are stained against tubulin (tub), F-actin (act), and the presynaptic markers Synapsin (Syn) and Bruchpilot (Brp). S indicates the soma, white arrowheads point to the GC. Mature neurons (48H) present complex axonal arborisation, as well as many presynaptic sites, compared to young neurons (6h). (**D-G**) Show GCs labelled against tubulin (green) and F-actin (magenta). The classification of GCs and MTs is indicated by the colour code and the patterns on the right bottom. Pointed GCs (**D**) have only filopodia, whereas lamellar GCs (**E-G**) present both filopodia and extensive lamellipodia. In case of MTs, bundled (**D-E**), spread (**F**) and looped (**G**) classes are distinguished depending on the morphology of MTs in the GC. (modified image, from [14])

Primary neuronal cell cultures are also particularly useful to study MT and F-actin dynamics with live-cell imaging. For instance, by expressing a fluorescently tagged form of end-binding protein 1 (EB1), an MT plus end associated protein, MT polymerisation and depolymerisation events become well-traceable in cultured cells (**Fig. 24**). Accordingly, F-actin dynamics can be investigated with a similar method. For example, GFP-tagged versions of fascin (a bundling factor of F-actin) or Myosin II (that integrates into F-actin retrograde flow) are suitable to visualise filopodia and/or F-actin dynamics. In addition, different drugs with selective effects on MTs or actin (for example Nocodazole, taxol, Cytochalasin D and Latrunculin A) can be applied simply in the culture media, therefore it gives the possibility to study the differential role of cytoskeletal components in axon advance [14].

Together, all these features make *Drosophila* primary neuronal cell cultures a versatile model system to study many aspects of cytoskeletal changes in detail, which can contribute to better understanding of the principal mechanisms of cytoskeletal dynamics during axon growth. Furthermore, combined with the available genetic manipulation tools, this technic can help us to identify the members of the molecular machinery that is responsible for the regulation of cytoskeletal dynamics in neurons.

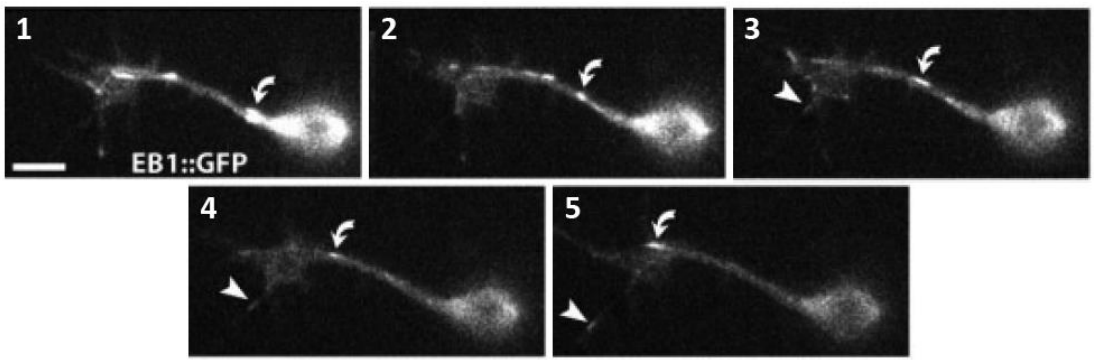

Figure 24. MT dynamics in cultured neurons

Primary cell cultures are suitable for investigating MT dynamics by expressing a GFP-tagged form of end-binding protein 1 (EB1::GFP) in cultured neurons during live-cell imaging. EB1::GFP comets can be seen in the sequence of images from a movie, representing anterograde movements of EB1::GFP puncta along the axon (curved arrows) and in a filopodium (arrowhead). Scale bar is 5 μm. (adapted from [14])

2. Aims

As it was described above, axon growth largely depends on the dynamic rearrangement of cytoskeletal elements in the GC. Although several cytoskeletal regulators have been identified in the recent years, it is still a key question what are those signalling pathways that gather guidance signals and activate the downstream regulators leading to cytoskeletal changes? Several studies demonstrated that Wnt/PCP signalling is involved in cytoskeletal remodelling [121-124], and that some members of the pathway play an important role in controlling axon growth during neuronal development (detailed in the *Introduction*, chapter 1. 2. 4.), however, their exact role remained largely elusive. Therefore, in this study our aim was to investigate the role of the Wnt/PCP signalling pathway in the regulation of neuronal cytoskeleton and to understand how this role contributes to axon growth, using the model organism *Drosophila melanogaster*.

In order to address these problems first we studied the localisation of the PCP proteins in the *Drosophila* embryonic nervous system, and next we asked whether their absence affects axon growth in the embryo. As another *in vivo* system, we also examined whether the PCP proteins are necessary for the stereotypical axonal development of the LN_v neurons in the adult brain. Since the LN_vs act as principal morning pacemakers of the fruit fly circadian clock [213, 218-221], the impact of reduced PCP function on the locomotor activity and the sleeping behaviour of the flies was also tested. Furthermore, as the subcellular function of the PCP proteins in neurons is largely elusive, we used primary neuronal cell cultures to study whether Wnt/PCP signalling controls the neuronal cytoskeleton. Finally, in order to identify a possible downstream effector of the Wnt/PCP signalling, we investigated the role of the formin DAAM in all the above described contexts.

3. Materials and methods

3. 1. Fly strains and genetics

Drosophila flies were kept and the crosses were made at 25˚C using standard fly food (containing corn flour, glucose, yeast and agar). We used the *Oregon R* wild type and w^{1118} fly strains as controls in our experiments. To study the expression of PCP proteins in neurons and in the nervous system several *in situ* EGFP-tagged lines were applied: *w; fmi-EGFP*, *w; fz-EGFP*, *w; EGFP-pk*, *w; P(acman)-stbm-EGFP* $stbm^{6}$, *yw* dsh^{V26}*; P(acman)-EGFP-dsh* and *w; P(acman)-EGFP-dgo* dgo^{380}. In case of Fmi, Fz and Pk the EGFP tag is inserted into the endogenous locus. For Stbm, Dsh and Dgo, the EGFP tag was integrated into the genome by using a P(acman) rescue construct. In addition, these lines also carry the appropriate mutant backgrounds to maintain normal gene dosage [222].

In order to investigate the role of core PCP proteins we used the following loss of function mutant alleles: fz^{K21}, fz^{R52}, $stbm^{6}$, dsh^{1}, *pk-sple*^{13}, pk^{30}, and fmi^{192}. The fz^{K21} and fz^{R52} alleles are amorphic alleles: fz^{K21} is associated with a chromosome inversion which impairs the function of the *fz* gene [223], while fz^{R52} is a nonsense mutation resulting in a truncated protein [224]. $stbm^{6}$ is a null allele, carrying a frameshift mutation that truncates most of the protein [140]. However dsh^{1} is a hypomorphic allele it is known to be a planar polarity null allele because the DEP domain of the protein, which is crucial in PCP signalling, is mutated [119, 141]. The *pk* locus expresses two alternatively spliced isoforms, these are the *pk* and *sple* (*spiny-legs*). *pk-sple*^{13} is a double mutant allele which deletes both the *pk* and *sple* isoforms, however, pk^{30} removes only the *pk* isoform [142, 225]. fmi^{192} is an X ray-induced null mutant allele [226].

In cases where the loss of function mutant alleles caused lethality in homozygosis the following marked balancer chromosomes were applied: *FM7 twist GFP*, *CyO twist GFP* and *TM3 twist GFP*. By using these balancers, we were able to collect homozygous mutant embryos to perform primary cell cultures.

In addition, the $DAAM^{Ex1}$ and $DAAM^{Ex68}$ loss of function mutant alleles were used to study the function of DAAM. The hypomorphic $DAAM^{Ex1}$ allele removes only the C-terminal end of the protein, while the null mutant $DAAM^{Ex68}$ allele is a bigger deletion, removing the C-terminal, the Diaphanous autoinhibitory domain and most of the FH2 domain of DAAM. [203] In some experiments, in order to reduce the level of maternal DAAM, homozygous $DAAM^{Ex1}$ females were crossed with $DAAM^{Ex68}/Y^{Dp(1;Y)Zs280}$ males to generate $DAAM^{Ex1}/DAAM^{Ex68}$ embryos in which maternal and zygotic *DAAM* functions are both impaired.

Furthermore, to investigate the role of DAAM in the regulation of microtubule dynamics in cultured neurons we used the *w⁻;elav-Gal4,UAS-EB1::GFP*, as control, and the $w^{-},DAAM^{Ex1}$*;elav-Gal4,UAS-EB1::GFP* strains. EB1 belongs to the family of proteins that are localised at the growing plus end of MTs (+TIPs), where they play a key role in controlling MT dynamics. In this case, EB1 is tagged with GFP and driven by the neuron-specific driver *elaV-Gal4*, therefore the dynamics of MT plus ends can be well-traceable in cultured neurons by this method.

3. 2. Embryo fixation, staining and dissection

3. 2. 1. Fixation

In order to collect stage 16 embryos, *Drosophila* flies were laying eggs for 4 hours and eggs were kept for 13 more hours at 25˚C. Following this, embryos were

dechorionised in 50% bleach for 2 min, washed in distilled water and transferred into a glass bottle with fixing solution which is a mix of 3ml heptane (Molar Chemicals, 06830), 2.7ml PBS and 300µl 37% formaldehyde (MERCK, 103999). After 20 min of fixation the bottom aqueous solution was removed. In the next step 3ml methanol was added, then embryos were vortexed for 45 sec and transferred from the bottom of the glass bottle into a new Eppendorf and washed with methanol. At this step the embryos can be stored in methanol at -20˚C.

3. 2. 2. Whole mount embryo staining

Prior to staining, embryos were rehydrated with washing steps in PBS with 0.1% Triton X-100 (PBT), then blocked for 1 hour at room temperature in PBT-BSA [0.2% Bovine Serum Albumin (Sigma, A2153) diluted in PBT]. Primary antibody staining with the anti-Fasciclin II antibody (1D4, 1:500, mouse, DSHB) was done overnight at 4˚C in blocking buffer. After washing steps in PBT embryos were incubated with biotin (1:500, anti-mouse, Vector Laboratories) secondary antibody for 90 minutes at room temperature, then washed for 1 hour in PBT. In the meantime, 3,3'-Diaminobenzidine (DAB, Sigma-Aldrich, D4168) and Urea-H_2O_2 (Sigma-Aldrich, D4168) solutions were prepared: 1 tablet DAB in 500µl H_2O and 1 tablet Urea-H_2O_2 in 500µl H_2O. The next step was a 30 min incubation with ABC mix at room temperature. The ABC mix (3µl buffer A and 3µl buffer B in 300µl PBT / genotype) needs to be prepared previously and stand for at least 30 minutes before use. Following washing steps in PBT for 1 hour at room temperature again, embryos were transferred to a well-plate and PBT was removed form embryos as much as possible. Then DAB and Urea-H_2O_2 solutions were mixed in 1:1, this mix was added to embryos and the reaction was monitored under dissection microscope. When the reaction was complete 1 ml PBT was added to stop the reaction, embryos were transferred to a new Eppendorf and further washes of PBT were applied for 1 hour at least.

3. 2. 3. Fluorescent staining

Similarly to the normal whole mount embryo staining, embryos were rehydrated in PBT but then blocked in PBS-BT [PBT with 0.2% BSA and 0.02% Na-azid (Reanal)] for 1 hour at room temperature. Overnight incubation with primary antibodies, anti-GFP (1:1000, rabbit, Invitrogen) either with BP 102 (1:500, mouse, DSHB) or anti-Fas II (1D4, 1:500, mouse, DSHB), was done at 4˚C in blocking buffer. After washing steps in PBT, secondary staining was done for 2 hours at room temperature using the corresponding Alexa-488 (1:600, anti-rabbit, Invitrogen) and Alexa-546 (1:600, anti-mouse, Life Technologies) antibodies, and finished by washes in PBT again.

3. 2. 4. Embryo dissection

All stainings were followed by a mounting step in glycerol:PBS (1:1), and stage 16 embryos were selected based on the morphology of the embryonic VNC. In cases where it was necessary VNCs were dissected to remove any other tissue material of the embryo in order to achieve better quality microscopic images.

To examine the peripheral motor nerves, we prepared embryo fillets: mounted embryos were stuck to a slide with a very small amount of glycerol:PBS (1:1), cut in the ventral midline by using insect pins and then laid out on the surface of the slide. Finally, the embryonic inner organs and tissues were gently removed.

3. 3. Adult brain dissection and staining

Adult *Drosophila* males were collected for one day and kept in fly vials at room temperature for three more days or one more week before dissection. In one batch,

15-20 adult brains per genotype were dissected in cold PBS, and fixed in 4% PFA (diluted in PBS) at room temperature for 20 min. A short movie, showing the method of adult brain dissection, is available at the following link: https://www.youtube.com/watch?v=u15xNrvNkPM. After washes in PBT, brains were blocked in PBS-BT for 1 hour, stained with primary antibodies overnight at 4˚C, and then washed in PBT again. Secondary antibodies were also applied overnight at 4˚C, and following washing steps in PBT, brains were mounted in glycerol:PBS (1:1). We used the PDF C7 primary antibody (1:200, mouse, DSHB) and the corresponding Alexa-546 coupled secondary antibody (1:600, anti-mouse, Invitrogen) for immunostaining. These antibodies were diluted in PBS-BT, and 200µl per genotype was added to the brains.

3. 4. Measurement of locomotor activity of the adult flies

Flies were reared on standard fly food at 25˚C with 12h light – 12h dark cycles (LD). To measure activity and sleep behaviour, upon eclosion of the progeny, 1-5 days old adult males were collected and were housed in glass tubes containing food with 5% sucrose (Sigma-Aldrich, S9378) and 2% bacto agar (Becton Dickinson, 214010). The locomotor activity was measured by the TriKinetics *Drosophila* Activity Monitor (Trikinetics Inc. USA) system in LD for 7 days, however, the first day of the recording was not analysed later in order to make sure all the flies are synchronised and entrained for the same conditions. In this system, the activity of individual flies is tracked by an infrared beam which detects every time when the fly crosses the way of the infrared light while moving in the glass tube. Afterwards, the number of counts is collected by an interface unit: this summarises the data depending on the experimental situation and sends it to a personal computer. In our case, the activity

was recorded by 1-min bins, and the sleep state was defined as 5 contiguous minutes of inactivity. The obtained data was analysed and charted by using the ShinyR-DAM program [227]. **Figure 25** shows a typical experimental setting to measure *Drosophila* locomotor activity.

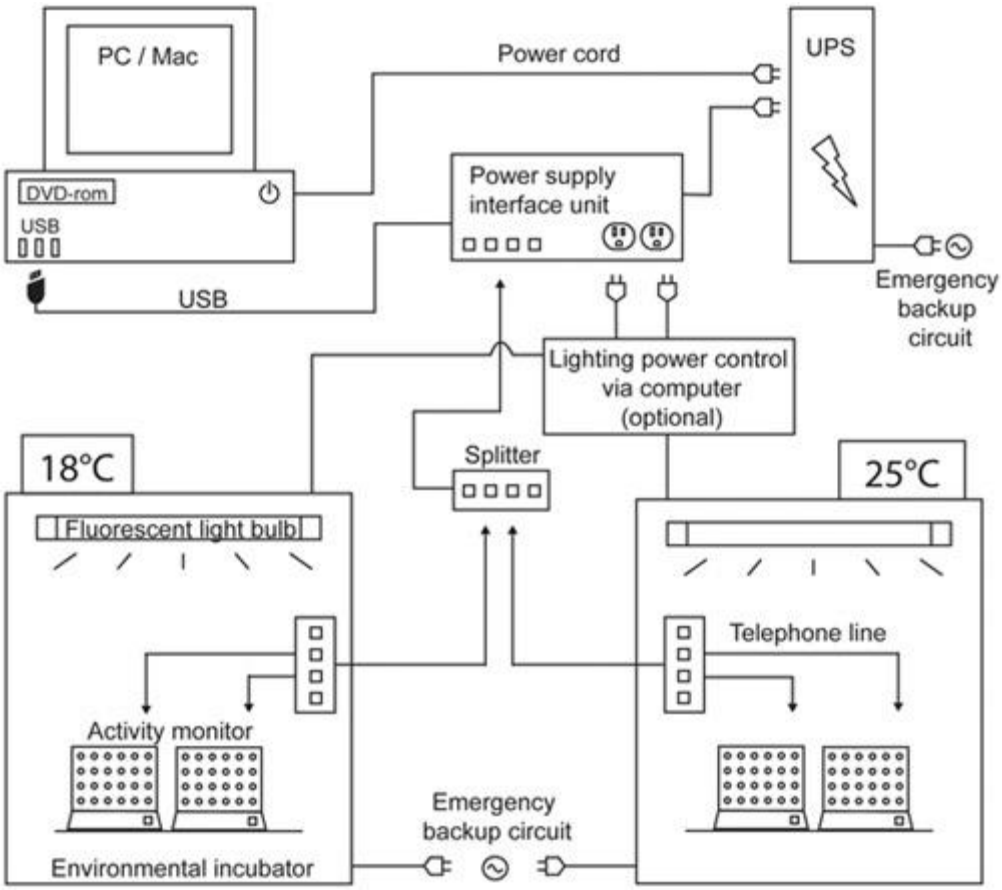

Figure 25. Components of the *Drosophila* locomotor activity data collection system
Activity monitors are housed inside incubators that control the temperature, humidity and lightning during the experiment. Monitors are connected to the Power supply interface unit which collects the locomotor activity counts of the flies and then sends this data to a dedicated computer to record. If available, all electrical appliances are connected to the emergency backup circuits in order to avoid interrupted monitoring during the experiment. (adapted from [228])

3. 5. Primary cell cultures and immunohistochemistry

3. 5. 1. The preparation of primary cell cultures

To perform primary neuronal cell cultures two different mediums were prepared first. To make the neuro-culture medium fetal bovine serum (Gibco, 10270) was mixed with fresh Schneider`s *Drosophila* medium (Life Technologies, 21720024) in a ratio 1:4, filtered with 0.22µm bacterial filter (Millex) and kept in dark at 26˚C for 3 days to make sure it is not contaminated, then 10µl of 10mg/ml insulin (Sigma-Aldrich, I0516) was added and pH was set to 6.8-6.9.

For dispersion media 30ml 10x Hanks' Balanced Salt Solutions (without calcium and magnesium, phenol red; Life Technologies, 14180046) was mixed with 3 ml penicillin-streptomycin solution (Life Technologies, 15140122), 0.01g phenylthiourea (Sigma-Aldrich, P7629) and solved in 167ml autoclaved distilled water, and then filtered. To make dispersion media freshly, 0.001g Collagenase (Type 1; Worthington, LS004214) and 0.005g Dispase II (Roche, 04942078001) was solved in 1-1 ml of this solution (37˚C, 30 min), mixed and filtered again.

Stage 11 *Drosophila* embryos were used to generate primary neuronal cell cultures. 24-30 embryos per genotype were selected (8-10 embryos per slide, 3 slides per genotype) using UV binocular microscope. Stage 11 embryos can be selected by a specific auto-fluorescence pattern of the embryo (**Fig. 26**).

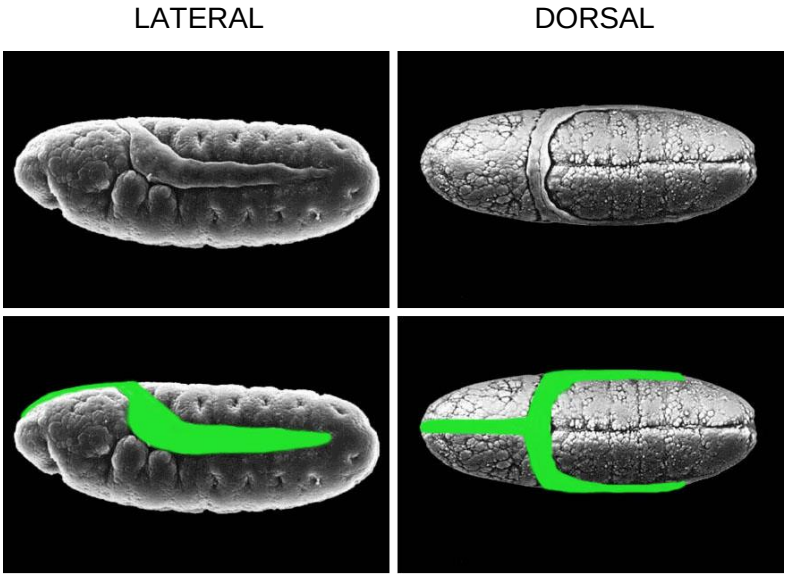

Figure 26. Lateral and dorsal view of a stage 11 embryo
The auto-fluorescence pattern of the embryo, which is used for selection, is shown in green.

First, the embryos were treated with 50% bleach for 30 seconds to remove the chorion, sterilised with 70% ethanol for 15-20 seconds and washed in 100µl sterile neuro-culture medium. In the next step the medium was changed to 100µl dispersion medium, then the embryos were gently homogenised with autoclaved plastic pellet pestles (Kimble-Chase, 749521-1500) and incubated for 3.5 minutes at 37˚C. After stopping the dispersion reaction by adding neuro-culture medium (200µl), the homogenised samples were centrifuged for 5 minutes at 900 g at room temperature and eventually re-suspended in the final volume of sterile neuro-culture medium (90µl per genotype). 30µl of cell suspensions were placed in special culture chambers (3 per genotype), covered with sterile coverslips (previously treated with acetone), and kept as hanging drop cultures facing upside-down with the coverslip. After 2 hours the chambers were turned back and further incubated up to 6 hours and 2 days at 26˚C. **Figure 27** shows the making of hanging drop cultures and the used culture chambers.

For live-imaging, cultured neurons were grown on 0.5 mg/ml Concavalin A (Sigma-Aldrich, C2010) coated coverslips for 6 hours at 26˚C, then medium was changed to fresh neuro-culture medium and cells were imaged without fixation and staining.

For treatments with the microtubule destabilising drug Nocodazole, neurons were plated onto coverslips coated with 0.5 mg/ml Concanavalin A and kept for 12 h at 22˚C. After 12 h, neurons were treated with either Nocodazole or vehicle for further 4 h at 22ºC. Dilutions of Nocodazole (100 uM, Sigma) in Schneider's medium were prepared from stock solutions in dimethyl sulfoxide (DMSO). For controls, equivalent concentrations of DMSO were diluted in Schneider's medium.

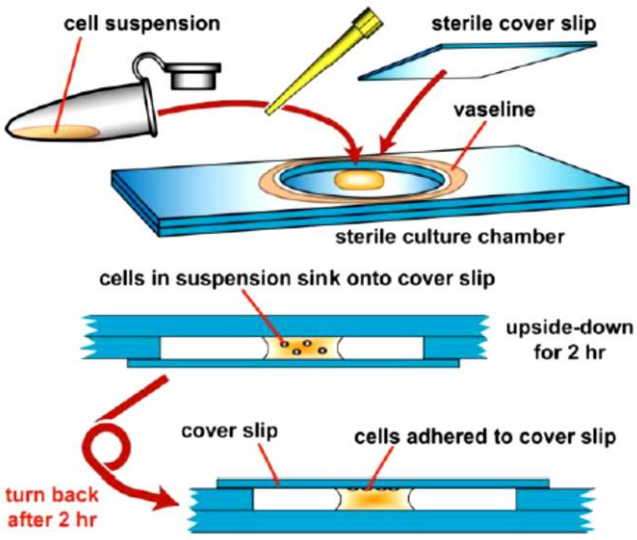

Figure 27. The preparation of hanging drop cultures (adapted from [229])
Culture chambers are made of two glass slides, stacked together, with a whole in the middle of one of them. Homogenised cell suspension is placed in the middle of the chamber and covered with a coverslip (vaseline is used in order to make the sealing air-tight). In the first 2 hours, culture chambers are placed upside-down to let the cells adhere on the surface of the coverslip. Following this, chambers are turned back and cells are further incubated.

3. 5. 2. Staining of primary cell cultures

After incubation cultured neurons were fixed in 4% paraformaldehyde (PFA) in 0.05 M phosphate buffer (pH 7-7.2) for 30 min at room temperature, then washed in PBS with 0.3% Triton X-100 (PBT). Overnight incubation in primary antibodies was done in PBT without blocking reagents at 4˚C; and the following primary antibodies were used: anti-tubulin (1:1000, mouse, Sigma-Aldrich), anti-synaptotagmin (1:1000, rabbit, Sigma-Aldrich). Following washing steps in PBT, neurons were incubated for 1.5 hours at room temperature in PBT using the corresponding FITC- and Cy3-conjugated secondary antibodies (1:100, Jackson Immuno Research). F-actin was stained with TRITC-conjugated Phalloidin (1:200, Sigma-Aldrich); Phalloidin is a toxin that specifically binds to F-actin. Before mounting, neurons were washed in PBT again and finally, the fixed and stained cultures were mounted using Vectashield medium (Vector Laboratories, H-1000).

3. 6. Documentation and data analysis

Images of neurons in primary cell cultures were taken using a QImaging Retiga 3000 Monochrome camera mounted on Nikon Eclipse 90i fluorescent microscope. Confocal images of adult brains, and time lapse movies of cultured cells for live imaging (45 frames with 2000ms intervals) were done using a 3i Marianas Spinning Disk Confocal microscope and a Hamamatsu Orca-Flash 4.0 Digital CMOS camera. Confocal images of embryos were captured on an Olympus FV1000 LSM microscope.

Microscopic image analysis, quantification and measurements were done in Image J software. To analyse MT dynamics, the Fiji plugin called Manual Tracking was used to trace trajectories of individual EB1::GFP comets and to calculate MT growth

velocity. Statistical analysis was done in GraphPad Prism 8. In the locomotor activity and sleep measurements the experimental data was obtained from the ShinyR-DAM program as mean+SEM, and further analysed in GraphPad Prism 8.

4. Results

4. 1. The expression pattern of the core PCP proteins in the embryonic nervous system

4. 1. 1. PCP proteins, except Dgo, are present in the ventral nerve cord

In order to investigate the *in vivo* function of the core PCP proteins in axon growth and guidance, first we examined the *Drosophila* embryo, particularly the expression of the PCP proteins in the embryonic nervous system. To this end, we used several fly lines that carry *in situ* EGFP-tagged forms of the PCP proteins, such as *EGFP-dgo*, *EGFP-pk*, *fz-EGFP*, *stbm-EGFP*, *EGFP-dsh* and *fmi-EGFP* [222]. In order to examine whether PCP proteins are expressed in the embryonic CNS, we applied BP102 staining to label all the axons in the VNC of stage 16 embryos. These axons form the neuropile which shows a ladder-like structure along the VNC, composed of the longitudinal connectives and the anterior and posterior commissures in each segment (**Fig. 28 A**). We found that Pk and Dgo cannot be detected in the VNC axons, whereas Fz, Stbm, Dsh and Fmi show a significant expression along the neuropile (**Fig. 28**).

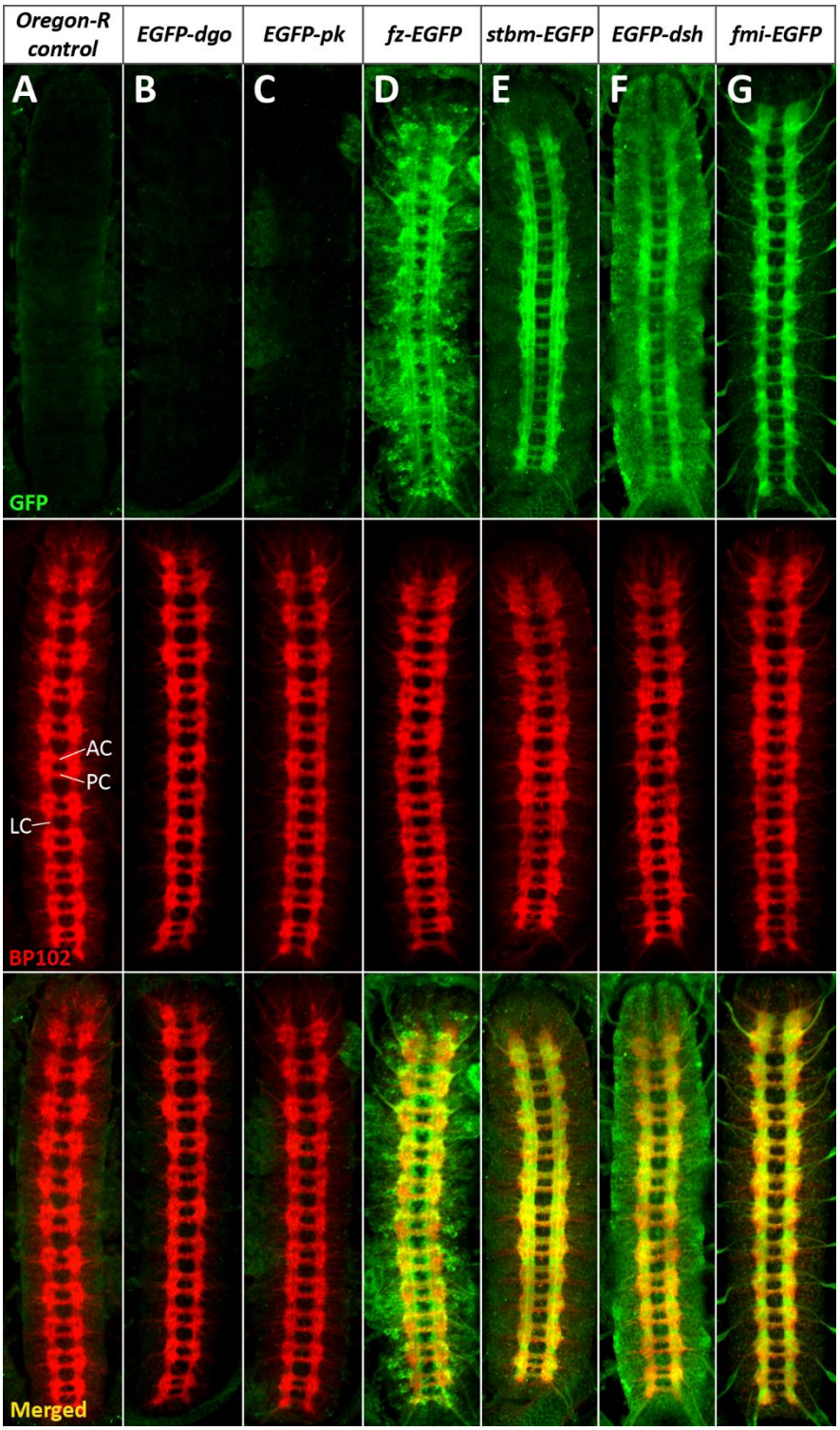

Figure 28. The expression of PCP proteins in the embryonic VNC

(**A**) Representative image of a wild type VNC of a stage 16 embryo stained with anti-GFP and BP102 antibodies; up is anterior. BP102 labels the neuropile, a ladder-like structure along the VNC, which is made up of longitudinal connectives (LC), anterior commissures (AC) and posterior commissures (PC). (**B-G**) Images of embryos showing the localisation of the PCP proteins in the embryonic VNC. (**B-C**) Dgo and Pk cannot be detected in the neuropile, whereas (**D-G**) Fz, Stbm, Dsh and Fmi exhibit strong expression in the VNC axons. (*Oregon-*

R, n=26; *EGFP-dgo*, n=17; *EGFP-pk*, n=20; *fz-EGFP*, n=23; *stbm-EGFP*, n=21; *EGFP-dsh*, n=20; *fmi-EGFP*, n=22. The n values indicate the number of examined embryos.)

Interestingly, Fz, Stbm, Dsh and Fmi display differences in their localisation in the VNC. Dsh and Fmi show a homogenous expression both in the longitudinal tracts and the commissures (**Fig. 28 F-G**). By contrast, Fz and Stbm exhibit a longitudinal tract pattern which is less uniform as compared to Dsh or Fmi, and it is partly similar to the pattern that can be revealed by Fas II staining. Fas II labels only a subpopulation of axonal fascicules in the embryonic nervous system by staining 3-3 parallel running longitudinal tracts in the VNC (**Fig. 29 A**). We found that, Fz and Stbm partially co-localize with these longitudinal fascicles (**Fig. 29**). However, in contrast to FasII, Fz and Stbm also stain the commissural axons crossing the midline.

In spite of that Pk displays no expression in the neuropile it occurs to be enriched in the neuronal cell bodies of the VNC. **Figure 30** shows a ventral plane of the VNC which contains the cell bodies of the neurons that send projections to form the neuropile. In contrast to the control, Pk forms aggregates in this plane (**Fig. 30 B**-**B'**) suggesting that this protein is present, most likely intracellularly, in the neuronal cell bodies.

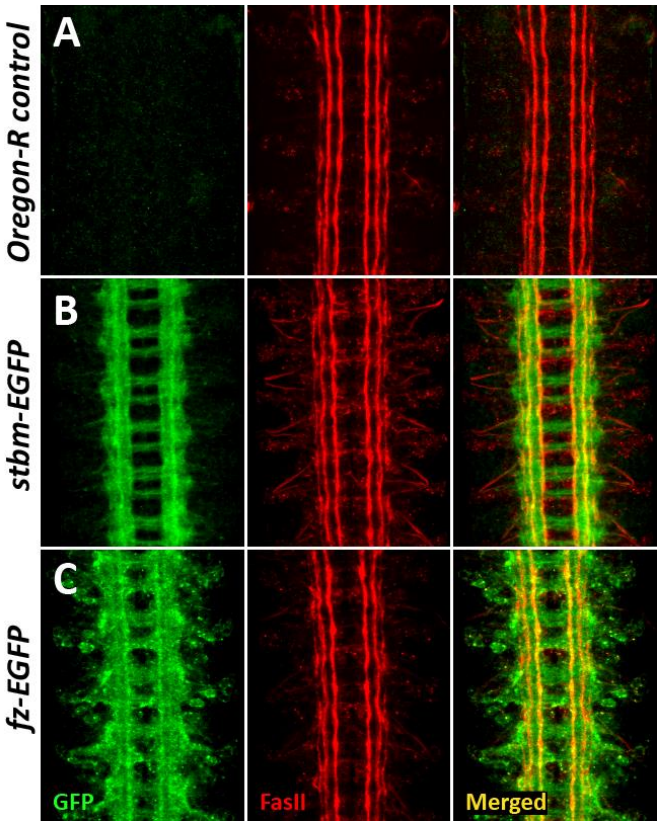

Figure 29. Fz and Stbm partially co-localize with the longitudinal axon tracts in the VNC
(**A-C**) Dissected VNCs of stage 16 embryos stained with anti-GFP and anti-FasII antibodies; up is anterior. (**A**) Section of a wild type VNC showing the 3-3 longitudinal axon fascicles in red. (**B**) Stbm co-localizes with the middle and the innermost fascicles, whereas (**C**) Fz accumulates in the innermost fascicles (indicated by white arrowheads). Both proteins are present in the commissures as well. (*Oregon-R*, n=24; *stbm-EGFP*, n=23; *fz-EGFP*, n=21. The n values represent the number of studied embryos.)

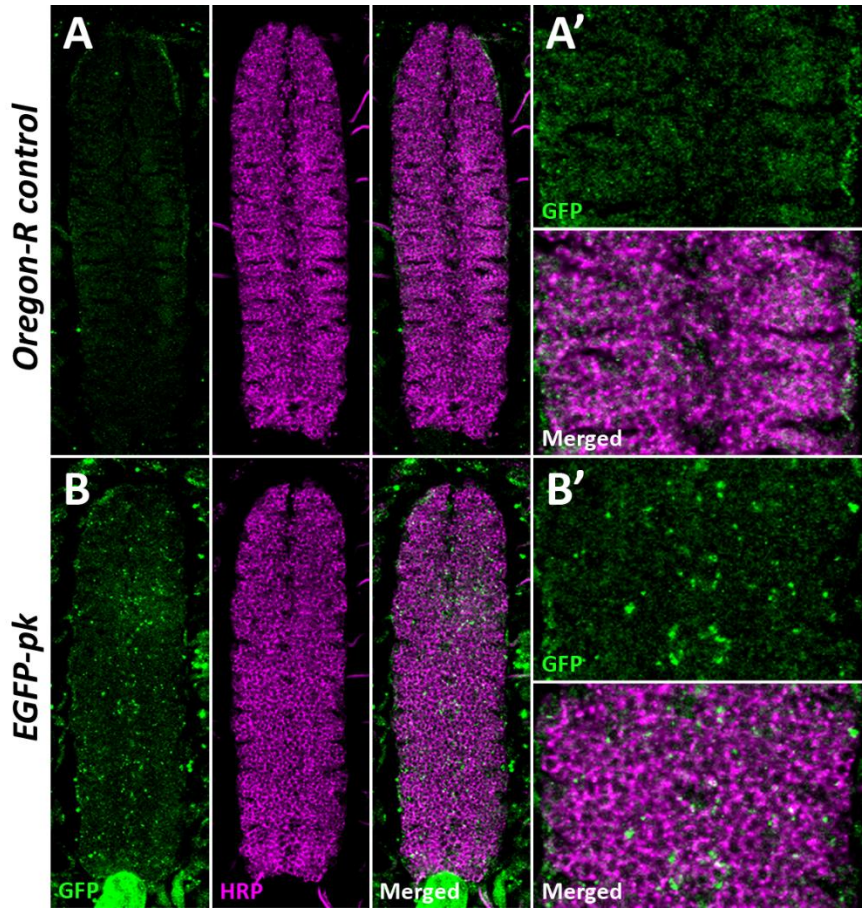

Figure 30. Pk forms aggregates in the cell bodies of VNC neurons

(**A**) Ventral plane of a wild type VNC stained with anti-GFP and anti-HRP antibodies, where HRP staining labels the neuronal cell bodies (magenta); up is anterior. (**B**) Anti-GFP staining reveals aggregates of Pk in this plane, most likely in the neuronal cell bodies. (**A'-B'**) Enlarged sections of the control and *EGFP-pk* VNCs. (Number of the examined embryos: *Oregon-R*, n=24; *EGFP-pk*, n=23)

4. 1. 2. Expression of the PCP proteins in the peripheral ISNb nerve

Subsequently, we investigated the localisation of the PCP proteins in the peripheral nervous system. In each hemisegment of the embryo muscle fibers are targeted by a particular motor nerve: the ISN, SNa and ISNb motor nerves project to the dorsolateral, lateral and ventrolateral muscles where they form neuromuscular junctions to innervate them. Besides the longitudinal axon tracts in the VNC, Fas II staining also reveals the structure of these peripheral motor nerves. Therefore, by

using stage 16 embryos that carry the previously described *in situ* EGFP-tagged forms of the PCP proteins, it is possible to detect whether PCP proteins are present in any of these nerves.

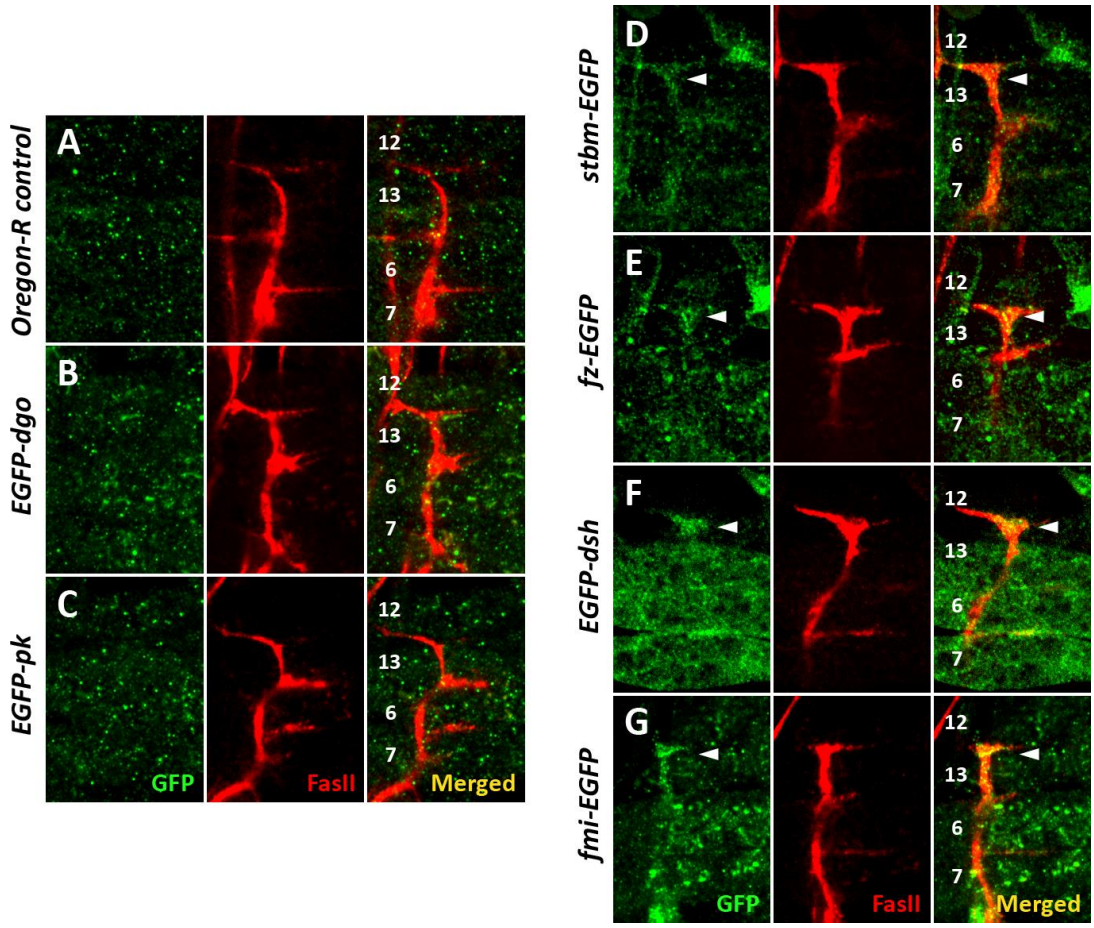

Figure 31. The expression of PCP proteins in the ISNb nerve

(**A-G**) Confocal images of the ISNb nerve in stage 16 embryos (fillet preparations) stained with anti-GFP and anti-FasII antibodies; up is dorsal, left is anterior. White numbers demonstrate the 12, 13, 6 and 7 ventrolateral muscles that are innervated by the ISNb. Compared to the control, (**D-G**) Stbm, Fz, Dsh and Fmi are present in the ISNb (white arrowheads), whereas (**B-C**) Dgo and Pk cannot be detected. Interestingly, Stbm and Fz show a weaker expression in the ISNb nerve than Dsh and Fmi. (*Oregon-R*, n=22; *EGFP-dgo*, n=15; *EGFP-pk*, n=19; *stbm-EGFP*, n=20; *fz-EGFP*, n=20; *EGFP-dsh*, n=19; *fmi-EGFP*, n=18. The n values indicate the number of embryos that were investigated.)

We found that the PCP proteins exhibit a similar expression pattern in the peripheral ISNb nerves as in the VNC axons: Dgo and Pk cannot be detected, whereas Stbm, Fz, Dsh and Fmi are present in these nerves. Interestingly, in comparison to our results from the embryonic VNC where all four proteins are strongly expressed in the neuropile, Stbm and Fz exhibit a weaker expression in the ISNb nerves than Dsh and Fmi (**Fig. 31**).

4. 2. PCP proteins have an impact on embryonic axon growth and guidance

After we saw that most PCP proteins are present in the embryonic VNC and in the peripheral motor nerves, we investigated whether these proteins affect axonal growth or guidance *in vivo* in the embryo. To this end we used several loss of function mutant alleles of the PCP proteins and examined their effect in stage 16 embryos. $stbm^{6}$, pk^{30} and dsh^{1} are homozygous viable alleles, of which $stbm^{6}$ is an amorphic allele [140], whereas pk^{30} and dsh^{1} are hypomorphic alleles. Although, pk^{30} deletes only one isoform of the *pk-sple* gene, we used this allele in our experiments since it was found to be neuron-specific in the mushroom body [177]. Despite the fact that dsh^{1} is a hypomorphic allele, it is considered to be a PCP-specific null mutant since the DEP domain of Dsh, which is crucial for PCP signalling, is mutated in this allele [119, 141]. fmi^{192} is a null mutant allele [226], and although it causes larval lethality, it is possible to collect homozygous embryos from a balanced fly stock and study its effect in the embryonic nervous system. In case of Fz we used the trans-heterozygous $fz^{K21/R52}$ combination in our experiments. fz^{K21} and fz^{R52} are null mutant alleles, however both are known to carry second site lethal mutations as well ([223, 224] and additional information from FlyBase). The trans-heterozygous combination is viable, thus this

has been chosen for our analysis in order to avoid the effect of the second site mutations. (The molecular nature of the above mentioned loss of function mutant alleles is described in *Materials and methods*, chapter 3. 1.)

Interestingly, we were able to identify changes in the VNC only in two cases. In *stbm*^{6} mutant embryos longitudinal fascicles, visualised by Fas II staining, show an increased number of discontinuities in which all 3 axon fascicles display gaps, at least on one side of the VNC (**Fig. 32 B**). In a few cases it occurs on both sides. In addition, *fmi*^{192} mutant embryos exhibit axon guidance defects characterized by an impaired midline crossing phenotype as revealed by anti-FasII staining (**Fig. 32 C**). Other PCP mutants showed no changes in the axonal fascicules of the VNC as compared to the control.

To further investigate this subject, the peripheral motor nerves of the embryos were analysed as well. We found that one type of these nerves, the ISNb, shows a strong axon stalling phenotype in some PCP mutants. In contrast to the wild type, where the ISNb innervates ventrolateral muscles 12, 13, 6 and 7, in *dsh*^{1} and *fmi*^{192} mutant embryos it fails to project to its target muscles, resulting in an early stalling (**Fig. 33**). These data are in line with our previous findings, since Dsh and Fmi showed a strong expression in the ISNb nerve. In addition, in *fmi*^{192} mutants the ISNb appears to be much thinner than in the wild type.

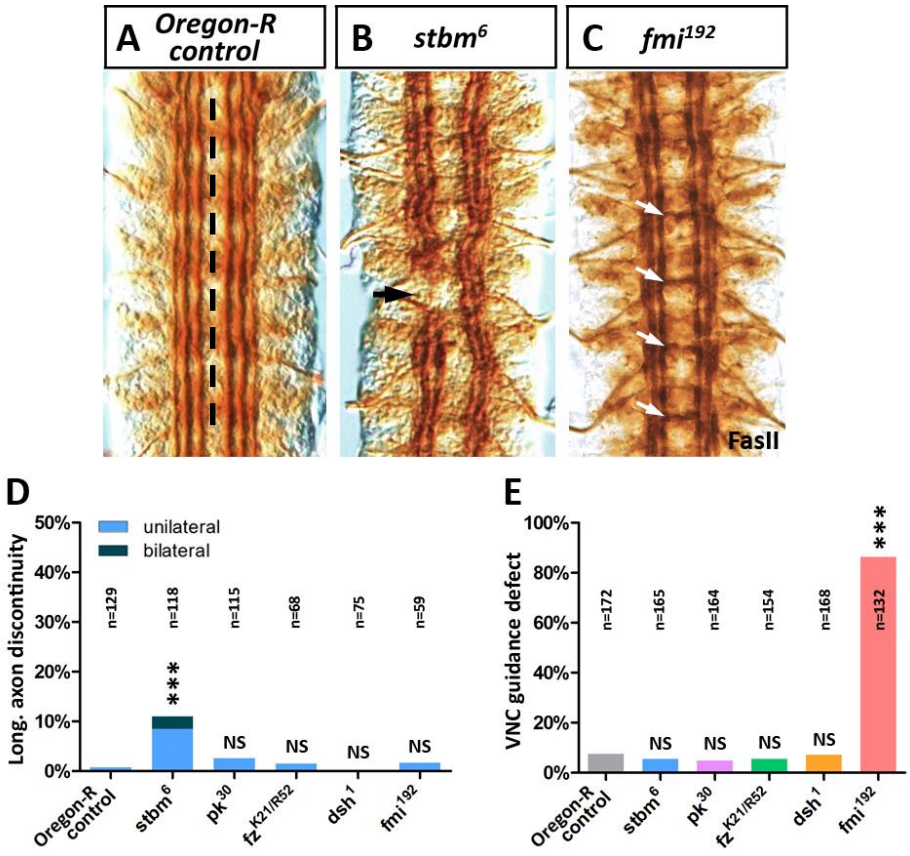

Figure 32. Phenotypes of the *stbm^{6}* and *fmi^{192}* mutant embryos in the VNC

(**A-C**) Dissected VNCs of stage 16 embryos stained with anti-Fas II antibody (**A**) Representative image of a wild type VNC showing the parallel longitudinal axonal tracts. The dashed line indicates the midline of the VNC; up is anterior. (**B**) VNC of a *stbm^{6}* mutant embryo; the black arrow points to the axonal discontinuity that can be seen in these mutants. (**C**) Image of a *fmi^{192}* mutant VNC, showing its axonal misguidance phenotype in several segments, indicated by the white arrows. (**D**) The number of embryos with axonal discontinuities in the VNC significantly increases in the loss of Stbm. These gaps occur mostly unilateral, but in some cases bilateral as well. Data sets were compared by Kruskal-Wallis test first (P<0.0001), then P values were calculated by Dunn's multiple comparisons tests: *Oregon-R* vs. *stbm^{6}*, P<0.0001; *Oregon-R* vs. *pk^{30}*, P>0.9999; *Oregon-R* vs. *fz$^{K21/R52}$*, P>0.9999; *Oregon-R* vs. *dsh^{1}*, P>0.9999; *Oregon-R* vs. *fmi^{192}*, P>0.9999 (multiplicity adjusted P values). *** P≤0.001; NS, not significant. The n values represent the number of embryos in each genotype. (**E**) The diagram shows the number of VNC segments with misguided axonal formations, which strongly increases in *fmi^{192}* mutants. To compare data sets, Kruskal-Wallis test was performed (p<0.0001), and P values were calculated by Dunn's multiple comparisons tests: *Oregon-R* vs. *stbm^{6}*, P>0.9999; *Oregon-R* vs. *pk^{30}*, P>0.9999; *Oregon-R* vs. *fz$^{K21/R52}$*, P>0.9999; *Oregon-R* vs. *dsh^{1}*, P>0.9999; *Oregon-R* vs. *fmi^{192}*, P<0.0001 (multiplicity adjusted P values). *** P≤0.001; NS, not significant. The n values indicate the number of VNC segments examined in each genotype.

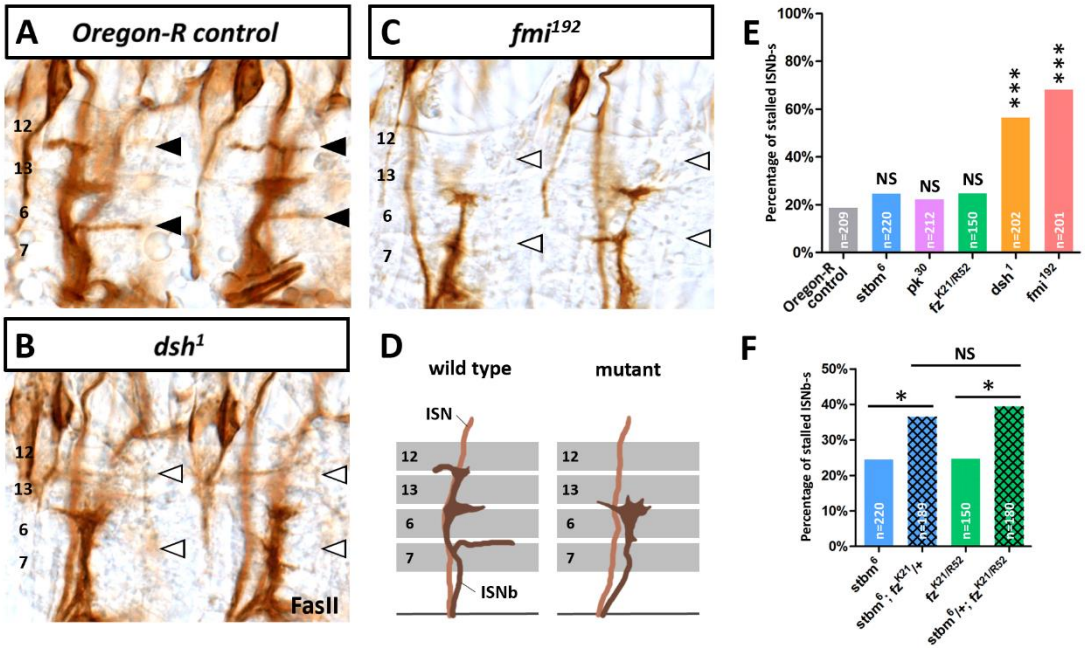

Figure 33. ISNb nerves show an early stalling phenotype in PCP mutants

(**A-C**) Fillet preparations of stage 16 embryos stained with anti-Fas II antibody to label the structure of the ISNb nerve; up is dorsal, left is anterior. (**A**) Image of a wild type ISNb: black arrowheads show the projections that innervate the 12, 13, 6 and 7 ventrolateral muscles. (**B-C**) ISNb nerves fail to innervate their target muscles, indicated by the empty arrowheads, in *dsh*^{1} and *fmi*^{192} mutant embryos. (**C**) In addition, *fmi*^{192} mutants present much thinner ISNb nerves than wild type embryos. (**D**) Schematic image of a wild type and a mutant ISNb nerve where it fails to project to its target muscles. (**E**) Quantification of the mutant phenotype in single PCP mutants. *dsh*^{1} and *fmi*^{192} mutants display a strong increase in the number of stalled ISNb-s. Data sets were compared by Kruskal-Wallis test (P<0.0001), followed by Dunn's multiple comparisons tests: *Oregon-R* vs. *stbm*^{6}, P>0.9999; *Oregon-R* vs. *pk*^{30}, P>0.9999; *Oregon-R* vs. *fz*^{K21}/*fz*^{R52}, P>0.9999; *Oregon-R* vs. *dsh*^{1}, P<0.0001; *Oregon-R* vs. *fmi*^{192}, P<0.0001 (multiplicity adjusted P values). *** P≤0.001; NS, not significant. (**F**) Quantification of the axon stalling phenotype in *stbm;fz* double mutants. *stbm* and *fz* show dominant genetic interaction with one another. Compared to the *stbm*^{6} homozygous mutant, one copy of *fz*^{K21} significantly increases the number of stalled ISNb-s in the double mutant. Similarly to this, the frequency of ISNb axon stalls increases in the *stbm*^{6}/+;*fz*^{k21}/*fz*^{R52} double mutants compared to the *fz*^{K21}/*fz*^{R52} trans-heterozygous combination. Following Kruskal-Wallis test (P=0.0013), P values were calculated by Dunn's multiple comparisons tests: *stbm*^{6} vs. *stbm*^{6};*fz*^{K21}/+, P=0.0373; *fz*^{K21}/*fz*^{R52} vs. *stbm*^{6}/+;*fz*^{K21}/*fz*^{R52}, P=0.0158; *stbm*^{6} vs. *fz*^{K21}/*fz*^{R52}, P>0.9999; *stbm*^{6};*fz*^{K21}/+ vs. *stbm*^{6}/+;*fz*^{K21}/*fz*^{R52}, P>0.9999 (multiplicity adjusted P values). * P≤0.05; NS, not significant. The n values indicate the number of examined ISNb nerves in each genotype, both in (**E**) and (**F**).

Despite the fact that only *dsh*^{1} and *fmi*^{192} mutants show a strong axon stalling phenotype, other PCP proteins may also be involved in controlling the growth of the ISNb nerves, especially because we found that Stbm and Fz are also present in the peripheral motor nerves, although their expression is not as strong as that of Dsh and Fmi. It is possible that the PCP components act in collaboration with one another in this process and may have redundant functions. To address this question we performed genetic interaction tests with double mutant combinations of *stbm* and *fz* first. We found that, compared to the single PCP mutants, one copy of *fz*^{K21} or *stbm*^{6} significantly enhances the frequency of ISNb axon stalls in the *stbm*^{6};*fz*^{K21}/+ and the *stbm*^{6}/+;*fz*^{K21}/*fz*^{R52} double mutant combinations (**Fig. 33 F**). This data suggests that *stbm* and *fz* are also necessary for the growth of the ISNb nerves and likely to act together in this process.

4. 3. Alterations in the growth and guidance of the LN_v axons in the brain of PCP mutant adult flies

Besides the embryonic nervous system, we also examined the adult brain to further investigate the potential *in vivo* role of the core PCP proteins in axon growth and pathfinding. For this purpose, we studied the simple and stereo-typical axonal pattern of the LN_v neurons that are key components of circadian regulation. These experiments were performed by using the same loss of function mutant alleles of the PCP genes as in the embryonic studies, with one exception: instead of *fmi*^{192} we used the hypomorphic *fmi*^{frz3} allele. In contrast to the *fmi*^{192} allele, this allele is homozygous viable, thus it can be applied to study the effect of Fmi loss in the adult fly brain.

LN_vs consist of two groups of neurons: s-LN_vs that send axons dorsally which terminate in the dorsal protocerebrum, and l-LN_vs, axons of which bifurcate close to their origin and innervate the medullae in both brain hemispheres. **Figure 34 A** shows the s-LN_v axons, as well as axonal projections of the l-LN_vs that form the posterior optic tract. Compared to the control, PCP mutant brains show strong guidance phenotypes in which ectopic axons originate from three different areas typically: (1) from the dorsal terminals of s-LN_vs, (2) from the middle section of s-LN_v axons and/or (3) from l-LN_v axons that grow through the posterior optic tract. Independent of their origin, most ectopic axons innervate the dorsomedial/medial region of the brain. Furthermore, l-LN_v axons in the posterior optic tract are strongly defasciculated in some cases (**Fig. 34 B-E**). With the exception of dsh^1, these phenotypes occur with a higher penetrance in PCP mutants than in the control, and seem to show a typical distribution among the three types of guidance problems. There is a small amount of brains even in the Oregon-R control that present ectopic axons mostly from s-LN_v dorsal terminals and from l-LN_vs, however, the number of these is much higher in some PCP mutants, such as in $fz^{K21/R52}$ and fmi^{frz3}. In the $stbm^6$ mutant brains majority of the ectopic axons emerge from the middle section of the s-LN_vs and from the l-LN_vs. Interestingly, pk^{30} mutants do not show a clear tendency: ectopic axons present a relatively even distribution among the three guidance phenotypes. In contrast to these, the number of brains with ectopic axonal projections is reduced in dsh^1 mutants as compared to its control or other PCP mutants (**Fig. 34 F-G**). Since the dsh^1 mutant chromosome also carries a w^{1118} marker mutation we tested whether this background affects LN_v axon guidance. As compared to the *Oregon-R* control, there are considerably more ectopic axons in the w^{1118} mutant flies, therefore it was necessary to use w^{1118} as a second control to the dsh^1 mutant flies.

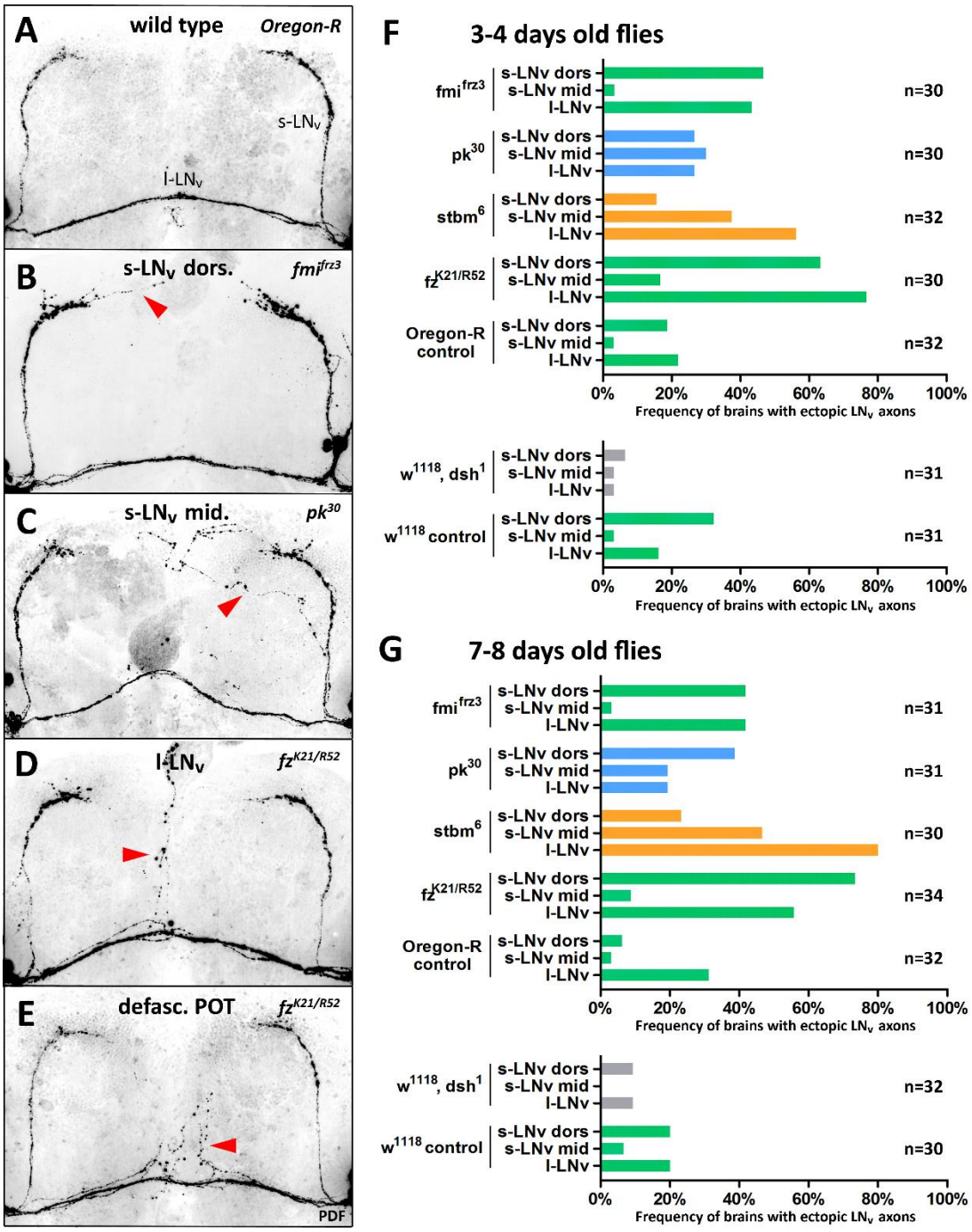

Figure 34. Mutant phenotypes of the LN_v neurons

(**A-E**) Confocal images of adult brains showing the axonal projections of s-LN_v and l-LN_v neurons (visualised by anti-PDF staining); up is dorsal. In contrast to the wild type, PCP mutants exhibit severe axon guidance problems that can be classified into three groups by their origin: ectopic axonal projections can emerge (**B**) from the dorsal terminals of s-LN_vs (s-LN_v dors.), (**C**) from the middle section of s-LN_v axons (s-LN_v mid.) and/or (**D**) from the axonal fascicles of l-LN_vs that grow through the posterior optic tract (l-LN_v). In addition, (**E**) the axonal fascicle of l-LN_v neurons is strongly defasciculated in the area of the posterior optic tract (POT) in some cases. These phenotypes are indicated by red arrowheads in the images. (**F-G**) Diagrams show the distribution of the different misguidance phenotypes in the PCP mutants,

both in 3-4 days old and 7-8 days old flies. Percentages represent the amount of brains that display a certain type of ectopic axonal projection (one brain can exhibit more than one misguidance phenotype). The n values indicate the number of brains that were studied in each genotype. The diagrams are colour coded: (1) in cases when the majority of ectopic axons come from the dorsal terminals of s-LN_vs and from the l-LN_vs the bars of the diagram are green. (2) Yellow bars indicate that ectopic axons originate mostly from the middle section of s-LN_vs and from the l-LN_vs. (3) When misguided axons does not show a clear preference among the three classes the bars are blue. (4) The *dsh*^{1} mutant flies present very few ectopic axons which is not ideal to include it in any of these categories, thus the bars are grey.

Initially we used 3-4 days old flies in these experiments as young adults, however, when we saw the dramatic axon guidance defects in the PCP mutants, we decided to use a second age group due to the following reason. The strong changes in the projection pattern of the LN_v axons suggested that there might be alterations also in the daily activity and/or sleep behaviour of the PCP mutants as the LN_v neurons are essential in these processes. To address this question, we performed experiments to measure the locomotor activity of the PCP mutants (described in the next section: chapter 4. 4.), in which 1-5 days old flies were monitored for 1 week. Therefore, in order to match the age of those flies, we also examined the axonal pattern of the LN_vs in 7-8 days old flies. These experiments revealed that the 3-4 days old and 7-8 days old flies exhibit nearly identical guidance phenotypes and show the same tendencies (**Fig. 34 F-G**).

We also found that the above described defects sometimes accumulate in the same adult brain, one brain can exhibit several ectopic axons and/or defasciculated l-LN_v axon tracts. In order to quantify this phenomenon, we defined the mild, medium and strong categories depending on the degree of the phenotypic aberrations in one brain (**Fig. 35 B-D**). Brains in the mild category exhibit only one type of these phenotypes (s-LN_v dors./s-LN_v mid./l-LN_v/defasc. POT; **Fig. 34 B-E**), two types in the medium category and three or more types in the strong category. Our results showed that the percentage of brains that show axon guidance problems significantly

increases in the PCP mutants, with the exception of *dsh*^{1}. Moreover, the medium and strong categories become much more represented in the PCP mutant brains then in the control (**Fig. 35 E-F**). The strongest misguidance phenotypes appear in *fz*$^{K21/R52}$ and *stbm*^{6} mutants, both in 3-4 days old and 7-8 days old flies. *fmi*^{frz3} and *pk*^{30} mutants also present a considerable increase in the number of ectopic axon projections, however, in the case of *pk*^{30} it occurs to be significant only in 3-4 days old flies. In contrast, *dsh*^{1} does not follow this tendency, the frequency of misguided axons is much lower in *dsh*^{1} mutants than in the other PCP mutants and even in its *w*^{1118} control.

In addition to these, we observed another defect that occurs to be independent from the axon guidance problems and seems to be specific to *fmi*^{frz3} mutants. Normally, the majority of the l-LN$_v$ cell bodies localise ventrally close to the origin of the s-LN$_v$ neurons, however, in *fmi*^{frz3} mutants a great number of these cell bodies appear to be misplaced to a more dorsal position (**Fig. 36**).

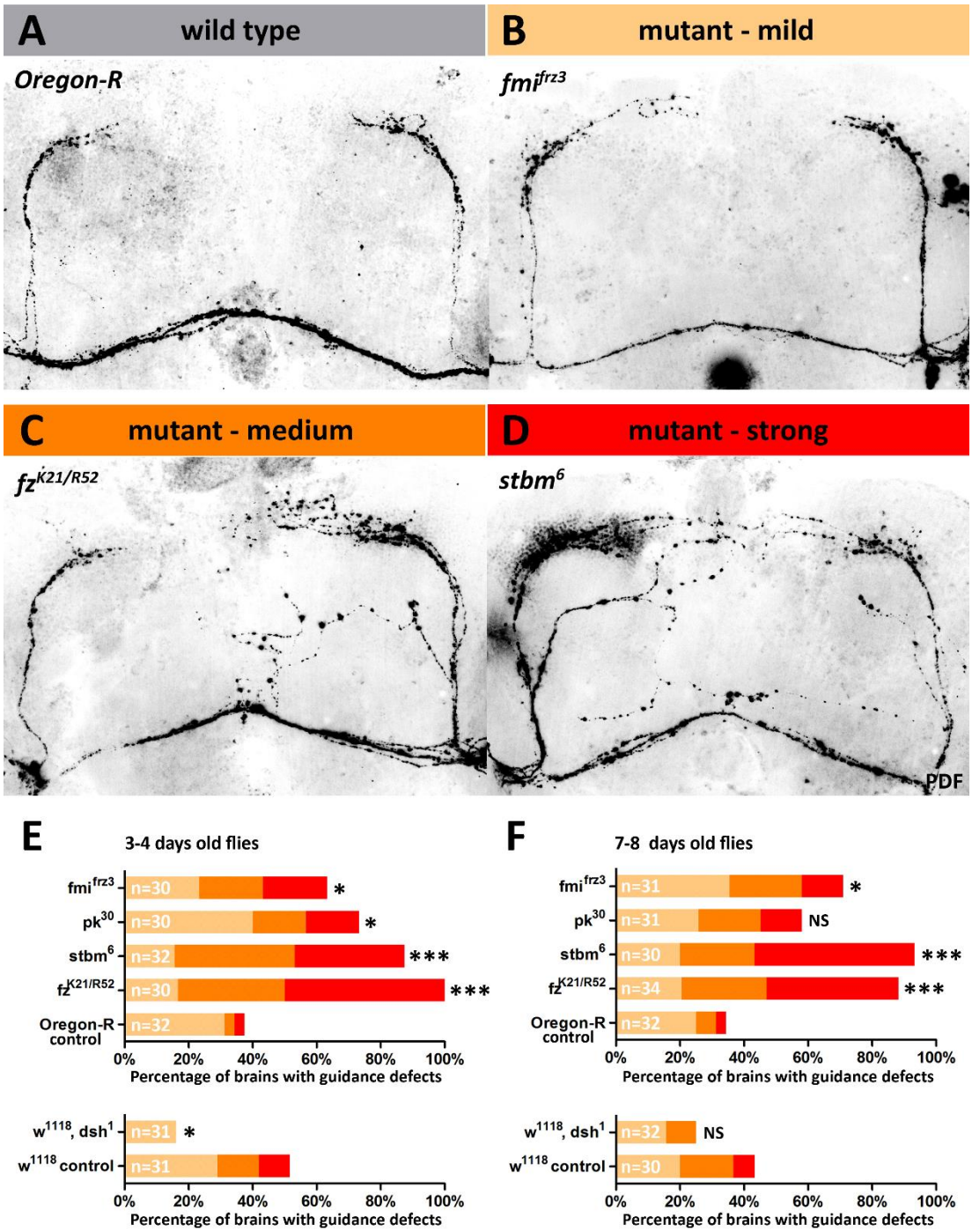

Figure 35. The rate of LN_v axon guidance defects is strongly enhanced in PCP mutants (**A-D**) Confocal images of adult brains: axonal projections of s-LN_v and l-LN_v neurons are visualised by anti-PDF staining; up is dorsal. (**B-D**) Images show the mild, medium and strong categories that were applied to quantify the accumulation of mutant phenotypes in the adult brains. In this classification system, the number of ectopic axonal projections and defasciculated l-LN_vs gradually increases from the mild to the strong categories. (**E-F**) Quantification of the mutant phenotypes in 3-4 days old and 7-8 days old flies. The colour code represents the previously described mild, medium and strong categories. The n values indicate the number of examined brains in each genotype. With the exception of *dsh*^{1}, PCP mutants

display a significant increase in the amount of axon guidance problems: not only the number of brains with ectopic axonal projections increases, but the medium and strong categories become much more represented in the PCP mutants than in the control. (**E**) Data sets were compared by Kruskal-Wallis test (P<0.0001), followed by Dunn's multiple comparisons tests to a fixed control: *Oregon-R* vs. $fz^{K21/R52}$, P<0.0001; *Oregon-R* vs. $stbm^{6}$, P<0.0001; *Oregon-R* vs. pk^{30}, P=0.0290; *Oregon-R* vs. fmi^{frz3}, P=0.0329 (multiplicity adjusted P values). The dsh^{1} mutants were compared to the w^{1118} control: P=0.0112 (chi-square test). * P≤0.05; *** P≤0.001. (**F**) The statistical analyses of the data from 7-8 days old flies was performed similarly. Kruskal-Wallis test: P<0.0001. Dunn's multiple comparisons tests: *Oregon-R* vs. $fz^{K21/R52}$, P<0.0001; *Oregon-R* vs. $stbm^{6}$, P<0.0001; *Oregon-R* vs. pk^{30}, P=0.1911; *Oregon-R* vs. fmi^{frz3}, P=0.0375 (multiplicity adjusted P values). Chi-square test for w^{1118} vs. dsh^{1}: P=0.2927. * P≤0.05; *** P≤0.001; NS, not significant.

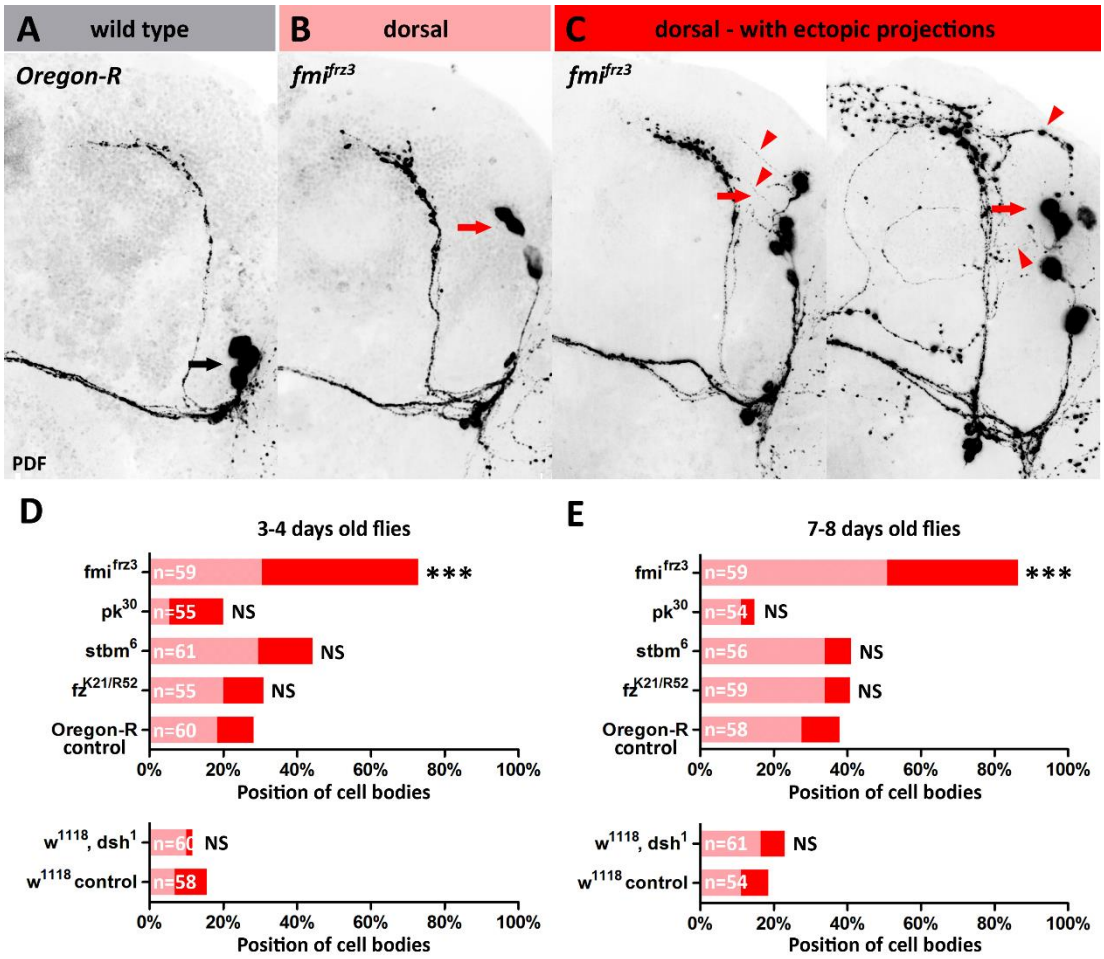

Figure 36. The position of l-LN$_v$ cell bodies in the PCP mutant adult flies

(**A-C**) Confocal images of the right hemisphere of adult *Drosophila* brains showing the position of l-LN$_v$ neurons. In the *Oregon-R* wild type (**A**) most cell bodies of l-LN$_v$ neurons are localised closed to the origin of s-LN$_v$ neurons (black arrow), however, (**B-C**) in some cases l-LN$_v$ cell bodies display a dorsal localisation (red arrows). Interestingly, (**C**) a small amount of these neurons grow ectopic axon projections dorsally (red arrowheads) and even innervate the dorsomedial brain. (**D-E**) shows the amount of dorsally localised cell bodies (with or without ectopic projections; the different categories are represented by the colour code) in 3-4 days old and 7-8 days old male flies. The n values indicate the number of hemispheres that were investigated in these experiments. Compared to the control, only *fmi^{frz3}* mutant flies show a strong and significant increase in the amount of dorsally localised l-LN$_v$s (many of them presents ectopic projections as well). Data sets were analysed by Kruskal-Wallis tests (3-4 days old flies, P<0.0001; 7-8 days old flies, P<0.0001), followed by Dunn's multiple comparisons tests: (**D**) 3-4 days old flies: *Oregon-R* vs. *fz$^{K21/R52}$*, P>0.9999; *Oregon-R* vs. *stbm^6*, P=0.4253; *Oregon-R* vs. *pk^{30}*, P>0.9999; *Oregon-R* vs. *fmi^{frz3}*, P<0.0001; (**E**) 7-8 days old flies: *Oregon-R* vs. *fz$^{K21/R52}$*, P>0.9999; *Oregon-R* vs. *stbm^6*, P>0.9999; *Oregon-R* vs. *pk^{30}*, P=0.0720; *Oregon-R* vs. *fmi^{frz3}*, P<0.0001 (multiplicity adjusted P values). The *dsh^1* mutant brains were compared to the *w^{1118}* control: 3-4 days old flies, P=0.2029; 7-8 days old flies, P=0.7134 (chi-square tests). *** P≤0.001; NS, not significant.

4. 4. PCP proteins regulate the daily activity and the sleeping behaviour of the adult flies

4. 4. 1. Alterations in the locomotor activity of the PCP mutant flies

LN_v neurons are key cellular components of the machinery that is responsible for circadian rhythms in *Drosophila*, and s-LN_v-s are well known as morning pacemakers which control the morning activity of the flies [218, 219]. In addition, l-LN_vs were also found to be important in regulating the sleeping behaviour of the flies. Specifically, l-LN_vs mediate light-induced arousal [213, 220, 221]. We found that upon loss of PCP components, LN_v axons display serious guidance defects, therefore we wondered whether PCP mutant flies display changes in their daily activity and/or their sleeping behaviour. For this purpose, the locomotor activity of 1-5 days old flies was recorded for one week in LD (12h light/12 h dark cycles) by using the previously described loss of function mutant alleles of PCP components. For analysing these results, we only used 5 days of our recorded data as the first day was eliminated to make sure that the flies are absolutely entrained for the experimental conditions, and we also removed the last day in order to reduce the number of dead flies, which may appear in the later stage of the experiment.

Our results showed that the loss of the PCP components affects the locomotor activity of adult flies, with the exception of Fmi, resulting in a decrease of their total activity. Notably, $stbm^{6}$, pk^{30} and $fz^{K21/R52}$ mutants exhibit a strong decrease in their activity. In contrast, the loss of Dsh seems to have an opposite effect, since the dsh^{1} mutant flies show an increased activity as compared to the w^{1118} control (**Fig. 37 A**). By examining the separate daytime and nighttime locomotor activity of the same flies, we found that the altered activity of the PCP mutants is caused by a strong decrease

in their daytime activity. Interestingly, *dsh*^{1} mutants present an increased activity during the daytime and the nighttime as well (**Fig. 37 B**).

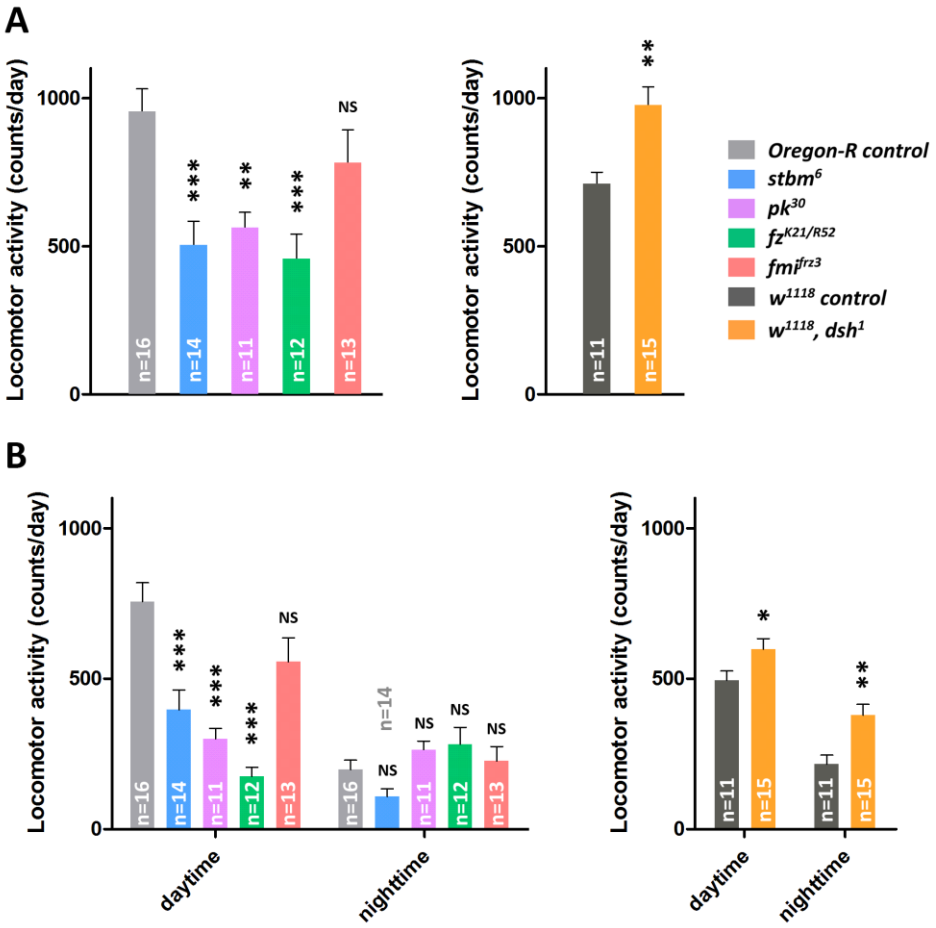

Figure 37. The loss of PCP components affects the locomotor activity of adult flies

(**A**) The total locomotor activity of adult male flies in LD for 5 days is shown by the diagram, indicating the mean (mean+SEM) of counts per day. Counts represent the number of events when a fly crosses the way of the infrared light while moving in the vial in the activity monitor (for further details see *Materials and Methods*, chapter 3. 4.). With the exception of the *fmi*^{frz3} and *dsh*^{1} mutants, PCP mutant flies exhibit a decreased activity compared to the control. The statistical analysis was done by using one-way ANOVA (P<0.0001), followed by Dunnett's multiple comparisons tests: *Oregon-R* vs. *stbm*^{6}, P=0.0006; *Oregon-R* vs. *pk*^{30}, P=0.0064; *Oregon-R* vs. *fz*$^{K21/R52}$, P=0.0003; *Oregon-R* vs. *fmi*^{frz3}, P=0.3795 (multiplicity adjusted P values). The *dsh*^{1} mutant flies were compared to the *w*^{1118} control: P=0.0026 (unpaired t test). ** P≤0.01; *** P≤0.001; NS, not significant. The n values indicate the number of flies in each genotype. (**B**) The diagram displays the locomotor activity (mean+SEM) of the same PCP mutant flies split into daytime and nighttime activity which reveals that, the lesser total activity

of the *stbm*^{6}, *pk*^{30} and *fz*$^{K21/R52}$ mutant flies is caused by a strong decrease in their daytime activity. In addition, *dsh*^{1} mutant flies display an increased activity during the daytime and the nighttime as well, compared to the *w*^{1118} control. The statistical analysis of the daytime and nighttime locomotor activity measurements was done similarly as described above. One-way ANOVA: daytime, P<0.0001; nighttime, P=0.0449. Dunnett's multiple comparisons tests (1) for daytime activity: *Oregon-R* vs. *stbm*^{6}, P<0.0001; *Oregon-R* vs. *pk*^{30}, P<0.0001; *Oregon-R* vs. *fz*$^{K21/R52}$, P<0.0001; *Oregon-R* vs. *fmi*^{frz3}, P=0.0609; (2) for nighttime activity: *Oregon-R* vs. *stbm*^{6}, P=0.2643; *Oregon-R* vs. *pk*^{30}, P=0.6028; *Oregon-R* vs. *fz*$^{K21/R52}$, P=0.3653; *Oregon-R* vs. *fmi*^{frz3}, P=0.9617 (multiplicity adjusted P values). Unpaired t tests to compare *dsh*^{1} mutant flies to the *w*^{1118} control: daytime, P=0.0449; nighttime, P=0.0035. * P≤0.05; ** P≤0.01; *** P≤0.001; NS, not significant.

Normally, when flies are entrained to the light-dark schedule, there are two activity maxima during the day, a morning peak and an evening peak (**Fig. 38 A**). Flies start to wake up and show an increasing activity (anticipation) prior to light exposure and they reach their activity maximum at the onset of the light (equal with dawn in the natural environment), producing a morning peak. Subsequently, their activity decreases to a lower level which is maintained during daytime. The evening peak is formed very similarly to this at the beginning of the dark period (equal with dusk in the natural environment). PCP mutant flies show a strong decrease in their morning activity which becomes severely disrupted in some cases. In *fz*$^{K21/R52}$, *stbm*^{6} and *pk*^{30} mutants the morning peak almost completely disappears, and although to a lower extent, evening activity of the *stbm*^{6} and *pk*^{30} mutant flies decreases as well. Furthermore, *fmi*^{frz3} mutant flies show a decrease both in their morning and evening activities. *dsh*^{1} seems to be an exception in this aspect as well because the morning and evening activity peaks of *dsh*^{1} mutants do not show a notable difference when compared to the *w*^{1118} control, however, the activity of the flies during the dark cycle increases remarkably. **Figure 38** displays the average activity profiles of the studied adult flies, moreover, daily activity profiles (*Appendix*, Fig. 1) and actograms

(*Appendix*, Fig. 2) in the *Appendix* provide additional detailed information about their activity.

Together these data show that loss of the PCP components strongly affects the locomotor activity of the adult flies resulting in a decrease of their daytime activity; moreover, the morning activity peak almost disappears in the PCP mutants. Interestingly, Dsh is an exception in this case since its loss leads to an increased activity throughout the whole day. Furthermore, these findings are also in accordance with our previous results regarding the axon guidance defects of the LN_v neurons given that the frequency of the ectopic LN_v axonal projections correlates quite well with the changes in the locomotor activity of the PCP mutant flies.

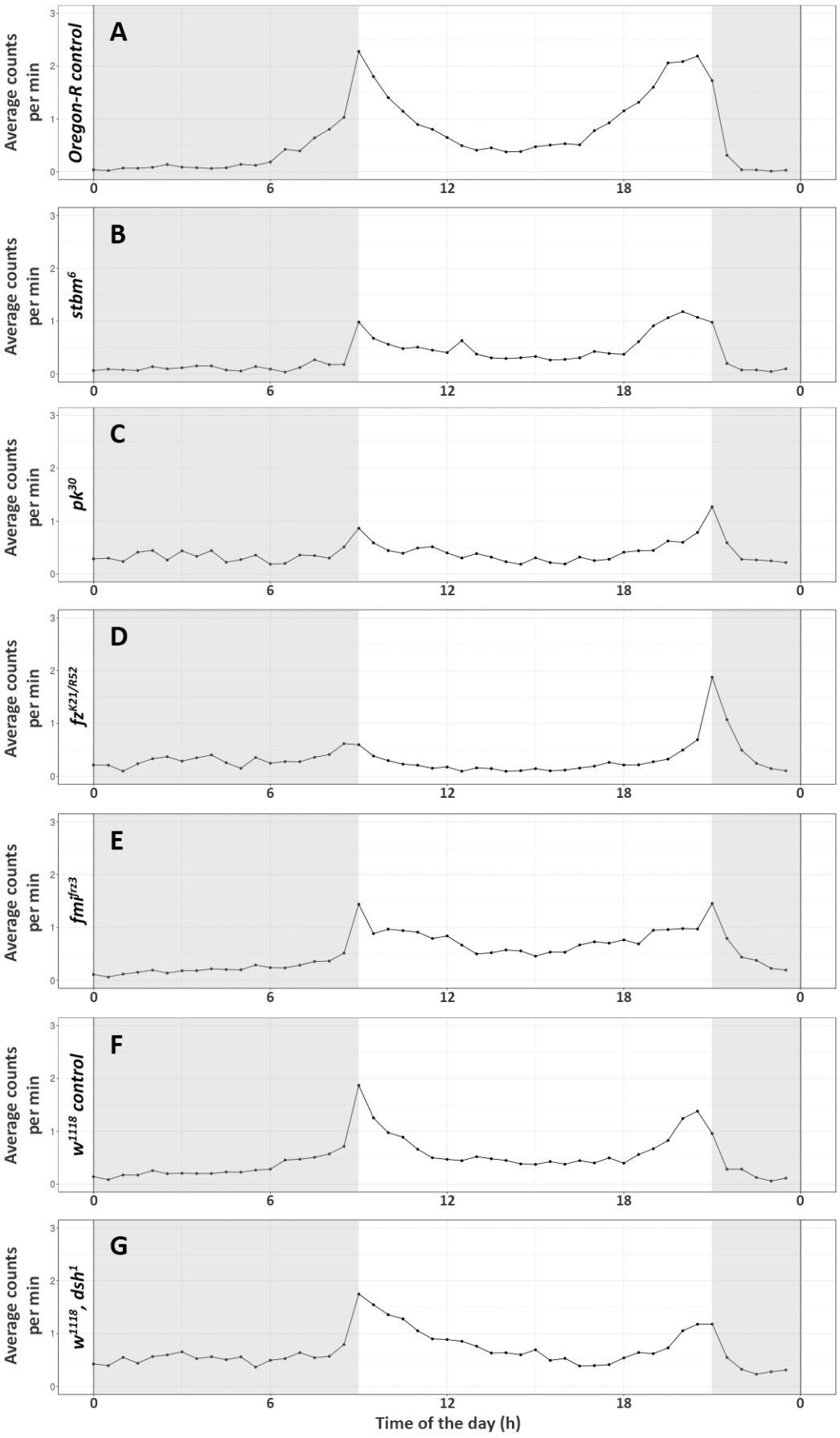

Figure 38. Average activity profiles of the PCP mutant adult flies (fig. legend continues)

(**A-G**) The diagrams show the average activity profiles of adult male flies in LD for 5 days (*Oregon-R*, n=16; *stbm*^{6}, n=14; *pk*^{30}, n=11; *fz*$^{K21/R52}$, n=12; *fmi*^{frz3}, n=13; *w*^{1118}, n=11; *w*^{1118}, *dsh*^{1}, n=15), representing the average of counts per min (counts are summarised into 30 min bins). White areas indicate the period of light exposure, whereas grey shaded areas indicate the dark periods.

4. 4. 2. Loss of the PCP proteins affects the sleeping behaviour of the adult flies

Parallel to their locomotor activity, the sleeping behaviour of the PCP mutant adult flies was also analysed. To this end, we used the same data set which was recorded in LD for one week, and defined the sleep state as a minimum of 5 contiguous minutes of inactivity. For the reasons mentioned before, only 5 days of the recording was used for the final analysis.

We found that loss of the PCP proteins impairs the sleeping behaviour of the flies (**Fig. 39**), and it is in accordance with the alterations in their locomotor activity. The total amount of sleep strongly increases in *stbm*^{6} and *fz*$^{K21/R52}$ mutants, while *pk*^{30} mutants also show a significant increase in the amount of sleep during the daytime. In addition, comparison of the daytime and nighttime recordings showed that the loss of these proteins affect the amount of sleep during daytime, which is in good agreement with our previous results from the locomotor activity analysis. Besides these, in accordance with the changes in the amount of sleep, the length of sleep episodes also increases upon the loss of Stbm or Fz, although this change is not significant in the case of Fz. Despite the fact that the sleep episode length is not altered in *pk*^{30} mutants, these flies exhibit significantly more episodes which can also explain the increased amount of sleep. Similarly to the previous experiments, the loss of Dsh induces opposite changes as compared to the other PCP mutants as the amount of sleep decreases in the *dsh*^{1} mutants in total, and in the nighttime. Moreover, these flies display shorter but more sleep episodes suggesting sleep

fragmentation. Interestingly, the loss of Fmi does not lead to changes in any of these parameters.

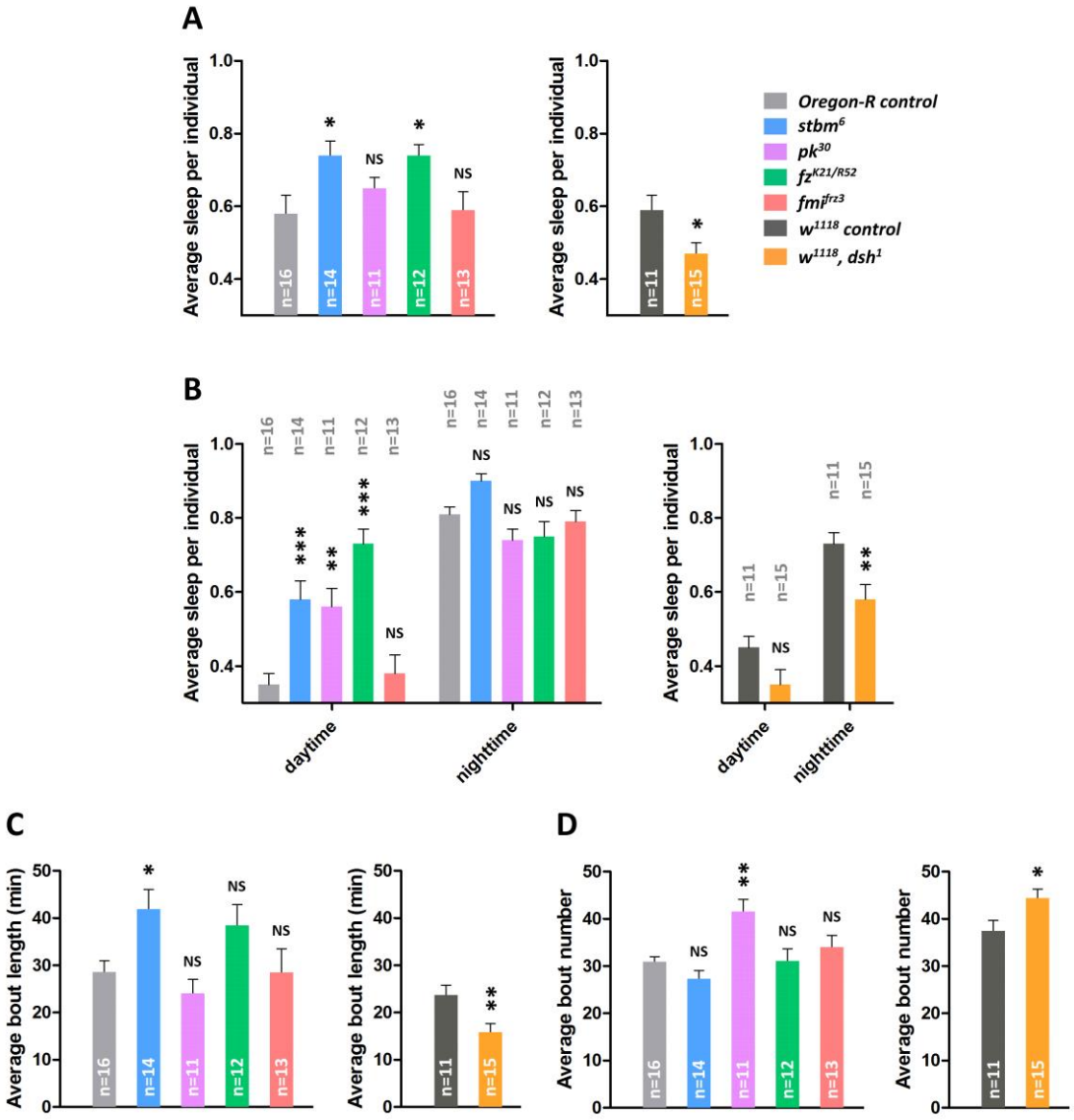

Figure 39. PCP mutant flies show altered sleep

(**A-B**) The diagrams show the amount of sleep in LD for 5 days (**A**) in total and (**B**) separated into daytime and nighttime sleep. (**A**) *stbm*^{6}, *pk*^{30} and *fz*$^{K21/R52}$ mutant flies exhibit an increased amount of sleep in total, moreover, (**B**) this change is even more explicit during the daytime. In accordance with these, (**C**) the length of sleep episodes (bout length) strongly increases in the *stbm*^{6} and *fz*$^{K21/R52}$ mutants. Although, *pk*^{30} mutants does not show changes in sleep episode length, (**D**) the number of these episodes (bout number) is significantly higher which can also result in an increased amount of sleep. Interestingly, the loss of Fmi does not lead to changes in any of these parameters. Dsh seems to have an opposite effect than the other

PCP proteins, (**A-B**) since the amount of sleep decreases in total and in the nighttime in these mutants. In addition, (**C-D**) *dsh*^{1} flies present shorter and more sleep episodes than the *w*^{1118} control. (**A-D**) All data are shown as mean+SEM in the diagrams, and the n values indicate the number of examined adult flies in each genotype. The statistical analysis of the experimental data was performed by using the same tests in every case: one-way ANOVA to compare data sets, then followed by Dunnett's multiple comparisons tests to compare *stbm*^{6}, *pk*^{30}, *fz*$^{K21/R52}$ and *fmi*^{frz3} to the *Oregon-R* control. In contrast to this, the *dsh*^{1} mutant flies were compared to the *w*^{1118} control by using unpaired t tests. The results of these analyses are as follows: (**A**) One-way ANOVA to average sleep: P=0.0144. Dunnett's tests to average sleep: *Oregon-R* vs. *stbm*^{6}, P=0.0254; *Oregon-R* vs. *pk*^{30}, P=0.6323; *Oregon-R* vs. *fz*$^{K21/R52}$, P=0.0343; *Oregon-R* vs. *fmi*^{frz3}, P=0.9993 (multiplicity adjusted P values). Unpaired t test to *dsh*^{1}: P=0.0219. (**B**) One-way ANOVA to average sleep during daytime: P<0.0001. Dunnett's tests to average sleep during daytime: *Oregon-R* vs. *stbm*^{6}, P=0.0008; *Oregon-R* vs. *pk*^{30}, P=0.0050; *Oregon-R* vs. *fz*$^{K21/R52}$, P<0.0001; *Oregon-R* vs. *fmi*^{frz3}, P=0.9672 (multiplicity adjusted P values). Unpaired t test to *dsh*^{1} (daytime): P=0.0736. One-way ANOVA to average sleep during nighttime: P=0.0011. Dunnett's tests to average sleep during nighttime: *Oregon-R* vs. *stbm*^{6}, P=0.0608; *Oregon-R* vs. *pk*^{30}, P=0.2472; *Oregon-R* vs. *fz*$^{K21/R52}$, P=0.3566; *Oregon-R* vs. *fmi*^{frz3}, P=0.9605 (multiplicity adjusted P values). Unpaired t test to *dsh*^{1} (nighttime): P=0.0098. (**C**) One-way ANOVA to average bout length: P=0.0098. Dunnett's tests to average bout length: *Oregon-R* vs. *stbm*^{6}, P=0.0418; *Oregon-R* vs. *pk*^{30}, P=0.8455; *Oregon-R* vs. *fz*$^{K21/R52}$, P=0.2183; *Oregon-R* vs. *fmi*^{frz3}, P>0.9999 (multiplicity adjusted P values). Unpaired t test to *dsh*^{1}: P=0.0081. (**D**) One-way ANOVA to average bout number: P=0.0003. Dunnett's tests to average bout number: *Oregon-R* vs. *stbm*^{6}, P=0.5244; *Oregon-R* vs. *pk*^{30}, P=0.0022; *Oregon-R* vs. *fz*$^{K21/R52}$, P>0.9999; *Oregon-R* vs. *fmi*^{frz3}, P=0.6399 (multiplicity adjusted P values). Unpaired t test to *dsh*^{1}: P=0.0228. * P≤0.05; ** P≤0.01; *** P≤0.001; NS, not significant.

Similarly to the locomotor activity analysis, we also studied the sleep profiles of the PCP mutant flies and found that the loss of Stbm, Pk and Fz leads to an increased daytime sleep which is most evident in the *fz*$^{K21/R52}$ mutants. According to the morning and evening activity peaks, flies present their sleep minima at the beginning of the light period (ZT0, Zeitgeber time) and the start of the dark period (ZT12) (**Fig. 40 A**). In *stbm*^{6}, *pk*^{30} and *fz*$^{K21/R52}$ mutants this sleep minimum is remarkably higher at ZT0 than in the *Oregon-R* control. In addition, as contrast to wild type flies that start to wake up before the end of the dark period which appears as a gradual decrease in

their sleep profiles, the loss of Stbm, Pk or Fz results in an extended sleep state during the dark period. *fmi*^{frz3} mutants do not show significant alterations in their sleep profile compared to the control, although these flies also exhibit increased sleep before the end of the dark period. Opposite to these observations, *dsh*^{1} mutant flies display less sleep during both daytime and nighttime. **Figure 40** shows the average sleep profiles of the PCP mutant flies, while the daily sleep profiles (*Appendix*, Fig. 3) in the *Appendix* provide further information about their sleeping behaviour.

Collectively, our data from the locomotor activity and sleep analysis show that the loss of Stbm, Pk and Fz leads to significant changes in the sleep and the morning activity of the flies. First, *stbm*^{6}, *pk*^{30} and *fz*$^{K21/R52}$ mutants exhibit an extended sleep period, represented by a fairly stable sleep state close to the end of the dark cycle. Moreover, these flies fail to wake up properly at light onset, which is also detectable by the loss of their morning activity peak, and stay in sleep and/or more frequently fall back to sleep during the light period as indicated by the increased amount of daytime sleep. Interestingly, *fmi*^{frz3} mutants show only mild changes compared to the other PCP mutants, whereas the loss of Dsh seems to have an opposite effect on the activity and sleep of the adult flies. These observations are also in accordance with our findings regarding the axonal guidance phenotypes of the LN_v neurons in the PCP mutants. *stbm*^{6} and *fz*$^{K21/R52}$ mutants present a high frequency of misguided axons which presumably is the main cause of the strongly altered locomotor activity and sleep in these flies. Although *pk*^{30} and *fmi*^{frz3} mutants both display LN_v axonal guidance defects, notable changes in their activity and sleep are only detectable in the *pk*^{30} mutant flies.

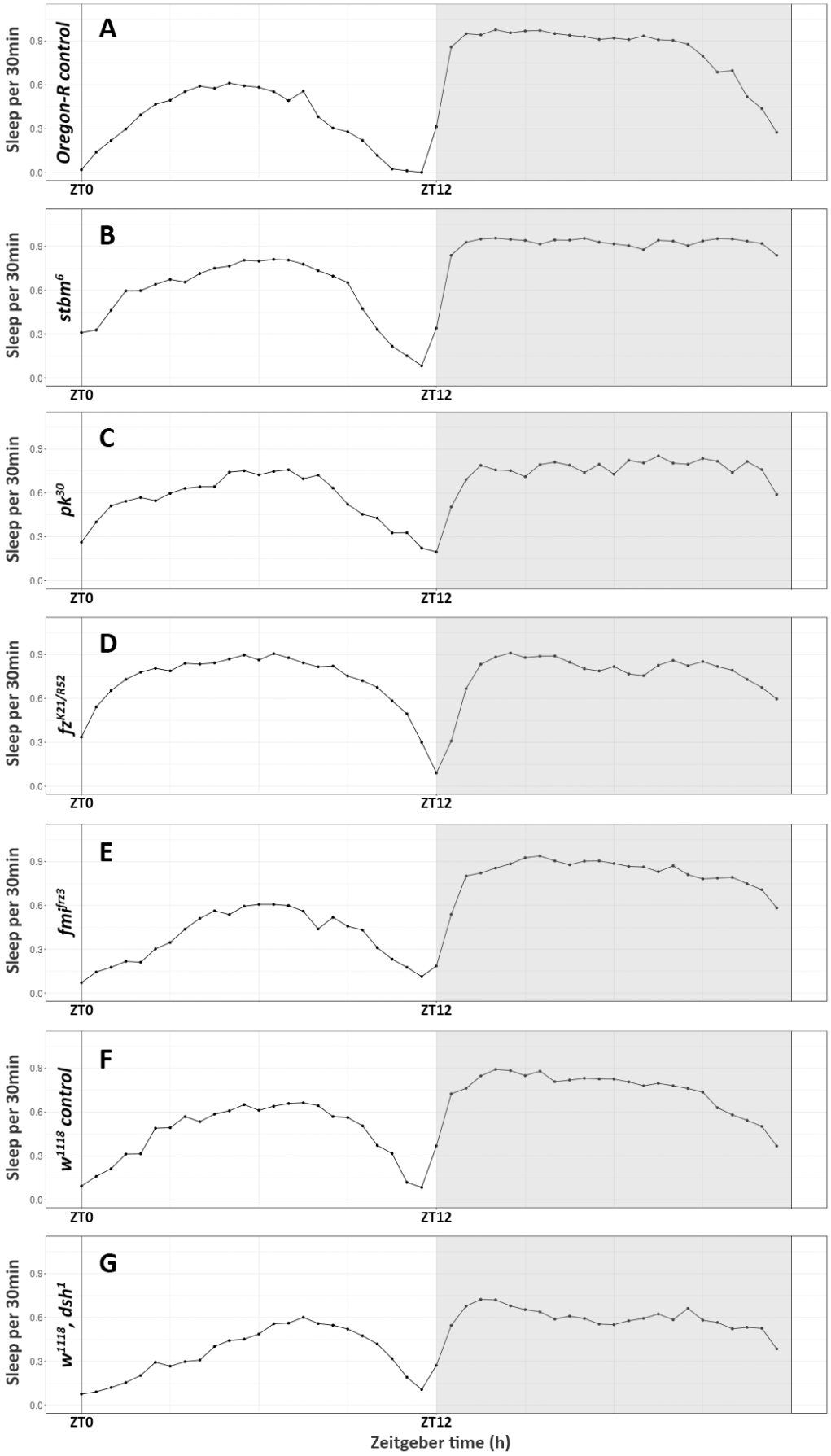

Figure 40. Average sleep profiles of the PCP mutant adult flies (fig. legend continues)

(**A-G**) The diagrams show the average sleep profiles of adult male flies in LD for 5 days (*Oregon-R*, n=16; *stbm*^{6}, n=14; *pk*^{30}, n=11; *fz*$^{K21/R52}$, n=12; *fmi*^{frz3}, n=13; *w*^{1118}, n=11; *w*^{1118}, *dsh*^{1}, n=15), representing the amount of sleep per 30 min. The time is shown in Zeitgeber time, in which ZT0 represents the start of the light period and ZT12 represents the start of the dark period. According to this, the light period is indicated by white areas, whereas, grey shaded areas show the dark period.

4. 5. The role of the PCP components in cytoskeleton regulation in cultured primary neuronal cells

The above presented data demonstrate that PCP proteins regulate axon growth and/or guidance both in the embryonic and the adult nervous system *in vivo*. Axon growth and pathfinding essentially depends on the neuronal cytoskeleton and its dynamic changes, therefore we wanted to investigate whether loss of the PCP proteins alters the neuronal cytoskeleton, and whether these changes affect axon growth. To this end, we used primary neuronal cell cultures which provide powerful readouts to determine the state of the neuronal cytoskeleton. Cell cultures were derived from *Drosophila* embryos (described in detail in the *Materials and Methods*, chapter 3. 5. 1.), and neurons were incubated typically for 6 hours or 2 days in culture. The previously applied loss of function mutant alleles of the PCP proteins were used in these experiments, with the additional null mutant *pk-sple*^{13} allele which deletes both isoforms of Pk [142, 225].

MTs and F-actin are the two key elements of the neuronal cytoskeleton with distinct roles in axon growth and guidance. In order to investigate the involvement of PCP proteins in their regulation, we studied different parameters of both the actin and the MT cytoskeleton in primary cell cultures which will be summarised in the following sections.

4. 5. 1. PCP proteins affect the actin cytoskeleton in cultured neurons

To study the effect of the loss of PCP proteins on the actin cytoskeleton we used two well-accessible readouts for our analysis: the number of filopodia and the morphology of GCs. Finger-like filopodia are actin rich structures normally present at the periphery of the GCs, but in *Drosophila* cultured neurons also along the whole length of the axons. These are easily detectable in primary neuronal cell cultures after 6 hours of incubation (**Fig. 41 A**). Changes in F-actin dynamics and/or in the state of the actin cytoskeleton can lead to alterations in filopodia formation, and subsequent differences in the number of filopodia. We found that the loss of some of the PCP proteins affects filopodia formation, since cultured neurons derived from pk^{30}, $fz^{K21/R52}$ *or* dsh^{1} mutant embryos have significantly less filopodia than the control neurons. Neurons obtained from $stbm^{6}$, $pk\text{-}sple^{13}$ and fmi^{192} mutant embryos show no detectable change in filopodia number (**Fig. 41 C**).

Besides filopodia, the peripheral zone of the GC is also actin-rich, therefore its morphology can also provide relevant information about the state of the actin cytoskeleton. In order to quantify whether PCP proteins control GC morphology we classified GCs by using the “pointed” and “lamellar” categories: pointed GCs present mostly filopodia with no or reduced lamellipodia, resulting in a narrow morphology, whereas lamellar GCs are characterised by the presence of filopodia and big prominent lamellipodia. In cases where GCs did not fit into any of these categories they were classified as “no class” (**Fig. 41 D**). Our results showed that there are significantly more neurons with pointed GCs in the $fz^{K21/R52}$ and dsh^{1} mutant cultures, whereas the other PCP mutant neurons do not display changes in the morphology of the GC (**Fig. 41 E**).

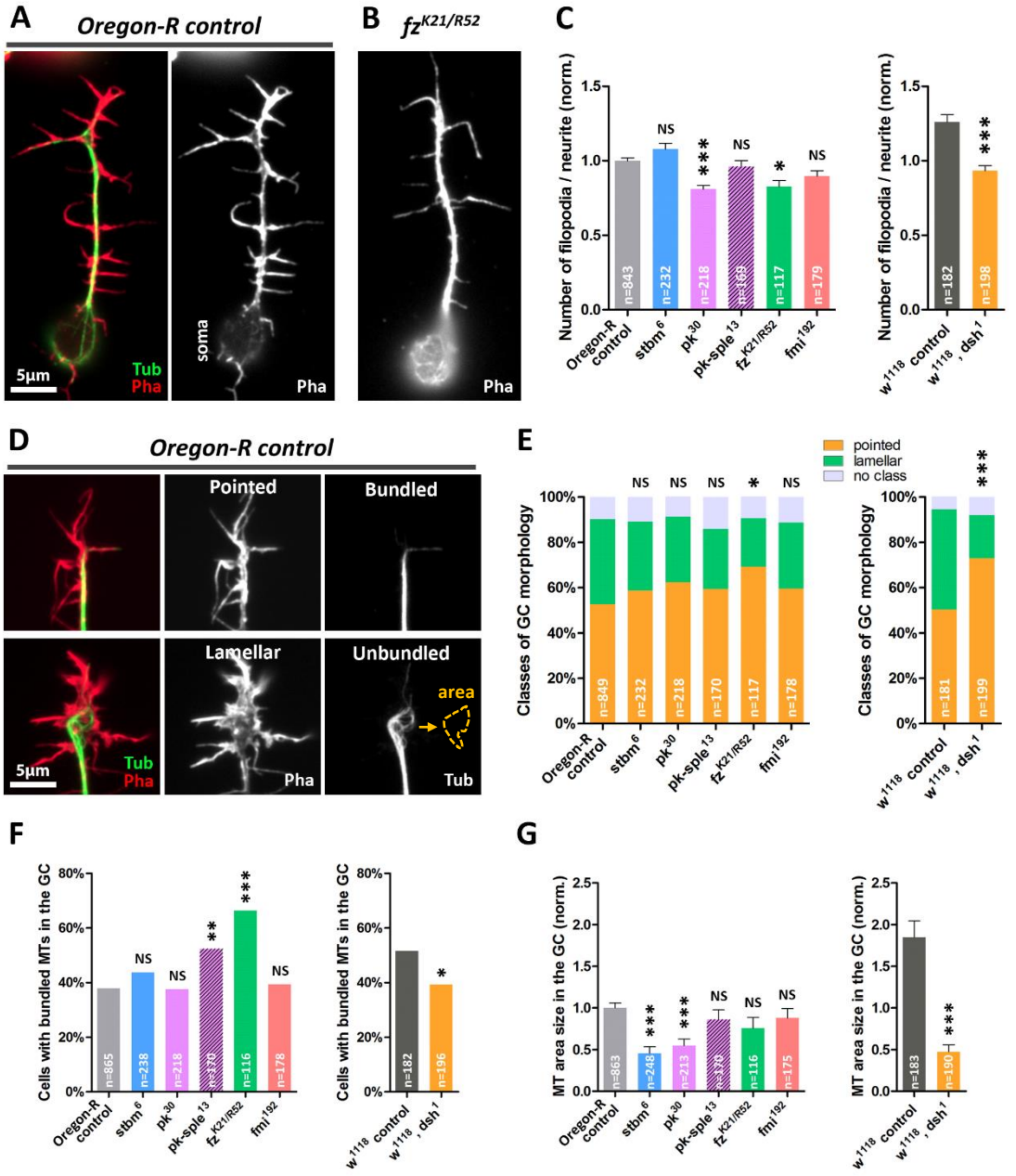

Figure 41. The loss of the PCP components leads to changes in the neuronal cytoskeleton

(**A**) Image of an *Oregon-R* control neuron in primary cell culture after 6 hours of incubation showing the actin and MT cytoskeleton (left): MTs are labelled by α-Tubulin (Tub) antibody staining, whereas actin is visualised by Phalloidin (Pha) staining. On the right, the image shows only the actin cytoskeleton of the same cell in grey, representing the finger-like filopodia along the axon. The loss of some of the PCP components leads to a decrease in the number of filopodia, (**B**) shows a $fz^{K21/R52}$ mutant cultured cell which display less filopodia than the control. (**C**) Quantification of the number of filopodia in the PCP mutant cultured neurons after 6 hours of incubation (mean+SEM; means represent the relative number of filopodia per neurite). pk^{30} and $fz^{K21/R52}$ mutant neurons exhibit significantly less filopodia than the *Oregon-R* control cells. Furthermore, the number of filopodia is significantly less in the dsh^{1} mutant cell

cultures compared to the w^{1118} control. D'Agostino-Pearson tests were performed to test whether the data sets are normally distributed: *Oregon-R*, P<0.0001; $stbm^{6}$, P<0.0001; pk^{30}, P<0.0001; $pk\text{-}sple^{13}$, P=0.0004; $fz^{K21/R52}$, P<0.0001; fmi^{192}, P=0.0038; w^{1118}, P<0.0001; dsh^{1}, P<0.0001. In addition, the data sets were compared by using Kruskal-Wallis test (P<0.0001), followed by Dunn's multiple comparisons tests: *Oregon-R* vs. $stbm^{6}$, P=0.2640; *Oregon-R* vs. pk^{30}, P=0.0001; *Oregon-R* vs. $pk\text{-}sple^{13}$, P>0.9999; *Oregon-R* vs. $fz^{K21/R52}$, P=0.0117; *Oregon-R* vs. fmi^{192}, P=0.0847 (multiplicity adjusted P values). The dsh^{1} mutant cells were compared to the w^{1118} control: P<0.0001 (Mann Whitney U test). * P≤0.05; *** P≤0.001; NS, not significant. (**D**) On the left, images show GCs of cultured control neurons after 6 hours of incubation stained with the same antibodies to visualise both F-actin (Pha) and MTs (Tub). The actin cytoskeleton of the same cells is showed in grey (middle) to reveal the structure of the GC. GCs were classified as pointed or lamellar in order to quantify morphological changes in the loss of the PCP proteins. The MT cytoskeleton is also shown separately in grey on the right to reveal the organisation of MTs in the GC. For classification, "bundled" and "unbundled" categories were used in order to study MT organisation. In addition to this, the size of the area that is covered by MTs in the GC was also measured as another readout. This area is indicated by the orange dashed shape in the image. (**E**) Quantification of the classes of GC morphology in the PCP mutant cultured neurons after 6 hours of incubation. The amount of pointed and lamellar GCs is represented by the orange and green colours in the graph, whereas the GCs that did not fit these categories are classified and indicated as "no class" (grey). Compared to the corresponding controls, the number of neurons with pointed GCs significantly increases in the $fz^{K21/R52}$ and dsh^{1} mutant primary cell cultures. The statistical analysis of the data was done by using Kruskal-Wallis test (P=0.0196), followed by Dunn's multiple comparisons tests: *Oregon-R* vs. $stbm^{6}$, P=0.9134; *Oregon-R* vs. pk^{30}, P=0.0816; *Oregon-R* vs. $pk\text{-}sple^{13}$, P>0.9999; *Oregon-R* vs. $fz^{K21/R52}$, P=0.0130; *Oregon-R* vs. fmi^{192}, P=0.8868 (multiplicity adjusted P values). The dsh^{1} mutant cells were compared to the w^{1118} control: P<0.0001 (chi-square test). * P≤0.05; *** P≤0.001; NS, not significant. (**F**) The graph shows the percentage of cells with bundled MTs in the GC. Compared to the *Oregon-R* control, there is a significantly higher number of neurons with bundled MTs in the $pk\text{-}sple^{13}$ and $fz^{K21/R52}$ mutant cell cultures. Interestingly, dsh^{1} mutant cell cultures show the opposite and present significantly less neurons with bundled MTs than the w^{1118} control. Based on the categorical nature of the data, Kruskal-Wallis test was used to compare data sets (P<0.0001), then P values were calculated by Dunn's multiple comparisons tests: *Oregon-R* vs. $stbm^{6}$, P=0.5492; *Oregon-R* vs. pk^{30}, P>0.9999; *Oregon-R* vs. $pk\text{-}sple^{13}$, P=0.0025; *Oregon-R* vs. $fz^{K21/R52}$, P<0.0001; *Oregon-R* vs. fmi^{192}, P>0.9999 (multiplicity adjusted P values). The dhs^{1} mutant cells were compared to the w^{1118} control: P=0.0175 (Fischer's exact test). * P≤0.05; ** P≤0.01; *** P≤0.001; NS, not significant. (**G**) Quantification of MT area size; means represent the relative size of the area that is covered by MTs in the GC (mean+SEM; normalised to the *Oregon-R* control). GCs of the $stbm^{6}$, pk^{30} and dsh^{1} mutant cultured neurons exhibit significantly smaller areas, occupied by MTs, than that of the corresponding control neurons. D'Agostino-Pearson tests were used

to test the normality of the data sets: *Oregon-R*, P<0.0001; *stbm*^{6}, P<0.0001; *pk*^{30}, P<0.0001; *pk-sple*^{13}, P<0.0001; *fz*$^{K21/R52}$, P<0.0001; *fmi*^{192}, P<0.0001; *w*^{1118}, P<0.0001; *dsh*^{1}, P<0.0001. Statistical analysis was done by using Kruskal-Wallis test (P<0.0001), followed by Dunn's multiple comparisons tests: *Oregon-R* vs. *stbm*^{6}, P<0.0001; *Oregon-R* vs. *pk*^{30}, P=0.0004; *Oregon-R* vs. *pk-sple*^{13}, P>0.9999; *Oregon-R* vs. *fz*$^{K21/R52}$, P=0.4717; *Oregon-R* vs. *fmi*^{192}, P>0.9999 (multiplicity adjusted P values). In addition, the *dsh*^{1} mutant cells were compared to the *w*^{1118} control: P<0.0001 (Mann Whitney U test). *** P≤0.001; NS, not significant. The n values in (**C**), (**E**), (**F**) and (**G**) indicate the number of examined cells in each genotype.

These data suggest that Fz and Dsh are responsible for controlling the actin cytoskeleton in cultured neurons since the loss of these proteins alters both filopodia number and GC morphology in primary cell cultures. In addition, Pk may regulate actin in filopodia but it seems to be dispensable for lamellipodia. Interestingly, Fmi might not influence the actin cytoskeleton in primary neuronal cell cultures since its loss does not lead to changes in any of these aspects.

Actin rich structures such as filopodia not only influence axonal growth but are also important for the formation of axonal branches [230]. Next we investigated whether the changes mentioned above influence branch formation in mature neurons. To this end the number of primary branches was counted after 2 days of incubation. Although we found that the neurons derived from *stbm*^{6}, *pk*^{30} and *fz*^{K21} mutant embryos have slightly less primary branches than the control neurons, these differences are not significant in any of these cases. (**Fig. 42 A-B**).

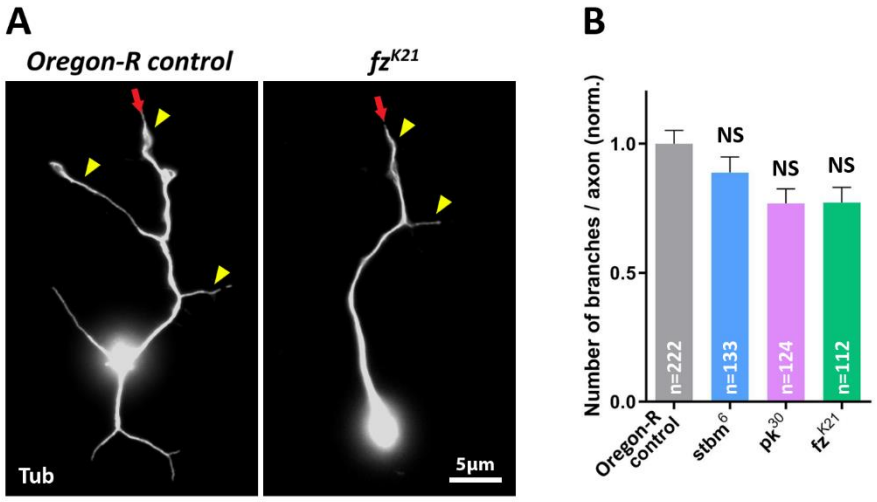

Figure 42. The effect of PCP loss of function on neuronal branch formation in culture

(**A**) Images of neurons in primary cell cultures after 2 days of incubation stained with α-Tubulin (Tub) antibody. Although the number of branches is used here to study the impact of actin cytoskeletal changes, branches are considered to be properly formed when they present stable MT bundles, thus MTs needed to be visualised for this experiment. Axons present several branches in the control neurons (left), whereas the number of these branches decreases in some of the PCP mutants, although not significantly, which is represented by the *fz*^{K21} mutant neuron (right). Red arrows show the main axon branches, and primary branches are pointed by the yellow arrowheads. (**B**) Quantification of the number of primary branches in some of the PCP mutant cultured cells, showing the relative number of branches per axon (mean+SEM, normalised to the control). Although, the number of primary branches decreases in the examined PCP mutant neuron cells it does not show a significant difference in any of these cases compared to the control. D'Agostino-Pearson normality tests: *Oregon-R*, P<0.0001; *stbm*^{6}, P=0.0015; *pk*^{30}, P=0.0029; *fz*^{K21}, P=0.0161. The data sets were compared by using Kruskal-Wallis test (P=0.0521), followed by Dunn's multiple comparisons tests: *Oregon-R* vs. *stbm*^{6}, P=0.6979; *Oregon-R* vs. *pk*^{30}, P=0.0534; *Oregon-R* vs. *fz*^{K21}, P=0.0870 (multiplicity adjusted P values). NS, not significant. The n values indicate the number of studied cells in each genotype.

4. 5. 2. Reduced function of the PCP proteins affects the organisation of the MT cytoskeleton in cultured neurons

Next we investigated whether the loss of PCP proteins affects the organisation of the MT cytoskeleton in the growth cone. The main shaft of the axonal MTs ends in the central zone of the GC, from which individual MTs can extend into lamellipodia and filopodia. Through the complex interactions of MTs and F-aktin, the exploratory behaviour of these splayed MTs is influenced by the actin cytoskeleton. In addition, the subsequent stabilisation of MTs into a certain direction is essential for the formation of a new axon segment during directed axonal growth. Therefore, the organisation and the behaviour of MTs within the GC has an impact on axon growth [6, 19, 20]. To examine MT organisation, we defined two categories: neurons that have a compact MT bundle in the GC are referred as “bundled”, whereas the “unbundled” category includes neurons in which MTs spread and leave the main MT bundle (**Fig. 41 D**). By using this classification, we found that there are significantly more neurons with bundled MTs in the cell cultures derived from *pk-sple*^{13} and *fz*$^{K21/R52}$ mutant embryos. In contrast to this, *dsh*^{1} mutant cultures contain significantly less neurons with bundled MTs in the GC compared to the *w*^{1118} control. The loss of Stbm and Fmi do not lead to changes in this binary system. (**Fig. 41 F**).

These results suggested that the loss of some of the PCP components influences the explorative behaviour of the MTs that leave the main MT bundle and invade into lamellipodia and filopodia. Therefore, we also measured the area that is covered by MTs in the GC as another method to study this phenomenon. This investigation revealed that MTs occupy a significantly smaller area in the *stbm*^{6}, *pk*^{30} and *dsh*^{1} mutant cell cultures, whereas the *pk-sple*^{13}, *fz*$^{K21/R52}$ and *fmi*^{192} mutant neurons do not display changes compared to the corresponding controls (**Fig. 41 G**).

Together these results indicate that Stbm, Pk, Fz and Dsh influence MT organisation in the GC since their loss leads to a reduction of spread or unbundled MTs. Interestingly, Fmi seems not to have a role in any of these aspects.

4. 5. 3. Loss of some of the PCP components leads to exacerbated axonal growth in culture conditions

The growth of axons requires coordinated function of both the actin and microtubule cytoskeleton [4, 6, 19]. Since defects in PCP signalling leads to changes in the actin and MT cytoskeleton, next we investigated to what degree axonal growth is affected upon mutations on PCP components. To this end we measured the net growth of axons after 6 hours of incubation in culture. We found that neurons in the *pk-sple*^{13}, *fmi*^{192} and *dsh*^{1} mutant cell cultures have slightly but significantly longer axons than the control neurons (**Fig. 43**), suggesting that these PCP components contribute to axon growth presumably by regulating the actin and/or the MT cytoskeleton.

The presence of subtle phenotypes concerning axon growth and readouts for the actin and the MT cytoskeleton led to hypothesise that PCP proteins could have redundant functions and/or act in collaboration with one another to control cytoskeletal changes. Therefore, similarly to the embryonic experiments, we started to investigate the genetic interactions between *stbm* and *fz* in primary cell cultures as well. Because the current level of this analysis is preliminary, these data are only shown in the *Appendix* (Fig. 4).

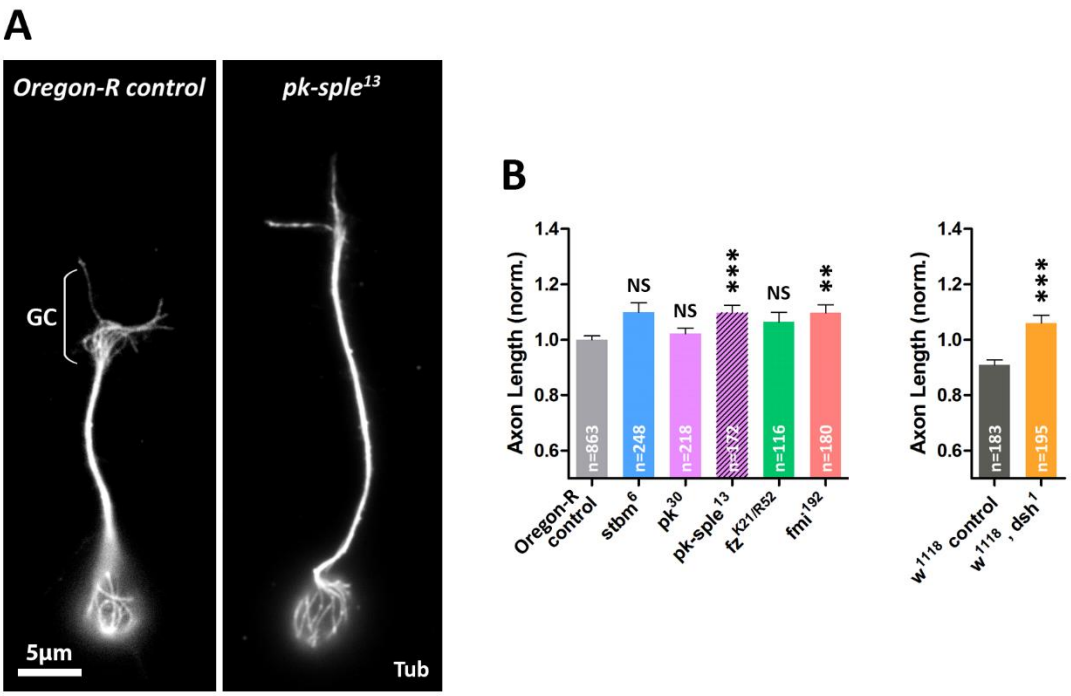

Figure 43. The loss of some of the PCP proteins increases axon length

(**A**) Images of cultured neurons after 6 hours of incubation, stained with α-Tubulin (Tub) antibody in order to label the MT cytoskeleton. Axon length was measured from the origin of the axonal MT shaft until its distal end. Compared to the control (left), the loss of some of the PCP components increases axon length in primary cell cultures as it is represented by a *pk-sple*^{13} mutant neuron (right). GC, growth cone. (**B**) Quantification of axon length; means represent the relative length of the axonal MT shaft (mean+SEM; normalised to the *Oregon-R* control). Neurons in the *pk-sple*^{13} and *fmi*^{192} mutant cell cultures display significantly longer axons than the *Oregon-R* control neurons, as well as *dsh*^{1} mutant cultured neurons have significantly longer axons compared to the *w*^{1118} control. To examine whether the data sets were normally distributed we used D'Agostino-Pearson tests: *Oregon-R*, P<0.0001; *stbm*^{6}, P=0.0004; *pk*^{30}, P=0.0269; *pk-sple*^{13}, P<0.0001; *fz*$^{K21/R52}$, P=0.0027; *fmi*^{192}, P<0.0001; *w*^{1118}, P<0.0001; *dsh*^{1}, P<0.0001. The statistical analysis was done by using Kruskal-Wallis test (P<0.0001), followed by Dunn's multiple comparisons tests: *Oregon-R* vs. *stbm*^{6}, P=0.0565; *Oregon-R* vs. *pk*^{30}, P=0.1647; *Oregon-R* vs. *pk-sple*^{13}, P=0.0003; *Oregon-R* vs. *fz*$^{K21/R52}$, P=0.1775; *Oregon-R* vs. *fmi*^{192}, P=0.0016 (multiplicity adjusted P values). The *dsh*^{1} mutant cells were compared to the *w*^{1118} control: P=0.0001 (Mann Whitney U test). ** P≤0.01; *** P≤0.001; NS, not significant. The n values indicate the number of examined cells in each genotype.

4. 6. The formin DAAM, a candidate to mediate the effect of PCP proteins in axon growth and guidance

DAAM belongs to the formin protein family which are evolutionary conserved actin assembly factors, mostly known for their function to promote the nucleation and elongation of actin filaments. Formins are multidomain proteins, and all of them are characterized by the presence of two formin homology domains, FH1 and FH2. The FH2 domain is responsible for actin nucleation and supports the elongation of actin filaments, whereas the FH1 domain recruits Profilin-bound actin monomers and promotes elongation [48, 231-234].

It was first shown by Habas et al. that Daam1 (a vertebrate DAAM ortholog) is required for convergent extension during gastrulation of the Xenopus embryo, and that it interacts with the PDZ and DEP domains (both are important for PCP signalling) of Dvl (a Dsh ortholog) [116]. Following this, the involvement of Daam in the Wnt/PCP signalling pathway was further supported by several vertebrate studies [235-237]. Despite the fact that DAAM does not seem to be required for the establishment of PCP in *Drosophila* [238], it was shown to play an essential role in different aspects of neuronal development. First, DAAM is strongly enriched in the *Drosophila* embryonic CNS where it is necessary for proper axon growth [203]. Accordingly, DAAM is present in primary cell culture neurons derived from Drosophila embryos, and regulates axon growth and filopodia formation [64, 203]. Curiously, a recent study demonstrated that DAAM acts in concert with the Wnt/PCP signalling components as a downstream effector protein, to control the axonal growth and guidance of the mushroom body neurons [177].

Based on the above notions, we hypothesised that DAAM might mediate the effect of the PCP proteins on axon growth and/or guidance in the neurons we examined

previously. To test this possibility, we mainly used the hypomorphic *DAAM*^{Ex1} mutant allele, although in one case the *DAAM*$^{mat/zyg}$ combination was also applied in which both maternal and zygotic DAAM functions are impaired (further description of the alleles can be found in *Materials and Methods*, chapter 3. 1.). While the *DAAM*^{Ex1} allele deletes only the C-terminal tail of the protein, this mutation results in a highly decreased level of DAAM in the adult *Drosophila* brain suggesting that it is suitable and helpful to investigate the function of DAAM in the nervous system [177, 203]. Figure 5 in the *Appendix* shows the reduced level of DAAM in the *DAAM*^{Ex1} mutant adult brain compared to the wild type. Interestingly, the C-terminal region of some formins was found to bind MTs *in vitro* [45, 239], therefore using this allele may provide a possibility to examine whether the C-terminal tail of DAAM shows any functional similarities to them.

4. 6. 1. DAAM is necessary for growth of the ISNb nerves in the embryo

Previous studies have shown that the single *Drosophila* DAAM ortholog is expressed in the embryonic nervous system and it accumulates in the neuropil of the VNC and in the peripheral motor nerves [203, 240]. It has also been shown that the loss of DAAM leads to morphological defects in the embryonic VNC, moreover, its activated form induces neurite outgrowth in embryonic nerve cord cultures [203]. These findings suggested that DAAM might be important to control the growth of the peripheral motor nerves as well. As our results revealed that the loss of most of the PCP proteins results in an early axon stall of the ISNb nerves, we investigated whether the lack of DAAM causes a similar phenotype. For this purpose, motor nerves were studied in stage 16 embryos and we found that, similarly to the PCP mutants, *DAAM*^{Ex1} mutant embryos exhibit significantly more ISNb-s that stall between the 13 and 6 ventrolateral muscles than the control embryos (**Fig. 44 B-C**). Independent of this experiment,

DAAM^{Ex68} null mutant embryos were also investigated in our lab and showed the same axon stalling phenotype [240]. As expected, frequency of the stalled ISNb-s occurs to be higher in the complete null mutants (63%) than in the hypomorphic mutant *DAAM*^{Ex1} (49%) embryos.

Together these findings suggest that, similarly to PCP proteins, DAAM also has an important role in controlling the growth of the ISNb nerves in the embryos. Moreover, DAAM is a possible candidate to mediate the effect of the PCP proteins in this process.

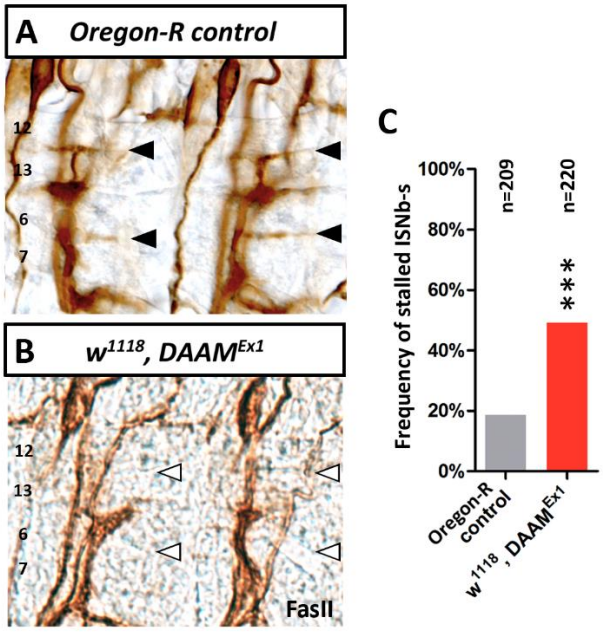

Figure 44. The loss of DAAM causes an early stalling of the ISNb nerves

(**A-B**) Fillet preparations of stage 16 embryos, stained with anti-Fasciclin (FasII) antibody, showing the structure of the ISNb nerves; up is dorsal, left is anterior. Compared to the control, (**B**) ISNb nerves fail to project to their target muscles (empty arrowheads) in the *DAAM*^{Ex1} mutant embryos and stall between the 13 and 6 ventrolateral muscles. (**C**) Quantification of the ISNb stalling phenotype. The frequency of stalled ISNb nerves is significantly higher in the *DAAM*^{Ex1} mutant embryos than in the control: $P<0.0001$ (Fisher's exact test). *** $P\leq0.001$. The n values indicate the number of examined ISNb nerves.

4. 6. 2. The loss of DAAM does not alter LN_v axon guidance

Since we found that, besides the PCP proteins, DAAM is also important in controlling axon growth in the *Drosophila* embryos, we investigated whether the loss of DAAM affects guidance of the LN_v neurons *in vivo* in the adult brain. To this end, the axonal pattern of LN_vs was studied in 3-4 days old and 7-8 days old male flies by using the adult viable $DAAM^{Ex1}$ allele. The $DAAM^{Ex1}$ mutant chromosome also carries a w^{1118} marker mutation, therefore we used w^{1118} flies as control to $DAAM^{Ex1}$ mutants.

In order to quantify the incidence of the LN_v axon guidance defects we applied the same classification system as described previously, including the mild, medium and strong mutant categories (**Fig. 45 B-D**). Although we found that the number of ectopic axons slightly increases in the $DAAM^{Ex1}$ mutants, both in 3-4 days and 7-8 days old flies, this change does not appear to be significant as compared to the w^{1118} control (**Fig. 45 E**). As it was described before, ectopic axons originate from three different places, either from the dorsal terminals of s-LN_v neurons (s-LN_v dors), from the middle section of s-LN_v neurons (s-LN_v mid) and/or from the axonal fascicles of l-LN_vs (l-LN_v). Although most PCP mutants display a characteristic pattern regarding to the origin of misguided axons, a clear preference amongst these three types cannot be detected in $DAAM^{Ex1}$ mutant flies (**Fig. 45 F**).

Based on these data, DAAM is not particularly important for controlling the guidance of the LN_v axons *in vivo*, since the loss of DAAM does not lead to notable changes in the number of ectopic axons. Furthermore, it also suggests that PCP proteins regulate LN_v axon guidance most likely independently from DAAM.

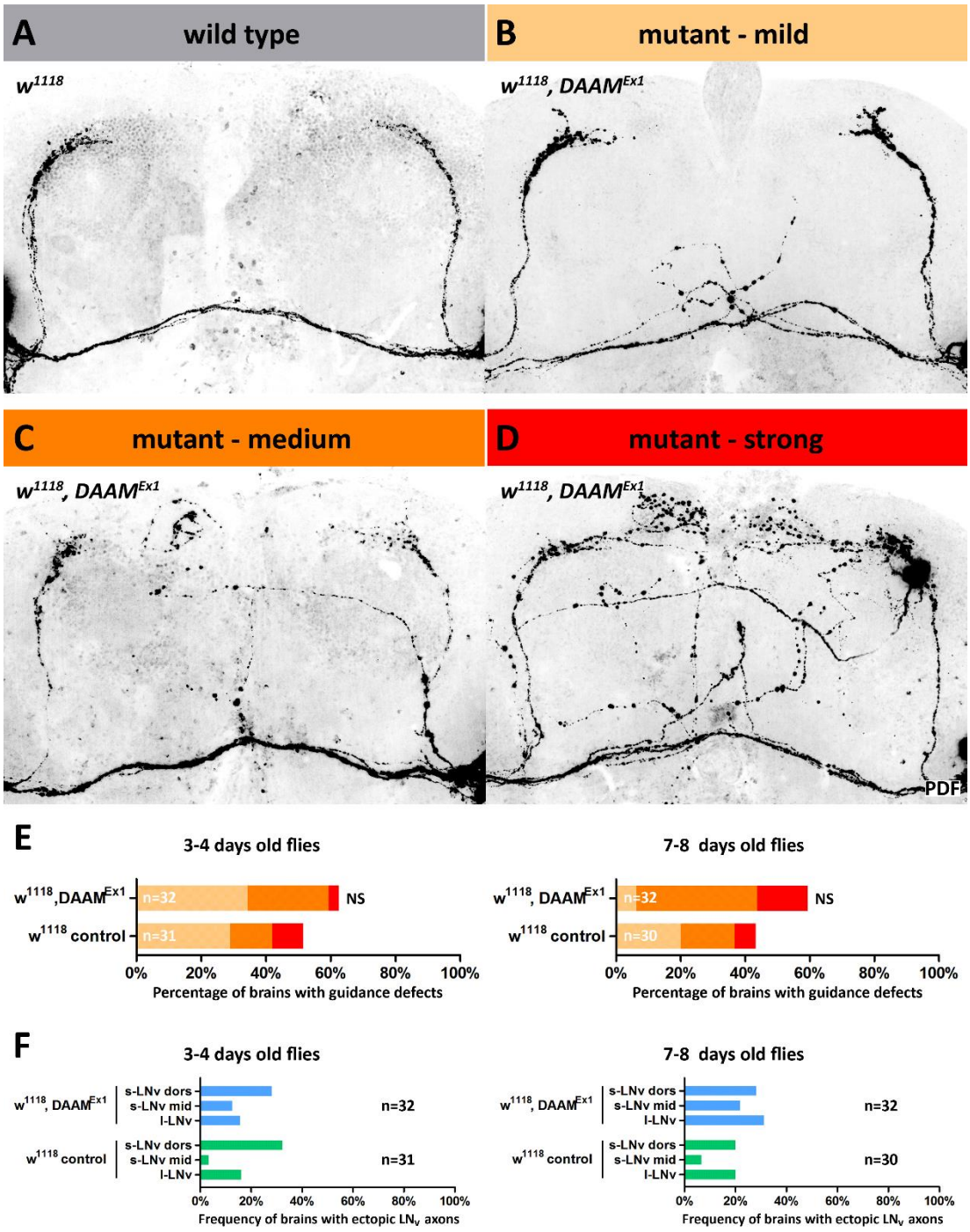

Figure 45. The loss of DAAM does not affect the guidance of LN_v axons

(**A-D**) Confocal images of adult brains showing the axonal projections of LN_v neurons (visualised by anti-PDF staining); up is dorsal. The images illustrate (**A**) the stereotypical axonal pattern of wild type LN_v neurons and (**B-D**) the mild, medium and strong categories that were used to measure the amount of ectopic LN_v axons in the adult fly brains. (**E**) The graphs show the percentage of brains with mild, medium or strong misguidance problems both in 3-4 days old and 7-8 old flies; the different categories are indicated by the colour code. Compared to the control, *DAAM*^{Ex1} mutant brains do not display a significant difference. P values were calculated by chi-square tests: 3-4 days old, P=0.4151; 7-8 days old, P=0.0842.

NS, not significant. (**F**) Quantification of the different misguidance phenotypes in 3-4 days old and 7-8 days old flies, depending on the origin of the ectopic axons (l-LN_v / s-LN_v mid / s-LN_v dors). Green bars of the w^{1118} control represents that most ectopic axons come from the dorsal terminals of s-LN_v neurons and from the l-LN_vs. In contrast to this, ectopic axons in the $DAAM^{Ex1}$ mutant brains does not show a clear preference among the three classes (blue bars). The n values indicate the number of examined brains both in (**E**) and (**F**).

4. 6. 3. The effect of DAAM on the locomotor activity and sleeping behaviour of adult *Drosophila*

Although the loss of DAAM does not seem to affect LN_v axon guidance, parallel to the PCP mutants, we also investigated whether $DAAM^{Ex1}$ mutant adult flies show altered locomotor activity and/or sleeping behaviour. To this end, the locomotor activity of 1-5 days old flies was recorded for one week in LD in this case as well, and we used only 5 days of the recording for further analysis (the first and the last day were eliminated for the previously described reasons).

Interestingly, we found that the loss of DAAM decreases the locomotor activity of the adult flies, and that this difference is typically caused by a decreased nighttime activity (**Fig. 46 A-B**). This finding is in contrast with our results from the PCP mutants, since the loss of Stbm, Pk and Fz decreases the daytime activity of adult flies. *Because the* dsh^1 mutants display an increased locomotor activity throughout the whole day, the effect of DAAM is not similar to that of Dsh either. In addition, although a lower level of nighttime activity can be detected in the activity profile of $DAAM^{Ex1}$ mutants, the morning and evening activity peaks are clearly detectable in the diagram (**Fig. 46 C-D**).

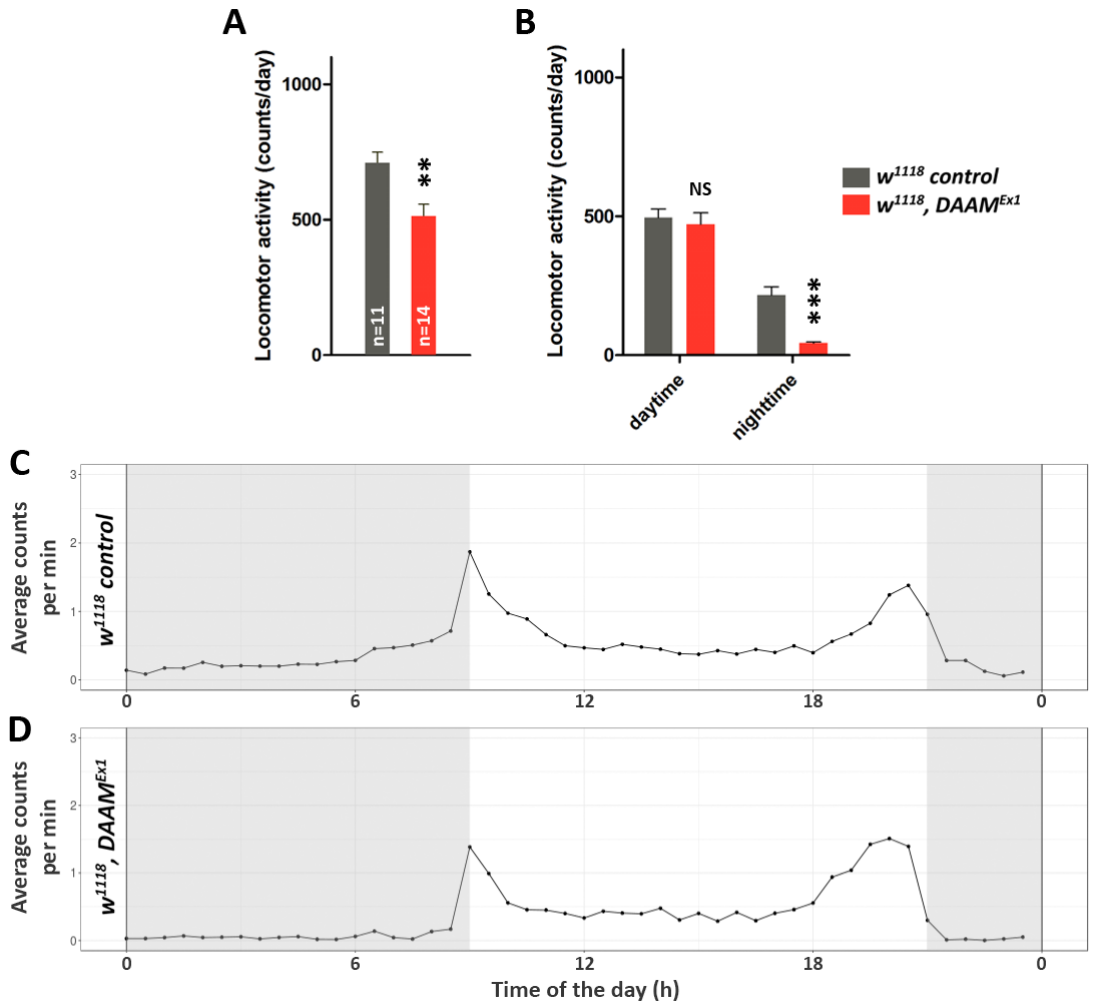

Figure 46. Alterations in the locomotor activity of the *DAAM^{Ex1}* mutant adult flies

(**A-B**) The graphs show the locomotor activity of adult male flies in LD for 5 days (**A**) in total or (**B**) distributed into daytime and nighttime activity, representing the mean of counts per day (mean+SEM). Compared to the control, (**A**) the total activity of the *DAAM^{Ex1}* mutant flies significantly decreases (P=0.0031), moreover, (**B**) this phenomenon comes mainly from the significantly less nighttime activity of these flies (P=0.0002). The daytime activity of the *DAAM^{Ex1}* mutant flies does not differ from that of the control (P=0.6630). P values were calculated by unpaired t tests, in the case of nighttime activity with Welch's correction since the variances were significantly different. ** P≤0.01; *** P≤0.001; NS, not significant. The n values indicate the number of adult flies that were examined. (**C-D**) Average activity profiles of the *w^{1118}* control and the *DAAM^{Ex1}* mutant adult male flies in LD for 5 days (*w^{1118}*, n=11; *w^{1118}, DAAM^{Ex1}*, n=14). The diagrams represent the average of counts per min, summarised into 30 min bins. White areas indicate the light periods, whereas the dark periods are shown by grey shaded areas. In contrast to the PCP mutants, there are no strong differences in the activity profiles of the control and the *DAAM^{Ex1}* mutant flies, although the decreased nighttime activity of the mutant flies is notable here as well.

To study the effect of DAAM on the sleeping behaviour of the adult flies, we used the same data set that was recorded in the locomotor activity experiment. For data evaluation, sleep state was defined as a minimum of 5 contiguous minutes of inactivity. Our results showed that the loss of DAAM significantly increases the amount of sleep during daytime and nighttime as well, however this difference is more evident in the nighttime sleep (**Fig. 47 A-B**). This finding is different from the ones for the PCP mutant flies since the loss of Stbm, Pk and Fz increases the amount of daytime sleep. In addition, the $DAAM^{Ex1}$ mutants exhibit significantly longer but fewer sleep episodes than the w^{1118} control flies (**Fig. 47 C-D**). Similarly to the activity profile, the sleep profile of the $DAAM^{Ex1}$ mutants do not show strong differences compared to that of w^{1118} flies. Although the diagram displays the increased amount of nighttime sleep, the sleep minima do not differ considerably, neither at ZT0 nor at ZT12, compared to the control (**Fig. 47 E-F**).

Together, these data show that the loss of DAAM alters the locomotor activity and sleeping behaviour of the adult flies, but surprisingly, the effect of DAAM is not similar to that of the PCP proteins. First, PCP proteins affect activity and sleep mainly during the daytime, whereas DAAM has an impact typically during the nighttime. Moreover, *stbm*, *pk* or *fz* mutant flies fail to wake up at light onset and display a strongly disrupted morning activity, however, the *DAAM* mutants exhibit no major changes in their morning activity. These results suggest that DAAM is unlikely to mediate the effect of the PCP proteins in these events, although it has a clear contribution to the regulation of these processes – presumably due to independent pathways from PCP signalling.

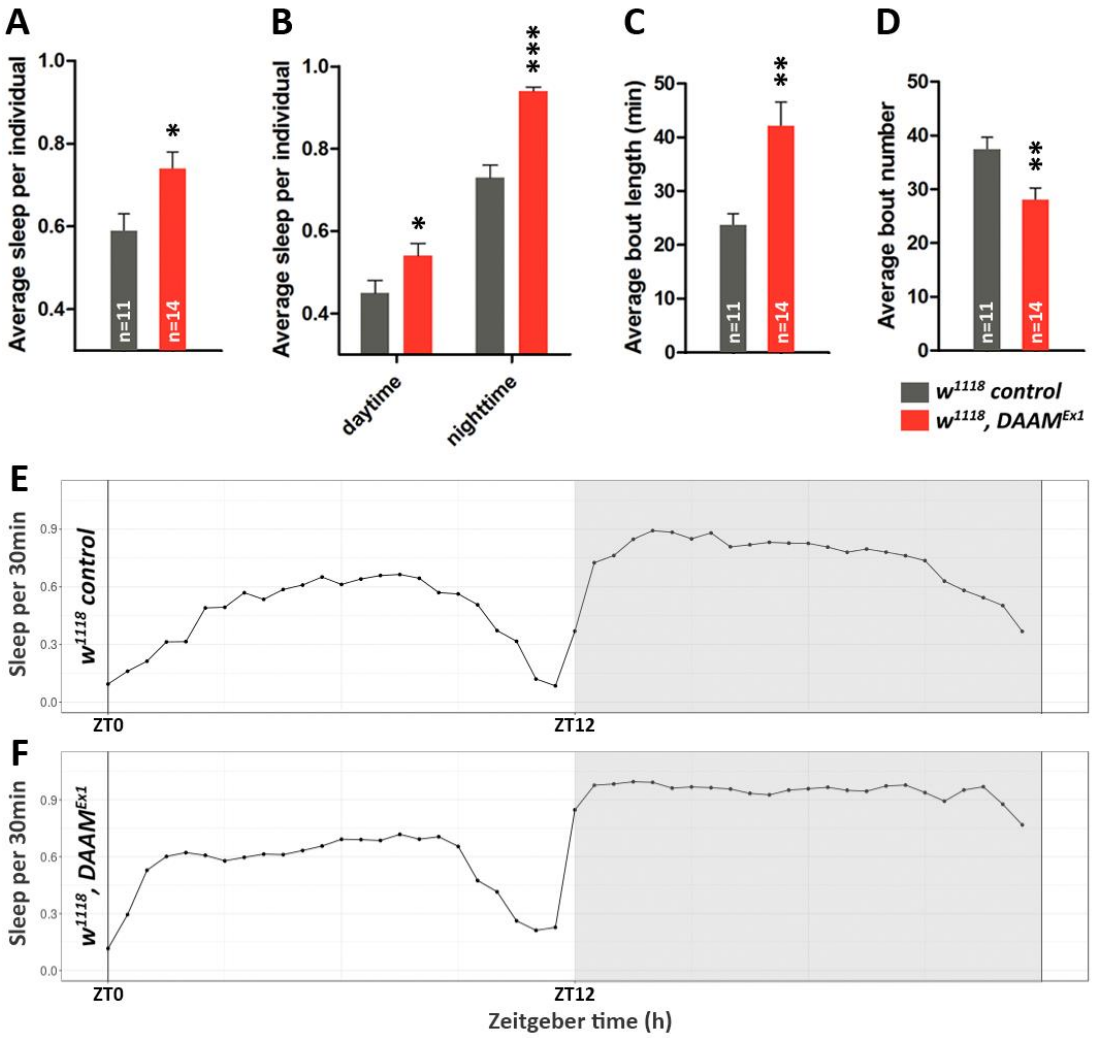

Figure 47. The loss of DAAM affects sleep in adult flies

(**A-B**) The graphs show the amount of sleep in LD for 5 days (mean+SEM). Compared to the control, *DAAM^{Ex1}* mutant flies display a significantly higher amount of sleep (**A**) in total (P=0.0156) and (**B**) during the daytime (P=0.0479) and nighttime (P<0.0001) as well. (**C-D**) Quantification of the length and the number of sleep episodes. *DAAM^{Ex1}* mutant flies present significantly longer (P=0.0012) and less (P=0.0065) episodes than the *w^{1118}* control. All P values were calculated by using unpaired t tests, in the case of nighttime sleep and episode length with Welch's correction. * P≤0.05; ** P≤0.01; *** P≤0.001. The n values indicate the number of adult flies that were studied. (**E-F**) Average sleep profiles of the adult male flies in LD for 5 days (*w^{1118}*, n=11; *w^{1118}, DAAM^{Ex1}*, n=14), representing the amount of sleep per 30 min. White areas indicate the light periods (start at ZT0), whereas grey shaded areas show the dark periods (start at ZT12). In contrast to the PCP mutant flies, the activity profile of the *DAAM^{Ex1}* mutants do not change drastically compared to the control, however an increased amount of nighttime sleep is detectable in these flies.

4. 6. 4. The role of DAAM in neuronal cytoskeleton regulation in primary cell cultures

To further investigate the possibility that DAAM may act as an effector molecule downstream of the core PCP machinery, we examined whether the loss of DAAM leads to similar changes to that of the PCP proteins in primary cell cultures. To this end, we studied both the actin and the MT cytoskeleton of cultured neurons by using the previously described readouts in *DAAM* loss of function mutant neurons.

4. 6. 4. 1. DAAM has an important role in controlling the neuronal actin cytoskeleton

Previous studies have shown that DAAM is present in cultured primary neurons and it shows a punctate localisation along the axon, in the GC and in filopodia. Moreover, by examining $DAAM^{mat/zyg}$ mutant neurons, these studies also proved that the loss of DAAM affects filopodia formation and results in the reduction of filopodia number and length [64, 203, 241]. In order to further investigate the role of DAAM in actin cytoskeleton regulation we used the hypomorphic $DAAM^{Ex1}$ mutant allele in homozygosis, and studied filopodia formation and GC morphology in our experiments.

We found that $DAAM^{Ex1}$ mutant neurons exhibit significantly less filopodia than the w^{1118} control neurons (**Fig. 48 B**). Furthermore, there are significantly more neurons with pointed GCs in the $DAAM^{Ex1}$ mutant cell cultures than in the control (**Fig. 48 D**). Beyond that these results are in agreement with the above mentioned findings regarding the function of DAAM in filopodia formation, they also show that the loss of DAAM affects filopodia number and GC morphology similarly to that of the PCP proteins, suggesting that DAAM may mediate the impact of the PCP proteins in these contexts.

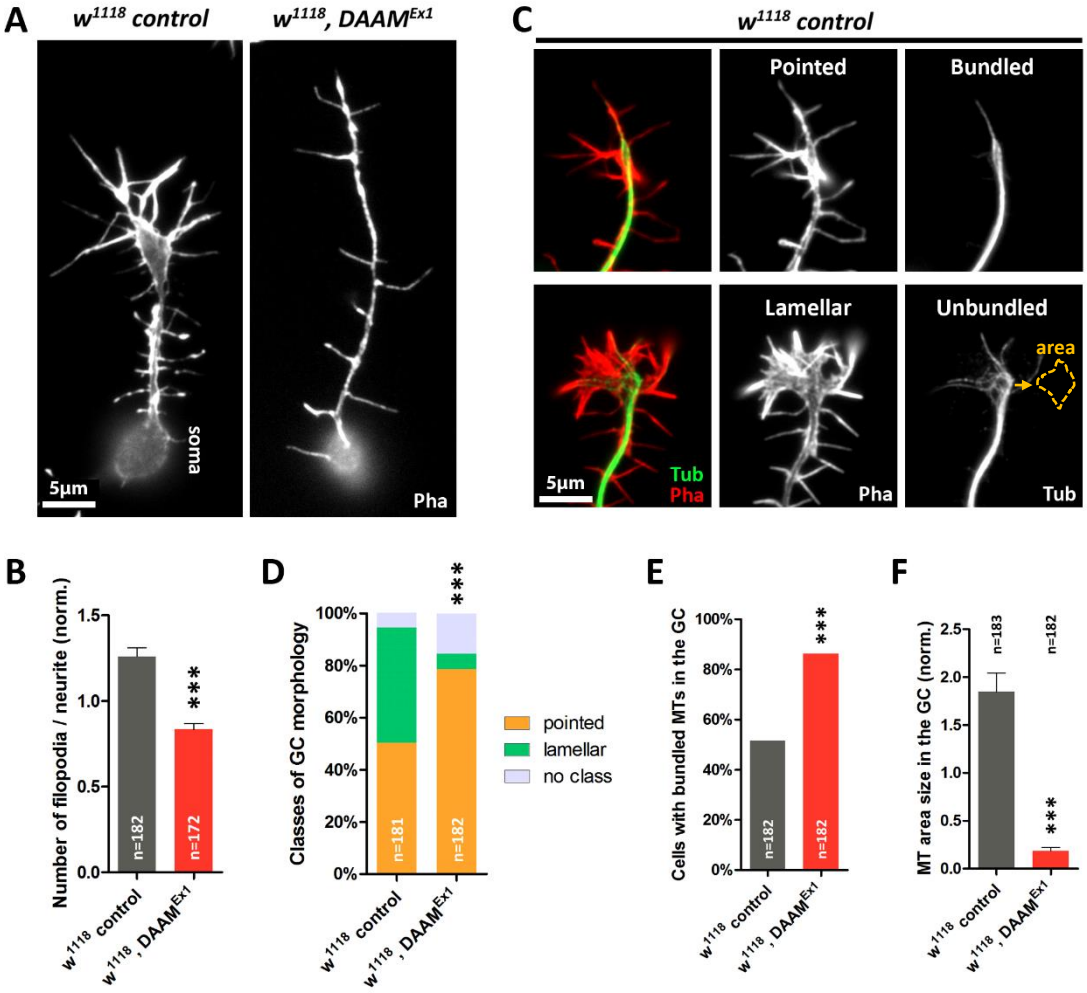

Figure 48. The loss of DAAM affects the neuronal cytoskeleton in primary cell cultures

(**A**) Images of neurons in primary cell cultures after 6 hours of incubation, stained with anti-Phalloidin (Pha) antibody to label F-actin along the axon. Compared to the control (left), the loss of DAAM decreases filopodia number in cultured neurons (right). (**B**) Quantification of the number of filopodia per neurite (mean+SEM) in cultured neurons. D'Agostino-Pearson tests were used to test whether data sets are normally distributed: w^{1118}, P<0.0001; $DAAM^{Ex1}$, P<0.0001. $DAAM^{Ex1}$ mutant neurons display significantly less filopodia than w^{1118} control neurons: P<0.0001 (Mann Whitney U test). (**C**) Images of GCs in primary cell culture after 6 hours of incubation demonstrating both the actin and MT cytoskeleton (left). MTs were visualised by α-Tubulin (Tub) staining, while F-actin was labelled with Phalloidin (Pha). The actin cytoskeleton of the GCs is shown separately in grey (middle panel), representing the "pointed" and "lamellar" categories that were used for GC morphology analysis. Images on the right display only the MT cytoskeleton of the GCs in grey, representing the "bundled" and "unbundled" MT organisational categories. The orange dashed shape indicates the area that is occupied by MTs in the GC, and was measured for statistical analysis. (**D**) Quantification of the neurons with pointed or lamellar GCs in primary cell cultures. As it is shown in the diagram, there are significantly more neurons with pointed GCs in the $DAAM^{Ex1}$ mutant cell cultures than in the control: P<0.0001 (chi-square test). (**E**) The percentage of cells with bundled MTs

in the GC is shown by the graph, which is significantly higher in the *DAAM*^{Ex1} mutant cell cultures than in the control: P<0.0001 (Fisher's exact test). In addition, (**F**) compared to the *w*^{1118} control, the size of the area that is covered by MTs in the GC is also significantly smaller in the *DAAM*^{Ex1} mutant neurons: P<0.0001 (Mann Whitney U test). Data are presented as mean+SEM in the graph; and the normality of the data sets was analysed by D'Agostino-Pearson tests: *w*^{1118}, P<0.0001; *DAAM*^{Ex1}, P<0.0001. In every graph (**B**, **D-F**), the n values indicate the number of examined neurons. *** P≤0.001. Although the graphs show normalised data in (**B**) and (**F**), the *w*^{1118} control does not appear to be 1 since all conditions were normalised to the *Oregon-R* control.

4. 6. 4. 2. DAAM is a key regulator of neuronal MTs as well

Although formins are primarily known as actin assembly factors, recent studies have shown that some formins are important in the crosstalk between actin and MTs, moreover, there are some formins that are able to directly regulate MT organisation and stability as well [45, 239, 242-244]. In addition, it was also found that many formins can bind MTs *in vitro* [45, 242, 243, 245-247]. While DAAM has clearly been shown to be able to facilitate actin nucleation and elongation, it was not known whether DAAM regulates any features of MTs as well, particularly in neurons. To address this, we first investigated whether the loss of DAAM impairs the organisation of the neuronal MT cytoskeleton in primary cell cultures by using the hypomorphic *DAAM*^{Ex1} allele.

Our results demonstrated that the loss of DAAM strongly alters MT organisation in cultured neurons. There are significantly more neurons with bundled MTs in the *DAAM*^{Ex1} mutant cultures than in the control. Moreover, the size of the area that is occupied by MTs in the GC is significantly smaller in the *DAAM*^{Ex1} mutant neurons (**Fig. 48 E-F**). These findings suggest that DAAM plays a role in controlling MT organisation, and most likely this could be one of the mechanisms whereby it contributes to axon growth regulation in cultured neurons.

After we established that MT organisation is strongly altered in the *DAAM* mutant neurons, we continued our investigations to examine whether the loss of DAAM affects MT dynamics and/or stability. An important property of MTs that greatly controls the growth of axons is their dynamic state, and in particular, the speed at which MTs polymerise. To study MT dynamics, we used a GFP-tagged form of EB1 (EB1::GFP). EB1 is a well-known MT-binding protein that localises to the plus end of the MTs, therefore, by expressing its GFP-tagged form, we are able to follow the dynamics of the MT plus ends. EB1::GFP was driven by the neuron-specific *elaV-Gal4* driver in cultured neurons, both in control and $DAAM^{Ex1}$ mutants, and live movies of neuronal GCs were taken after 6 hours of incubation. **Figure 49 A** is a sequence of images from a movie showing the movements of the EB1::GFP puncta in the GC of a control neuron. We found that the loss of DAAM significantly increases the velocity of EB1::GFP comets as compared to the control (**Fig. 49 B**), which suggests that DAAM regulates MT growth velocity in primary neuronal cell cultures.

In addition, to study the role of DAAM in controlling MT stability, cultured neurons were treated either with the MT destabilising drug Nocodazole (100μM) or with vehicle (DMSO) for 4 hours, following the overnight incubation of primary cell cultures at 22˚C. In this experiment, both $DAAM^{Ex1}$ and $DAAM^{mat/zyg}$ mutant cell cultures were examined and we found that DAAM stabilises MTs against Nocodazole treatment. Compared to the DMSO-treated cells, neurons display several gaps in the axonal MT shaft after Nocodazole treatment (**Fig. 50 A-B'**). The number of these gaps is significantly higher in both $DAAM^{Ex1}$ and $DAAM^{mat/zyg}$ mutant neurons after Nocodazole treatment, whereas the loss of DAAM does not induce gap formation in neurons treated only with DMSO (**Fig. 50 C-D**). These findings indicate that the presence of DAAM in cultured neurons is necessary to protect MTs against the effect of Nocodazole, further supporting the view that DAAM is responsible to control MT stability in primary cell cultures. These data contributed to the following publication: Szikora et al. 2017 Journal of Cell Science.

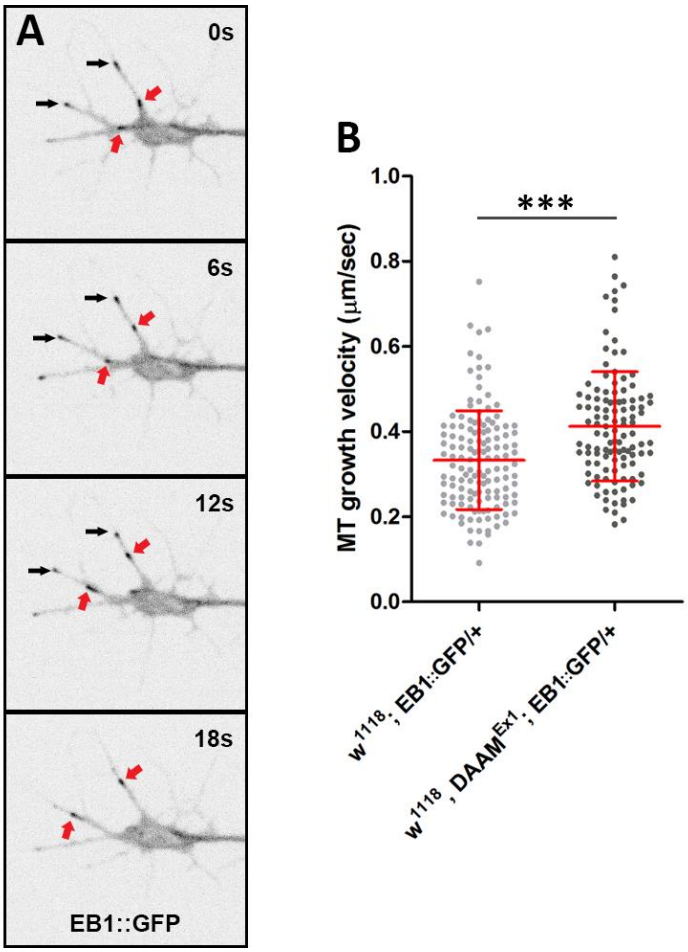

Figure 49. The loss of DAAM alters MT dynamics in cultured neurons

(**A**) Series of images from a live movie showing EB1::GFP comets in the GC of a neuron after 6 hours of incubation in primary cell culture. Red arrows point to comets that move anterogradely along filopodia, whereas black arrows indicate fairly static EB1::GFP puncta at filopodia tips. (**B**) Quantification of MT growth velocity: scatter plots represent the mean growth velocity (mean±SD) of EB1::GFP comets in the GC of *w*^{1118} control and *DAAM*^{Ex1} mutant cultured neurons showing that, the loss of DAAM significantly increases MT growth velocity ($P<0.0001$, Mann-Whitney U test). D'Agostino-Pearson normality tests were used to see whether data sets are normally distributed (*w*^{1118}*; EB1::GFP/+*, $P=0.0005$, n=138; *w*^{1118}, *DAAM*^{Ex1}*; EB1::GFP/+*, $P=0.0014$, n=114). *** $P\leq0.001$.

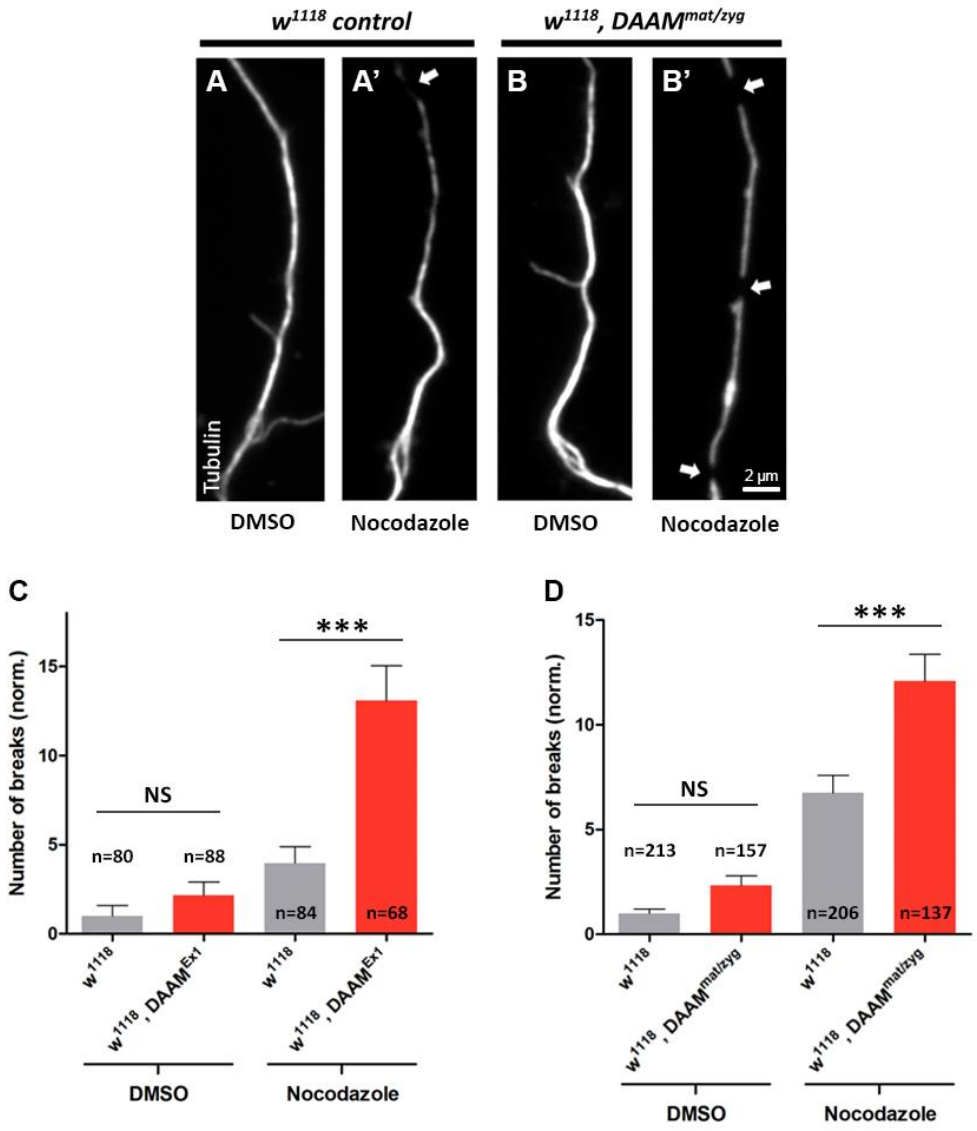

Figure 50. DAAM stabilises MTs in primary neuronal cell cultures

(**A-B'**) Images of axon segments of cultured neurons after 16 hours of incubation at 22˚C, stained with α-Tubulin antibody to label MTs. In the last 4 hours of incubation neurons were treated (**A'-B'**) either with 100µM Nocodazole (**A-B**) or with vehicle (DMSO). As it is shown in the figure, (**A'-B'**) Nocodazole treatment leads to gap formation along the axonal MT shaft (indicated by white arrows). (**C-D**) Quantification of breaks in the axonal MT shaft of the *DAAM*^{Ex1} and *DAAM*$^{mat/zyg}$ mutant neurons in primary cell cultures (mean+SEM). Compared to the *w*^{1118} control, Nocodazole treatment significantly increases the number of breaks in both *DAAM* mutants. In addition, the loss of DAAM does not induce gap formation in DMSO-treated neurons which suggests that, DAAM is responsible for stabilising MTs against Nocodazole treatment in cultured neurons. (**C**) D'Agostino-Pearson tests were performed to test whether data sets are normally distributed: *w*^{1118} DMSO, P<0.0001; *w*^{1118} Nocodazole, P<0.0001; *DAAM*^{Ex1} DMSO, P<0.0001; *DAAM*^{Ex1} Nocodazole, P=0.0083. Data sets were compared and P values were calculated by Kruskal-Wallis test (P<0.0001), followed by Dunn's multiple comparisons tests: *w*^{1118} DMSO vs. *w*^{1118} Nocodazole, P=0.0339; *DAAM*^{Ex1} DMSO vs.

DAAM^{Ex1} Nocodazole, P<0.0001; *w*^{1118} DMSO vs. *DAAM*^{Ex1} DMSO, P>0.9999; *w*^{1118} Nocodazole vs. *DAAM*^{Ex1} Nocodazole, P<0.0001 (multiplicity adjusted P values). (**D**) The normality of data sets was tested by D'Agostino-Pearson tests: *w*^{1118} DMSO, P<0.0001; *w*^{1118} Nocodazole, P<0.0001; *DAAM*$^{mat/zyg}$ DMSO, P<0.0001; *DAAM*$^{mat/zyg}$ Nocodazole, P<0.0001. Data sets were compared by Kruskal-Wallis test (P<0.0001), and P values were calculated by Dunn's multiple comparisons tests: *w*^{1118} DMSO vs. *w*^{1118} Nocodazole, P<0.0001; *DAAM*$^{mat/zyg}$ DMSO vs. *DAAM*$^{mat/zyg}$ Nocodazole, P<0.0001; *w*^{1118} DMSO vs. *DAAM*$^{mat/zyg}$ DMSO, P=0.5646; *w*^{1118} Nocodazole vs. *DAAM*$^{mat/zyg}$ Nocodazole, P<0.0001 (multiplicity adjusted P values). *** P≤0.001; NS, not significant. The n values indicate the number of neurons that were investigated both in (**C**) and (**D**).

4. 6. 4. 3. Axon growth is strongly altered in the absence of DAAM

As it was described above, the loss of DAAM leads to considerable changes in both the actin and MT cytoskeleton of cultured neurons, proposing that axon growth might be affected as well. To test this, we measured axon length in primary cell cultures, and found that neurons derived from *DAAM*^{Ex1} mutant embryos exhibit significantly longer axons than the control neurons (**Fig. 51**). This finding suggests that DAAM contributes to axon growth, moreover, since the loss of DAAM increases axon length similarly to that of the PCP proteins, it is possible that DAAM acts as a downstream effector of the signalling pathway and mediates the impact of the PCP proteins on axon growth.

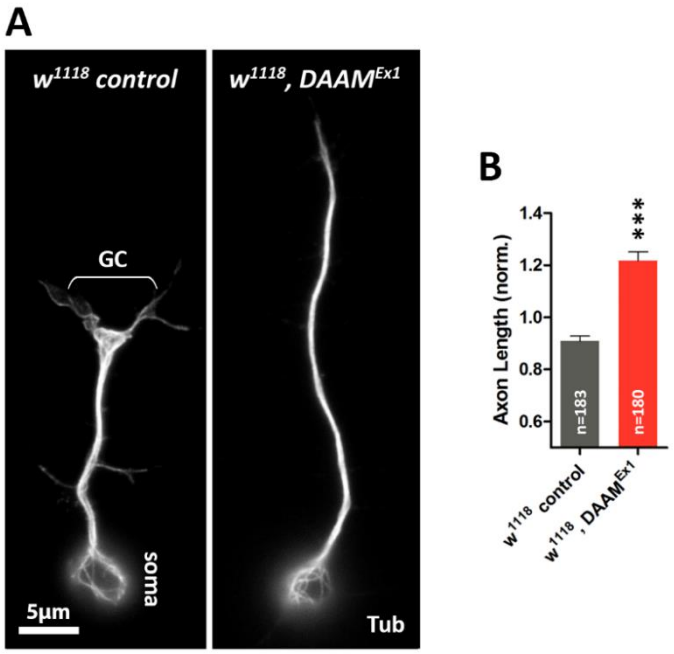

Figure 51. The loss of DAAM strongly increases axon length

(**A**) Images of neurons in primary cell cultures after 6 hours of incubation stained by α-Tubulin (Tub) antibody to visualise MTs along the axon and in the GC. Compared to the control (left), *DAAM*^{Ex1} mutant neurons display longer axons in which MTs show a simpler and more bundled organisation (right). GC, growth cone. (**B**) Quantification of axon length. D'Agostino-Pearson tests were used to analyse whether the data sets are normally distributed: *w*^{1118}, P<0.0001; *DAAM*^{Ex1}, P<0.0001. Axons are significantly longer in the *DAAM*^{Ex1} mutant neurons than in the control: P<0.0001 (Mann Whitney U test). *** P≤0.001. The n values indicate the number of neurons that were examined. Despite the fact that the data shown in the graph is normalised, the *w*^{1118} control is not equal to 1 since all conditions were normalised to the *Oregon-R* control.

5. Summary and Discussion

5. 1. Stbm, Fz, Dsh and Fmi regulate axon growth in the *Drosophila* embryonic nervous system

Involvement of the PCP proteins in controlling axon growth have been shown in many studies from vertebrates to *Drosophila* (for details see Introduction, chapter 1. 2. 4.), although their exact role remained elusive in most cases. In the *Drosophila* embryo, *fmi* was found to interact with *pk* to control the axonal advance of peripheral sensory neurons [173, 174] but other PCP components have not been reported in such mechanisms.

Our investigation revealed that Stbm, Fz, Dsh and Fmi are strongly enriched in the neuropil region of the VNC in stage 16 embryos. Although we were not able to detect the presence of Pk along the VNC axons, it displays a punctate localisation in the cortex suggesting that Pk may form aggregates in the cell bodies of the VNC neurons. By contrast, we found no evidence for Dgo expression in the VNC. Beyond the VNC, our examination also revealed that Stbm, Fz, Dsh and Fmi are present in the ISNb motor nerves, albeit Stbm and Fz display a slightly weaker expression level than that of Dsh and Fmi. Opposite to this, Pk and Dgo are not detectable in these nerves. Together these findings show that four of the core PCP members, such as Stbm, Fz, Dsh and Fmi, are present both in the VNC axons and in the peripheral ISNb nerves suggesting that these proteins might be involved in controlling the development of these axons.

Interestingly, we found that the loss of the PCP proteins led to axon growth or guidance defects only in two cases in the VNC. $stbm^{6}$ mutants exhibit discontinuities of longitudinal axon tracts, whereas fmi^{192} mutant embryos show axon guidance

problems. Thus, these effects seem to be specific to Stbm and Fmi, since the other PCP mutants do not display any differences compared to the control.

In addition, we were able to demonstrate that some PCP proteins influence the growth of the ISNb nerves in the embryo. Out of the three studied peripheral motor nerves, ISNb-s show a strong axon stalling phenotype in the absence of Dsh or Fmi. This result is in agreement with our previous findings that Dsh and Fmi are strongly expressed in the ISNb-s of wild type embryos, therefore their absence in the mutants could explain the early stalling of these nerves. Besides that, the loss of Fmi leads to a similar ISNb stalling phenotype than that of Dsh, fmi^{192} mutants exhibit much thinner ISNb nerves, suggesting that a subset of motor axons stall in an even earlier stage of growth in these mutants. A previous study has shown that, other peripheral motor nerves also become much thinner and display growth defects upon the loss of Fmi [173], which suggests that Fmi may have an additional, PCP-independent role in axon growth regulation.

Although the ISNb nerves display normal morphology in $stbm^{6}$ and $fz^{K21/R52}$ mutant embryos, it is possible that Stbm and Fz are also involved in controlling the growth of these nerves, but it may not be detectable for some reasons, especially because both proteins are present in the peripheral motor nerves. To address this question, we performed genetic interaction tests and found that $stbm^{6}; fz^{k21}$/+ and $stbm^{6}$/+; $fz^{K21/R52}$ double mutant embryos exhibit the same ISNb stalling phenotype, although with a lower degree than Dsh or Fmi. Therefore, we can assume that *stbm* and *fz* genetically interact with one another and act redundantly in this process. Based on our recent data, we can hypothesize further possibilities regarding to the interactions between *stbm*, *fz* and *dsh*. Since the lack of either Stbm or Fz is insufficient to induce ISNb nerve growth defects, and frequency of the ISNb stalls is lower in the double mutants than in the dsh^{1} mutant embryos, it is possible that Dsh is downstream of Stbm and Fz, and may gather signalling information from both proteins (**Fig. 52**). This situation would be very similar to what we know about the signalling mechanisms of the core

PCP components, and further genetic interaction tests are planned to investigate it in more details.

5. 2. DAAM may mediate the effect of PCP proteins on ISNb nerve growth

Similarly to Stbm, Fz, Dsh and Fmi, we found that the formin DAAM is also important for controlling the growth of the ISNb motor nerve. The loss of DAAM induces a very similar ISNb stalling phenotype than that of the above mentioned PCP proteins, which suggest that DAAM may act in concert with these proteins to regulate axon growth in the ISNb nerve. Vertebrate studies showed that Dvl (a Dsh ortholog) and Daam1 (a DAAM ortholog) directly interact with one another, and that Dvl activates Daam1 by binding to its C-terminal autoinhibitory domain [116, 235]. In addition, it was also suggested by a recent study in *Drosophila* that DAAM acts downstream of Dsh to control axon growth in the adult mushroom body [177]. By analogy with those findings, we propose a mechanism in which PCP proteins regulate the activity of DAAM, through its interaction with Dsh, to control ISNb nerve growth (**Fig. 52**).

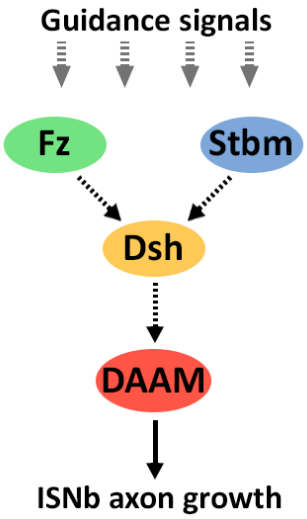

Figure 52. Hypothetical model for Wnt/PCP signalling, through DAAM, in ISNb axon growth

The 7-pass transmembrane protein Fz serves as the receptor of Wnt/PCP signalling [136, 137] and most likely receives guidance cues for the growth of ISNb axons. Based on our findings we propose that Fz and Stbm is likely to act redundantly, upstream of Dsh which may convey signalling information from both proteins. Presumably Dsh controls the activity of DAAM, through their interaction demonstrated before [116, 186, 236], which probably acts as a downstream effector of the signalling pathway and regulate ISNb axon growth.

5. 3. Fz, Stbm, Pk and Fmi are responsible for guiding LN_v axons *in vivo* in the *Drosophila* brain

We found that LN_v neurons show severe guidance problems in *fz*, *stbm*, *pk* and *fmi* mutants as demonstrated by the appearance of ectopic LN_v axons defasciculating from the main axonal tracts and projecting to the dorsomedial section of the adult brain. The frequency of these ectopic axons is significantly higher in the $fz^{K21/R52}$, $stbm^{6}$, pk^{30} and fmi^{frz3} mutant brains than in controls suggesting that all these four PCP proteins are essential for the guidance of the LN_v axons. Surprisingly, LN_v axons display no guidance defects in dsh^{1} mutant brains, instead, it seems like the loss of

Dsh may have an opposite effect than that of the other PCP components since *dsh*^{1} mutants exhibit even less ectopic axons than the control brains.

Ectopic LN_v axons originate from three different regions specifically: (1) from the dorsal terminals of s-LN_vs, (2) from the middle section of s-LN_vs and/or (3) from the axonal fascicles of l-LN_v neurons. Interestingly, PCP mutant brains show a relatively clear tendency and can be classified based on the types of origin of LN_v axons. In the absence of Fz or Fmi, most ectopic axons come from the dorsal terminals of the s-LN_vs and from the l-LN_vs, whereas in *stbm*^{6} mutant brains they defasciculate typically from the middle section of the s-LN_v neurons and from the l-LN_vs. Finally, although the *pk*^{30} mutants do not show a clear preference amongst these three types, there is a notable increase in the number of misguided axons from the middle section of the s-LN_vs, similarly to *stbm*^{6} mutants. These findings suggest that Fz-Fmi and Stbm-Pk may form functional subgroups which have slightly different roles in controlling LN_v axon guidance (summarised in **Fig. 53**).

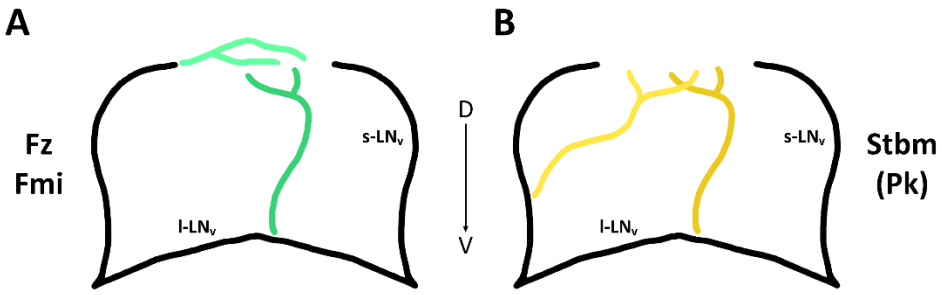

Figure 53. Schematic diagram of LN_v axon guidance defects

Schematic drawings show the stereo-typical axonal pattern of s-LN_v and l-LN_v neurons in black. Ectopic LN_v axons (in colour) target the dorsomedial brain typically. Although, Fz, Fmi, Stbm and Pk are all required for proper LN_v axon guidance, their contribution seems to be slightly different based on the origin of ectopic axons. Besides that, misguided axons from l-LN_vs are presented with a high degree in each case, (**A**) the loss of Fz and Fmi also promotes ectopic axon formation from the dorsal terminals of s-LN_vs, (**B**) whereas the loss of Stbm and Pk induces ectopic axon formation from the middle section of s-LN_vs as well.

LN_v neurons start to grow axons during the larval life and finish their development by the end of the pupal stage [214], thus they can fulfil their function in the freshly hatched imago. In this study, we investigated 3-4 days old and 7-8 days old adult flies and found that the LN_v axons show the same tendencies and display quite similar axon guidance phenotypes in both age groups upon the loss of the PCP proteins. These observations support that these ectopic axons are not only temporary structures in the adult brain. Most likely they are formed during development, together with the other LN_v axons, and presumably are maintained throughout the entire life of the flies.

In addition, we were able to detect a phenomenon which appears to be independent from the previously described axon guidance defects, and that is specific to Fmi. Normally, cell bodies of most l-LN_v neurons are localised ventrally, close to the origin of the s-LN_vs, however, in the *fmi*^{frz3} mutant brains many of them are positioned dorsally. Additionally, some of these dorsal neurons display ectopic axons growing towards the dorsomedial brain. Since these phenotypes can only be observed in the absemce of Fmi, it suggests that, similarly to the embryonic role of this protein, Fmi may have additional PCP-independent functions in these neurons.

In summary, for the first time we show that Fz, Stbm, Pk and Fmi are necessary for proper guidance of the LN_v axons *in vivo* in the *Drosophila* brain. Nevertheless, there are a couple of important questions that we could not answer at this level of the analysis. First, in spite of that ectopic axons originate from different regions, we were not able to distinguish whether these axons come from the s-LN_v neurons or the l-LN_v neurons or both. Moreover, it would also be interesting to know whether the PCP proteins act cell-autonomously in the LN_v neurons, for instance by receiving and transmitting guidance signals from the environment, or we revealed non-cell-autonomous effects. To address these questions, currently we are using several RNAi constructs of the PCP components and different LN_v-, s-LN_v- and l-LN_v-specific drivers

to silence the PCP genes specifically in these neurons. Furthermore, we are also studying PCP protein localisation in the LN_v neurons.

5. 4. LN_v axon targeting appears to be independent from DAAM

Although we found that DAAM may mediate the effect of the PCP proteins on ISNb nerve growth in the *Drosophila* embryo, and it was shown previously to act in cooperation with the PCP proteins to regulate axonal growth and guidance of the mushroom body neurons in the adult brain [177], LN_v axon guidance remains unaffected in the absence of DAAM. There is no significant difference in the frequency of the ectopic LN_v axons between the $DAAM^{Ex1}$ mutant and control flies. Although $DAAM^{Ex1}$ is a hypomorphic mutant allele, this mutation was shown to strongly reduce the level of DAAM in the *Drosophila* brain. Moreover, this allele has been successfully used in genetic studies for the characterisation of axon morphological defects [177, 203], therefore we conclude that DAAM is unlikely to contribute to LN_v axon guidance during neuronal development. Consequently, the PCP proteins most likely act independently of DAAM in this process.

5. 5. Stbm, Fz and Pk are necessary for the morning arousal of adult *Drosophila* most likely by regulating the guidance of LN_v axons

LN_v neurons are essential regulators of the morning sleep/wake transition during the circadian cycle of *Drosophila* [209-213], therefore the severe axon guidance problems present in the PCP mutants indicated that these flies may exhibit an aberrant morning behaviour. We found that the presence of ectopic axons strongly correlates with altered locomotor activity and sleep. In agreement with their axon misguidance phenotypes, adult flies are less active and spend more time in sleep during the daytime in the absence of Stbm, Pk or Fz. Accordingly, these flies also show differences in the duration and the number of sleep episodes as $stbm^{6}$ and $fz^{K21/R52}$ mutants display longer episodes (with unaltered episode number), whereas pk^{30} mutants exhibit more episodes (with no change in duration) than the control flies. Interestingly, Fmi is an exception in this case because although the number of ectopic LN_v axons increases in the fmi^{frz3} mutants, these flies display no changes in any of these parameters. In addition to this, the analysis of the activity and sleep profiles of the PCP mutant flies revealed other abnormalities. $stbm^{6}$, $fz^{K21/R52}$ and pk^{30} mutant flies exhibit an extended sleep state during the night and fail to properly wake up at light onset. According to it, the morning activity of these flies is also strongly disrupted. By contrast, fmi^{frz3} mutants show only weak alterations in their activity and sleep profiles. Together these findings suggest that the altered locomotor activity and sleep of adult flies most likely appears as a consequence of the LN_v axon guidance problems, induced by the absence of Stbm, Fz and Pk.

The *Drosophila* circadian clock is regulated by several groups of neurons, out of which the LN_vs are responsible for controlling the sleep-wake transition and the morning activity of the flies. In response to light, LN_v neurons start to express and

secret the neuropeptide PDF which serves as a wake-promoting signal and induces arousal, however, s-LN_v and l-LN_v neurons have different roles in this process. s-LN_vs are morning pacemakers that specifically control the morning anticipatory activity before light onset, whereas the l-LN_vs become activated upon light exposure and provoke arousal by inhibiting sleep and activating the motor control centre in the brain [213, 218-221, 248, 249]. Based on these, our findings can be explained by the lack of both s-LN_v and l-LN_v functions. The extended sleep state during the night most likely indicates the loss of s-LN_v anticipatory function. Furthermore, the fact that flies fail to wake up after light onset and stay in sleep, and/or more frequently fall back into sleep during the daytime suggest that l-LN_v functions are also impaired. Collectively, these findings suggest that Stbm, Fz and Pk control locomotor activity and sleep indirectly, unlike the classical regulators of the circadian system. Presumably, the dysfunction of LN_v neurons is caused by the axon guidance problems present in the above described PCP mutants. Ectopic axons project to inappropriate target sites, therefore the original targets loose adequate signals from the LN_v neurons. The downstream targets of the LN_vs are largely unknown, nevertheless it was shown that PDF secretion inhibits sleep-promoting neurons and activates the motor control centre in the *Drosophila* brain [249, 250]. Consequently, loss of the PDF signal at these targets can lead to an impaired sleep-wake transition and decreased arousal (**Fig. 54**).

Because the loss of Dsh seems to reduce the LN_v axon guidance problems, even when compared to the control, it appears likely that Dsh regulates locomotor activity and sleep differently than the other PCP components. In accordance with this, *dsh*^{1} mutant flies exhibit increased activity and less sleep both during the daytime and nighttime, and the loss of Dsh results in an aberration called fragmented sleep, which is defined by the presence of shorter and more sleep episodes. In addition, unlike that of the other PCP mutants, morning activity of the *dsh*^{1} mutants shows no alterations as compared to wild type. Taken together, Dsh clearly seems to have a different role

in controlling activity and sleep. Although the molecular mechanism is elusive, it remains possible that Dsh plays an antagonistic role as to Stbm, Fz and Pk during the regulation of LN_v axon guidance, which leads to opposite changes in the locomotor activity and sleeping behaviour of adult flies.

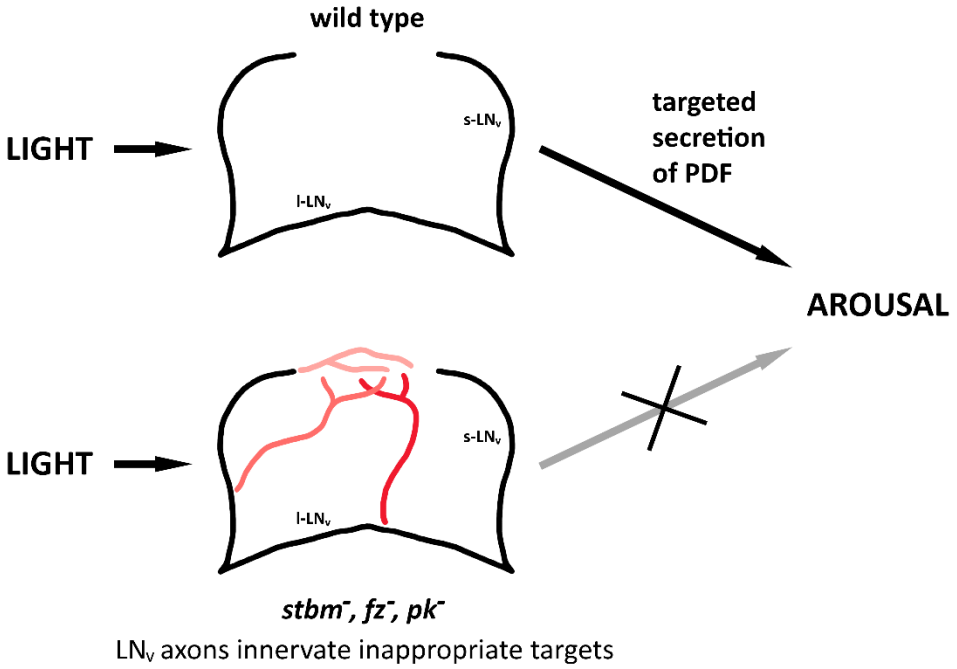

Figure 54. Hypothetical model for the role of PCP proteins in arousal

Due to light exposure LN_v neurons secrete PDF, a wake-promoting neuropeptide, which leads to arousal through the inhibition of sleep and the activation of locomotion. Stbm, Fz and Pk are required for the proper guidance of LN_v axons, therefore the loss of these proteins results in the formation of ectopic LN_v axons that project to inappropriate target sites. Consequently, the original targets of LN_v neurons loose adequate PDF signal which inhibits arousal by enhancing sleep and silencing locomotion.

5. 6. DAAM regulates locomotor activity and sleep independent of the PCP proteins

Interestingly, although DAAM seems not to control guidance of the LN_v neurons, we found that it influences the locomotor activity and sleeping behaviour of the adult flies. In contrast to the PCP proteins, the loss of DAAM results in less activity and increased sleep during the nighttime. In addition, the *DAAM*^{Ex1} mutant flies are characterized by a fairly intact morning activity that is opposite to the PCP mutants. Together, these findings suggest that DAAM contributes to the regulation of locomotor activity and sleep differently than Stbm, Fz, Pk or Dsh, presumably by influencing other groups of pacemaker neurons in the adult brain. Therefore, it is unlikely to mediate the effect of the PCP proteins in the light-induced morning arousal of the flies. With regard to *DAAM*, which might be an interesting novel sleep gene, further studies will be required to investigate whether it has a direct or indirect effect on the locomotor activity of the flies.

5. 7. PCP proteins influence the neuronal actin and MT cytoskeleton in primary cell cultures

PCP proteins are emerging as important regulators of axonal growth across species, yet their mechanism of function and the subcellular processes they regulate remain unknown. In this work we investigated whether PCP proteins act on the neuronal cytoskeleton by studying several parameters of both the actin and MT cytoskeleton in primary neuronal cultures (summarised in **Table 3**).

	GC morphology	filopodia No.	MT organisation	MT area size	axon length
stbm ^{6}	-	-	-	smaller	-
pk ^{30}	-	less	-	smaller	-
pk-sple ^{13}	-	-	more bundled	-	longer
fz $^{K21/R52}$	more pointed	less	more bundled	-	-
fmi ^{192}	-	-	-	-	longer
dsh ^{1}	more pointed	less	less bundled	smaller	longer
DAAM ^{Ex1}	more pointed	less	more bundled	smaller	longer

Table 3. Summary of the phenotypes of PCP and DAAM mutants in culture

The table shows the phenotypes of cultured neurons, derived from PCP and DAAM mutant embryos, related to the actin and MT cytoskeleton and axon growth. "-" signs indicate that cultured neurons display no significant phenotype with the certain mutation.

The actin cytoskeleton in the peripheral zone of the GC is particularly important for determining the directionality of axon extension, and it also contributes to axon growth, through its interaction with MTs [6, 19, 20]. Therefore, examining the actin-rich filopodia and lamellipodia was indispensable to study the potential function of the PCP components. We found that some of the PCP proteins regulate the actin cytoskeleton in cultured neurons. The loss of Fz or Dsh reduces lamellipodia formation in the GC which results in a more pointed GC morphology. In addition, filopodia formation seems to be controlled by Pk, Fz and Dsh since primary neurons exhibit less filopodia in their absence. In contrast to these, the loss of Stbm and Fmi does not affect any of these aspects (**Table 3**). Although *pk*^{30} mutant neurons show no change in GC morphology, Pk may still be important in filopodia formation, whereas Fz and Dsh seem to regulate F-actin both in filopodia and lamellipodia. (**Table 3**).

While the actin cytoskeleton is particularly important for directional growth, axon extension is known to primarily depend on MT function, and it is significantly influenced by the organisation of MTs in the GC [4, 6, 19, 20]. Our results showed

that Stbm, Pk and Fz are likely to contribute to control MT organisation as their loss leads to the reduction of unbundled or spread MTs (**Table 3**). These data suggest that these PCP components may promote polymerisation of the MTs away from the main bundle, and thereby increase the explorative behaviour of the MTs into the GC periphery. This could be achieved by a direct effect on the MTs, which seems to be the case with Stbm, although Sanchez-Soriano and colleges found that defective regulation of the actin cytoskeleton leads to hyper-bundled MTs in the GC [14]. Therefore, it is possible that the impact of the PCP components on MTs is mediated by their role in actin regulation in some cases.

In spite of that, we found subtle changes in the actin and MT cytoskeleton with the applied readouts it is still possible that the PCP proteins have an important role in controlling cytoskeletal changes in neurons, which could be explained by the potential functional redundancy between these proteins. To address this question, we are currently performing genetic interaction tests with double mutant combinations of the PCP components.

Finally, the loss of Pk, Fmi and Dsh leads to an increase in net axon growth in cultured neurons (**Table 3**). Since the PCP proteins, except Stbm and Fmi, seem to affect both the actin network and the MTs in cultured neurons, they could possibly contribute to axon growth regulation through both cytoskeletal components. For instance, Pk and Dsh affect several parameters of the actin and the MT cytoskeleton as well, and for this reason increased axon length could be a result of a cumulative impact in these cases. Conversely, the example of Fmi represents a different situation again as it regulates axon growth, but seems not to be involved in controlling the neuronal cytoskeleton. In addition to these, it is important to mention that the slight changes in axon length of the PCP mutant neurons can be explained by a technical limitation of primary cell cultures. In cell culture, neurons are in an *in vitro* environment where they lack the proper guidance cues that would be provided in a tissue *in vivo*. Considering that essential signals of the Wnt/PCP pathway are likely to be absent

from the culture system, the effect of PCP loss of function on axon growth may only be partially detected by examining individual PCP mutant neurons.

Compared to our *in vivo* findings, it appears contradictory that the loss of the PCP components leads to stalled axons and pathfinding defects *in vivo* but lengthening of the axons in culture. Nonetheless, a similar finding was reported for mutations in several actin regulators which also induced shortening *in vivo* and increased axonal length *in vitro* [14]. These similarities suggest that PCP function on axonal growth could be achieved through the regulation of the actin cytoskeleton.

5. 8. DAAM is essential for controlling actin and MTs in primary neurons, and possibly mediates the effect of the PCP proteins

Although the formin family member, DAAM was already known to regulate the neuronal actin cytoskeleton in primary cell cultures [203], it has not been reported to control MTs in neurons before. Our investigation revealed that DAAM strongly affects both the actin and MT cytoskeleton as judged by our major readouts. Moreover, the alterations that were caused by the loss of DAAM follow the same tendencies that we observed in the PCP mutants. Primary neurons, derived from *DAAM*^{Ex1} embryos, display more pointed GCs and less filopodia along the whole axon suggesting that DAAM is particularly important for controlling F-actin both in filopodia and lamellipodia. In addition, we found that DAAM is essential for organising the neuronal MTs as well since its loss leads to a drastic decrease of the unbundled and/or spread MTs in the GC, and results in the formation of a compact MT shaft at the axonal tips. Accordingly, axon growth is strongly altered and neurons exhibit significantly longer axons in the absence of DAAM (**Table 3**). Based on these findings, DAAM appears to play a very similar role in GCs as the PCP proteins, raising the possibility that it

may act in concert with the PCP components and may be an important factor in mediating their effect on the neuronal cytoskeleton.

Interestingly, DAAM seems to affect the actin and MT cytoskeleton much stronger than the PCP proteins. If we hypothesise that DAAM act as a downstream effector protein of the Wnt/PCP signalling cascade, as it was suggested before [177, 235], it could be explained by a possible redundant function of the PCP proteins in controlling the activity of DAAM. In this scenario, the absence of only one PCP component would not lead to a drastic change as strong as the loss of DAAM. Another alternative would be that other signalling pathways, acting in parallel to Wnt/PCP signalling, are also involved in cytoskeleton remodelling through DAAM. For instance, Rac GTPases are known to control DAAM function during *Drosophila* embryonic VNC development and in the mushroom body neurons [177, 203]. Rac GTPases receive regulatory input from several guidance cues and integrate many upstream signalling pathways [77-79], therefore it is entirely conceivable that the Wnt/PCP signalling module is not the only activator of DAAM.

Beyond that DAAM is a key regulator of the neuronal actin cytoskeleton, it appeared to have a robust impact on MT organisation in the GC which may not be a consequence of disrupted actin function in filopodia and lamellipodia only. Recent studies showed that several formins control MT organisation and stability, and are able to bind MTs in vitro [45, 239, 242, 243, 245-247], suggesting that DAAM may also have a MT regulatory function and affects MTs directly. Similarly to others who demonstrated that the formin-MT interaction holds back dynamic parameters of MTs [242, 251], we found that the loss of DAAM increases MT growth velocity in the GC of primary neurons. In addition, the presence of DAAM was necessary to prevent MTs from depolymerisation in cultured neurons, induced by the drug Nocodazole, suggesting that DAAM is a potential MT-stabilising factor.

With one exception, in our experiments we used the hypomorphic $DAAM^{Ex1}$ allele in homozygosis. This allele deletes only the C-terminal end of the protein [203],

therefore in theory it could provide means to study whether the C-terminal tail of DAAM is involved in MT binding. Unfortunately however, this mutation affects the stability of the DAAM protein as it results in a strongly reduced protein level in the adult brain [177]. Therefore, although this is a unique allele, it was not possible to use it to distinguish between the MT-related versus general effects, not to mention that the C-terminal tail of DAAM is also implicated in actin binding [252]. In this case we conclude that novel mutations with selective effects on the cytoskeletal elements will be necessary to unambiguously separate the actin and MT-related formin effects.

6. Acknowledgements

First of all, I would like to thank my supervisors József Mihály and Natalia Sánchez-Soriano for the opportunity to do my PhD work in their labs. I am very grateful for their guidance during these years which was indispensable for my professional and personal development and helped me to gain a significant experience in planning, organising and performing a research project.

In addition, I am thankful to Rita Gombos, Gabriella Gazsó-Gerhát and Monika Chojnovska-Monga for their effort and contribution to the experimental work. I would like to thank Dávid Farkas and István Földi for the meaningful discussions about theoretical and practical problems; and Szilárd Szikora, Pilar Okenve-Ramos, Krisztina Tóth and Anikó Berente for their help with any technical issues. Furthermore, the technical support and the contribution of Áron Szabó, Zoltán Asztalos and András Viczián to set up and perform fly behavioural assays is very appreciated.

Last but not least, I would also like to thank my parents Klára Magda Szinek and János Kaltenecker who were always there to help in all these years, and also my friends Viktória Temesfői, Tomás Zakar and Aitor Martinez-Zarate for their friendship and support.

7. Appendix

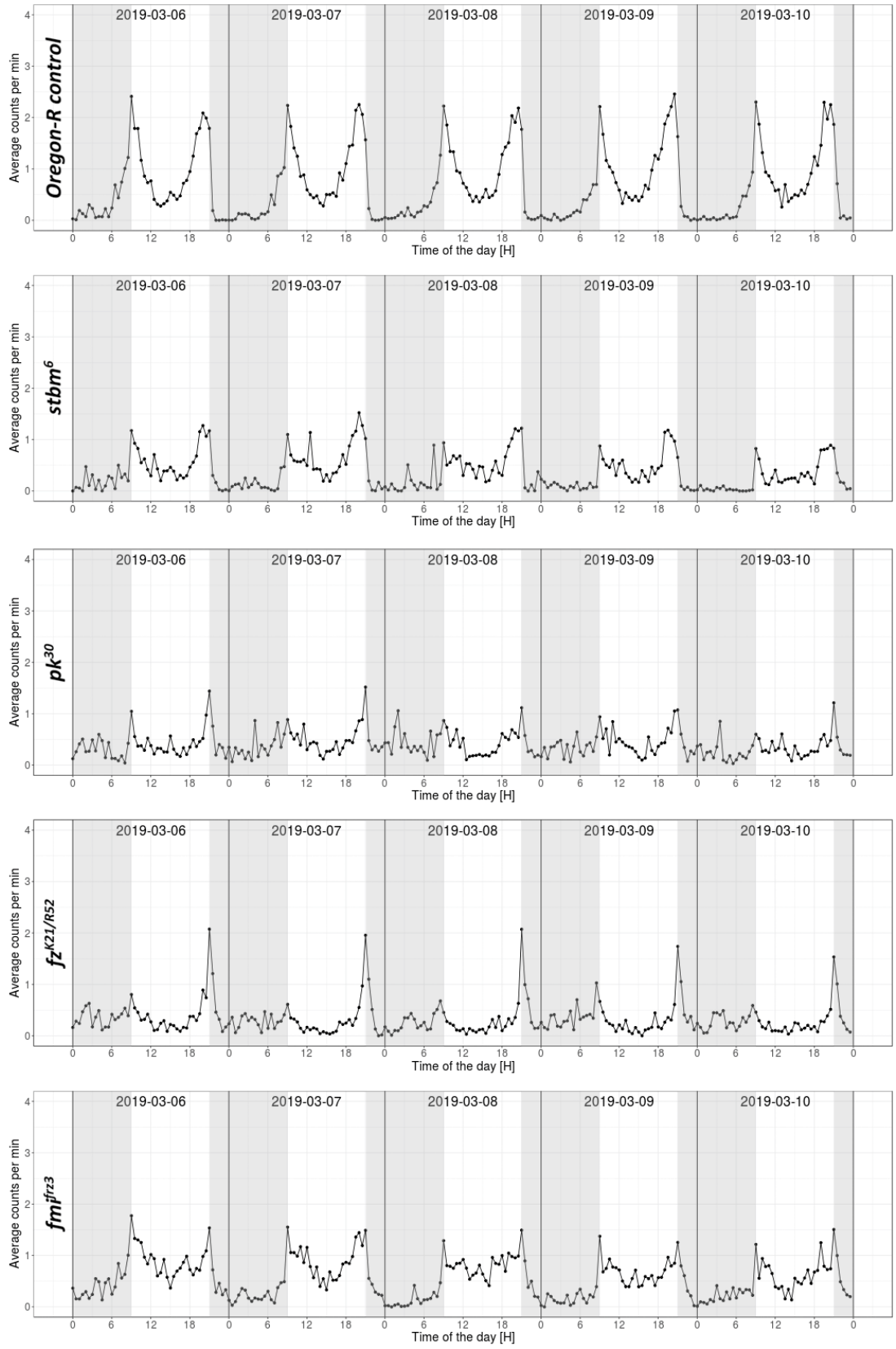

(The figure continues on the next page.)

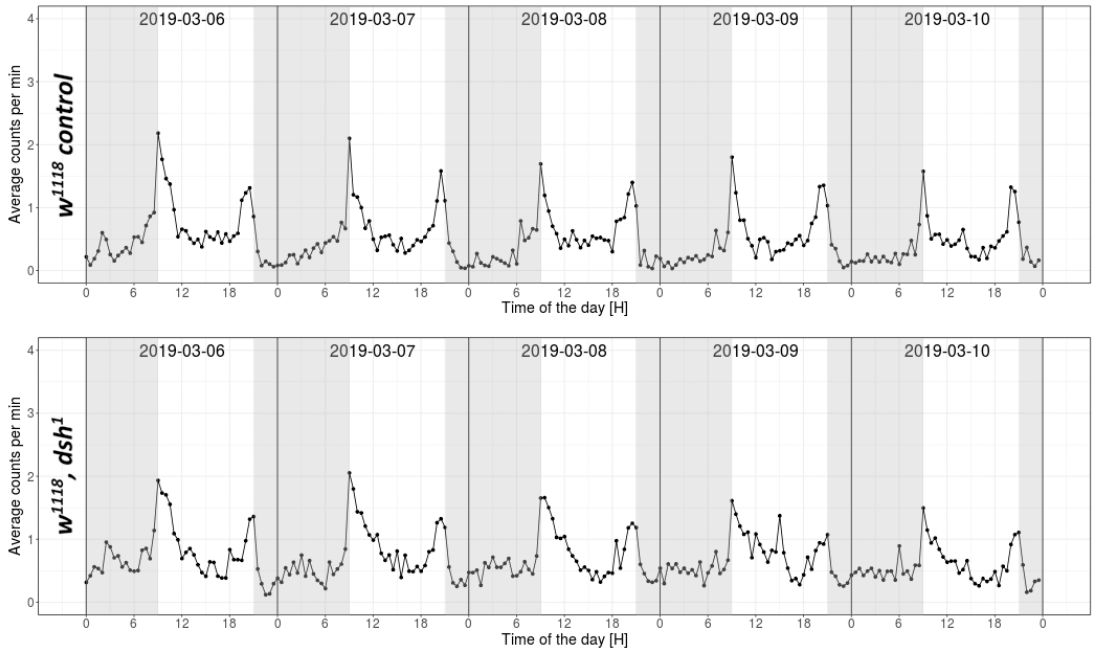

Figure 1. Daily activity profiles of the PCP mutant adult flies

The diagrams show the daily activity profiles of adult male flies in LD for 5 days (*Oregon-R*, n=16; *stbm*^{6}, n=14; *pk*^{30}, n=11; *fz*$^{K21/R52}$, n=12; *fmi*^{frz3}, n=13; *w*^{1118}, n=11; *w*^{1118}*, dsh*^{1}, n=15). White areas represent the light periods, whereas grey shaded areas indicate the dark periods.

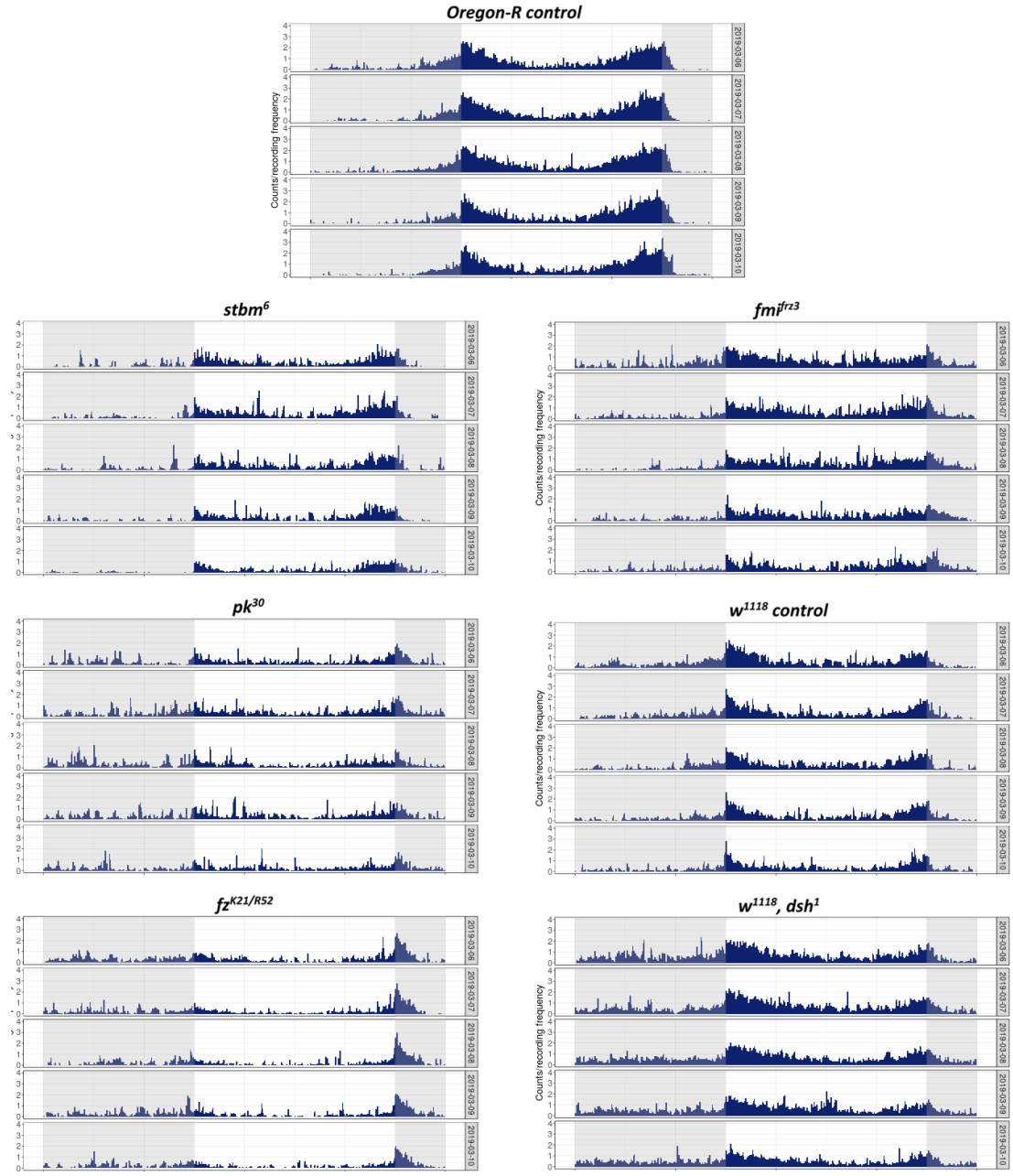

Figure 2. Actograms of the PCP mutant adult flies

Mean actograms show the circadian activity of adult male flies in LD for 5 days (*Oregon-R*, n=16; *stbm*^{6}, n=14; *pk*^{30}, n=11; *fz*$^{K21/R52}$, n=12; *fmi*^{frz3}, n=13; *w*^{1118}, n=11; *w*^{1118}, *dsh*^{1}, n=15). Blue vertical bars represent the mean of counts, and each horizontal row represents one day of recording. White areas indicate the light periods, whereas grey shaded areas show the dark periods.

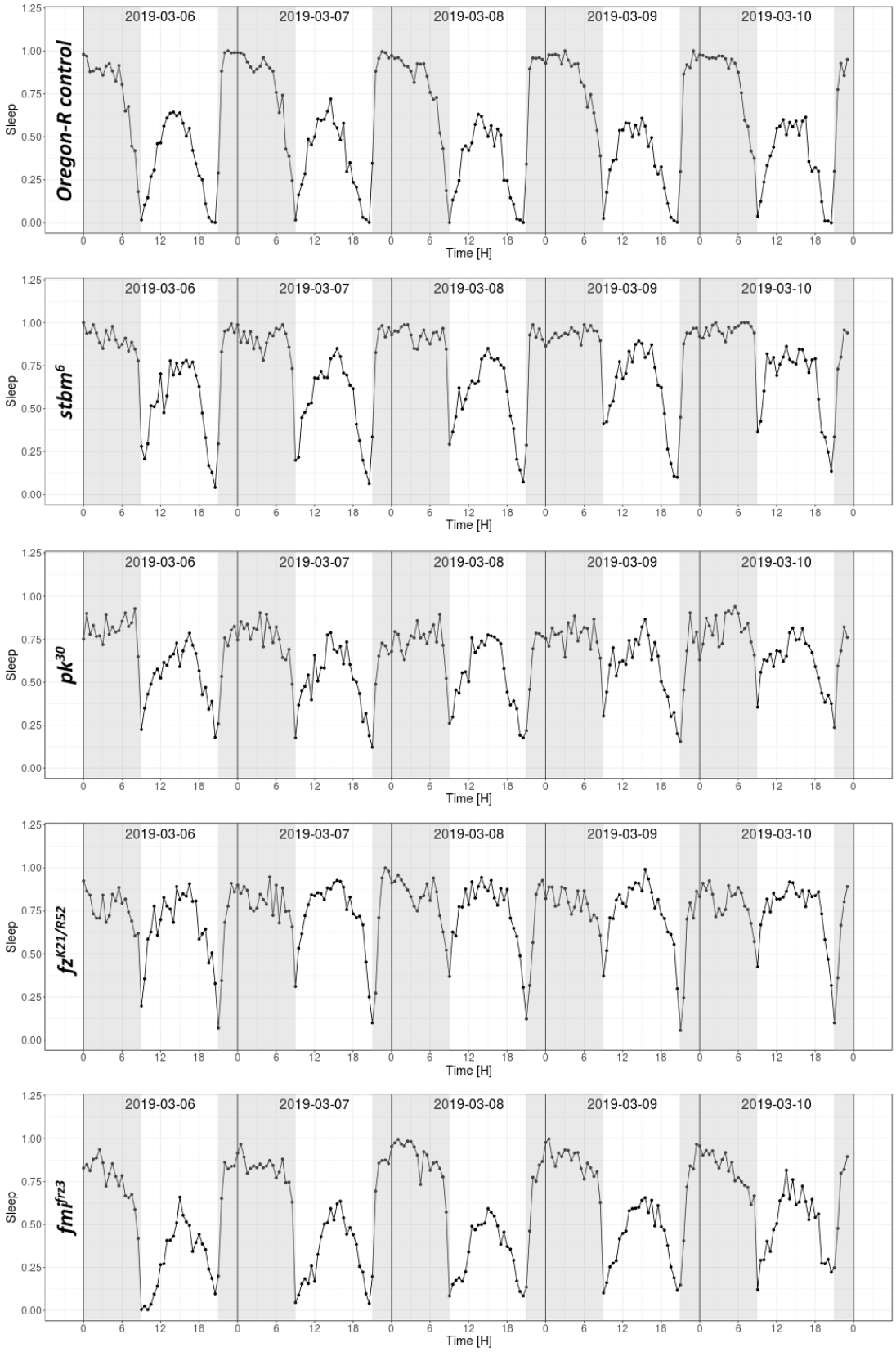

(The figure continues on the next page.)

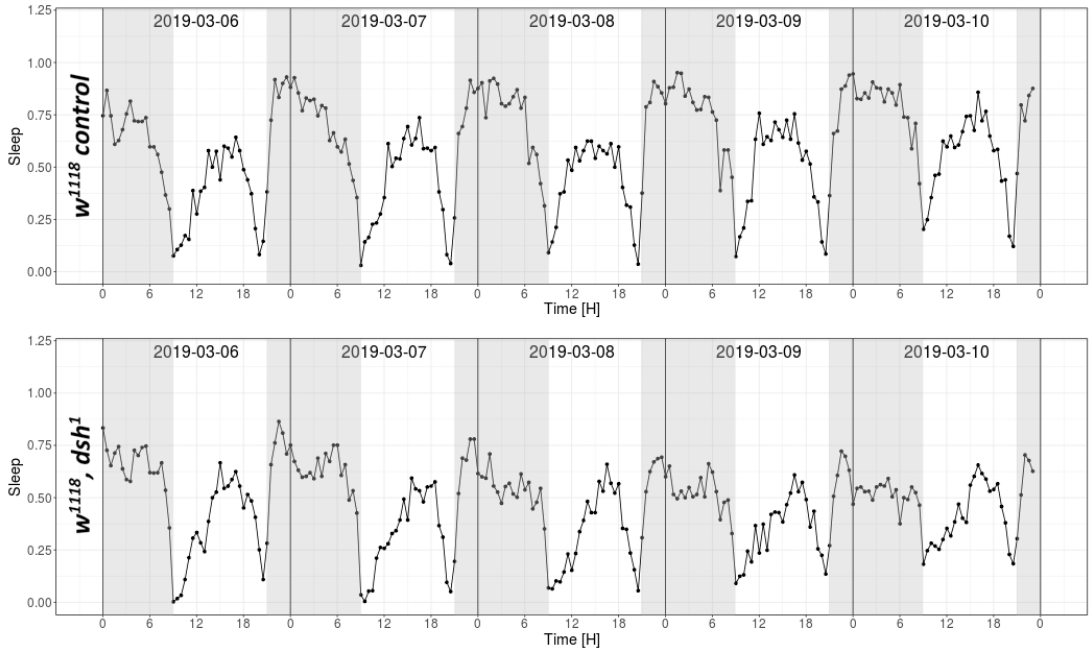

Figure 3. Daily sleep profiles of the PCP mutant adult flies

The diagrams show the daily sleep profiles of adult male flies in LD for 5 days (*Oregon-R*, n=16; *stbm*^{6}, n=14; *pk*^{30}, n=11; *fz*$^{K21/R52}$, n=12; *fmi*^{frz3}, n=13; *w*^{1118}, n=11; *w*^{1118}*, dsh*^{1}, n=15). The light periods are indicated by white areas, whereas grey shaded areas show the dark periods.

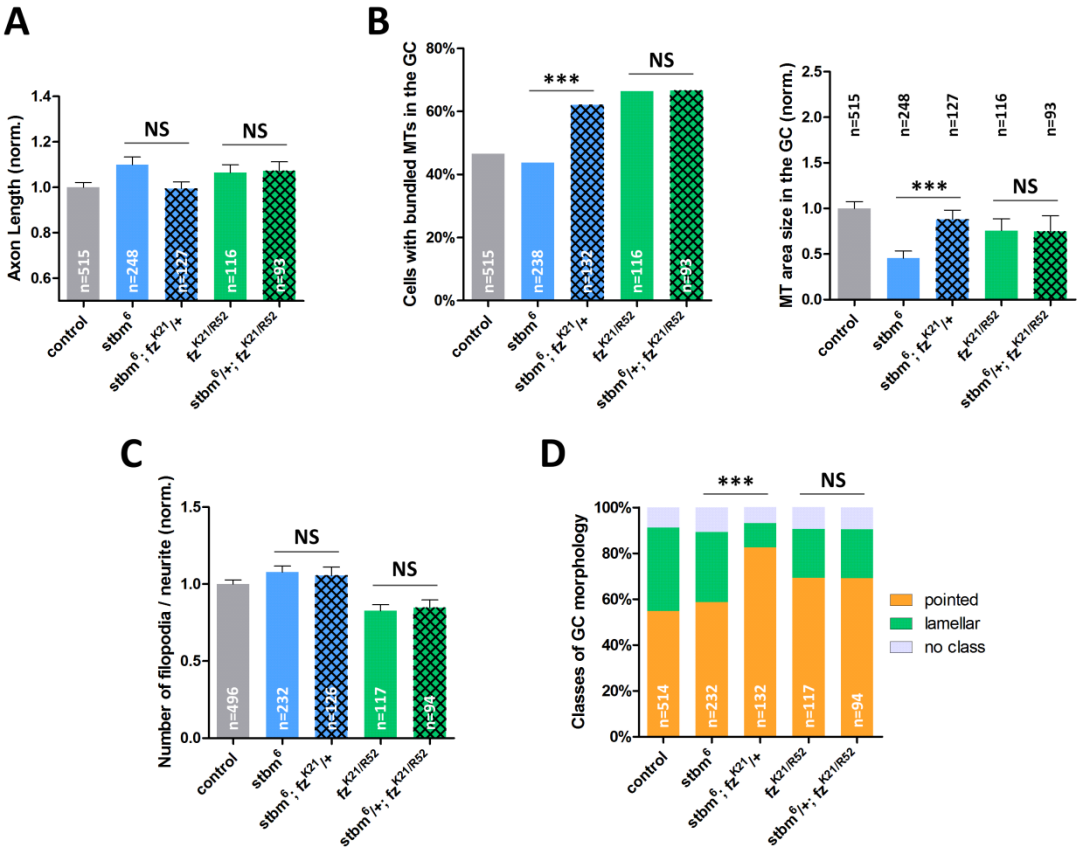

Figure 4. Genetic interactions between *stbm* and *fz* in cultured neurons

(**A**) Quantification of relative axon length of the *stbm* and *fz* double mutant combinations. In comparison to the *stbm*^{6} and *fz*$^{K21/R52}$ mutants, the double mutant combinations do not show any significant change. (**B**) Quantification of MT organisation and MT area size in the GC. One copy of *fz*^{K21} results in a significantly higher number of cells with bundled MTs in the GC of the *stbm*^{6}*; fz*^{K21}/+ double mutant primary cell cultures compared to the corresponding single mutant cultures. In addition, *stbm*^{6}*; fz*^{K21}/+ double mutant cells also display significantly bigger areas that are occupied by MTs in the GC, although this phenomenon is difficult to explain since the loss of Fz does not seem to affect MT area size by itself. In contrast, *stbm*^{6}/+*; fz*$^{K21/R52}$ double mutant neurons do not display any difference compared to the *fz*$^{K21/R52}$ mutants. (**C**) Quantification of relative filopodia number. Interestingly, the number of filopodia in the double mutant combinations do not differ from that of the corresponding single mutants. (**D**) The graph represents the percentage of cells that show pointed or lamellar GC morphology. Compared to the *stbm*^{6} mutant, one copy of *fz*^{K21} significantly increases the amount of cells with pointed GCs in the *stbm*^{6}*; fz*^{K21}/+ double mutant. In contrast to this, *stbm*^{6}/+*; fz*$^{K21/R52}$ double mutants do not show changes in GC morphology.

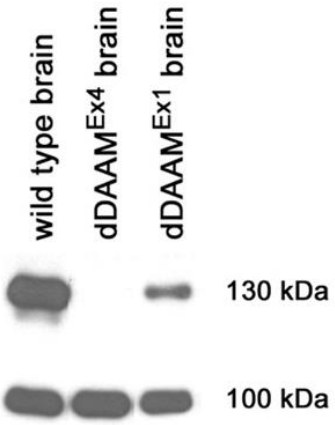

Figure 5. Western blot analysis of DAAM in the *Drosophila* brain (adapted from [177])

The figure shows the level of DAAM protein from adult brain extracts (5 brains per genotype). The 130 kDa band indicates the DAAM protein, whereas the 100kDa band represents α-glycogen phosphorylase which was used as the loading control. Compared to the w^{1118} control (indicated as wild type), the level of DAAM is highly reduced in the $DAAM^{Ex1}$ mutant brains, and it is barely detectable in the $DAAM^{Ex4}$ mutants.

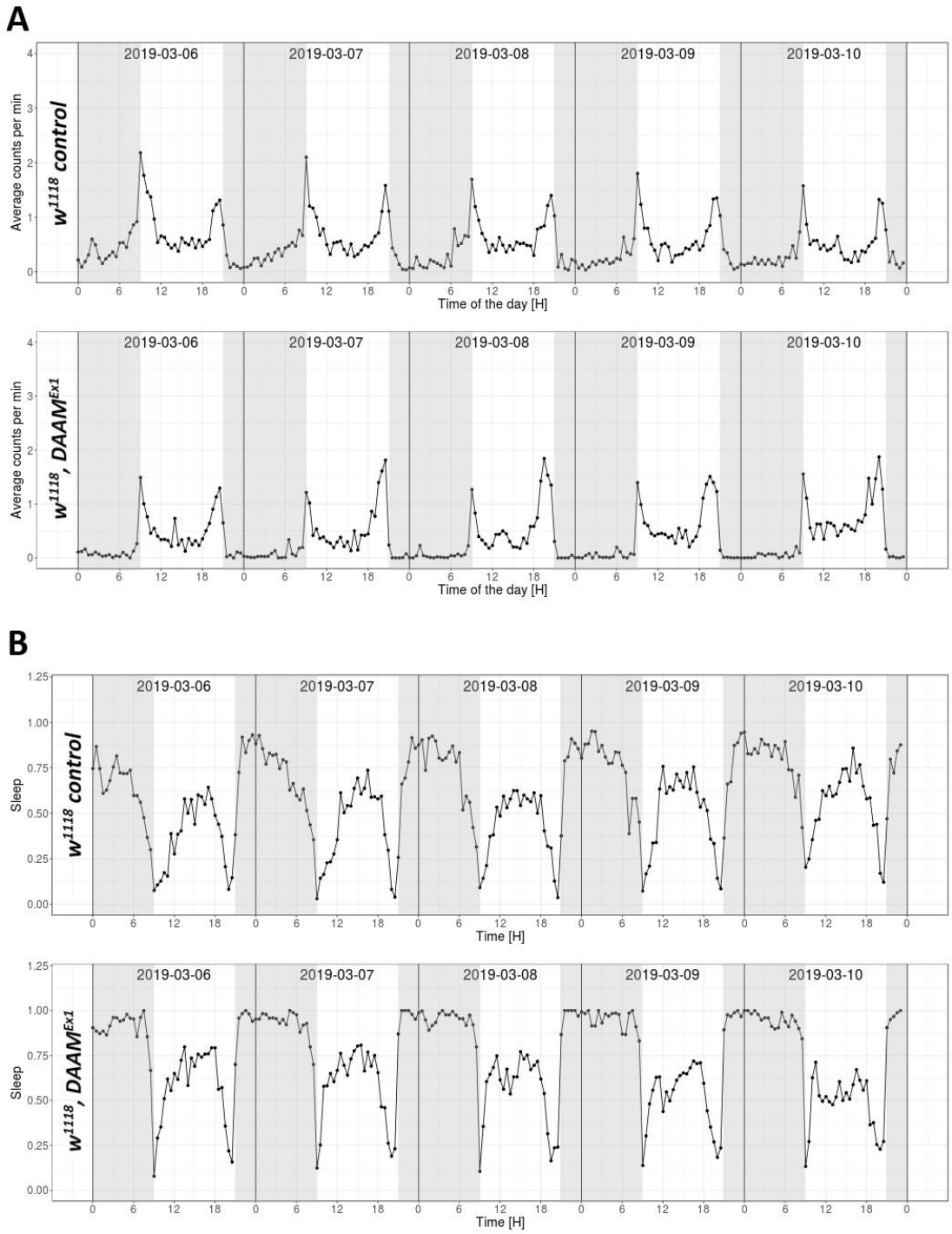

Figure 6. Daily activity and sleep profiles of the *DAAM^{Ex1}* mutant adult flies

The diagrams show (**A**) the daily activity profiles and (**B**) the daily sleep profiles of the *DAAM^{Ex1}* mutant adult male flies in LD for 5 days (*w^{1118}*, n=11; *w^{1118}, DAAM^{Ex1}*, n=14). The light periods are indicated by the white areas, whereas grey shaded areas indicate the dark periods.

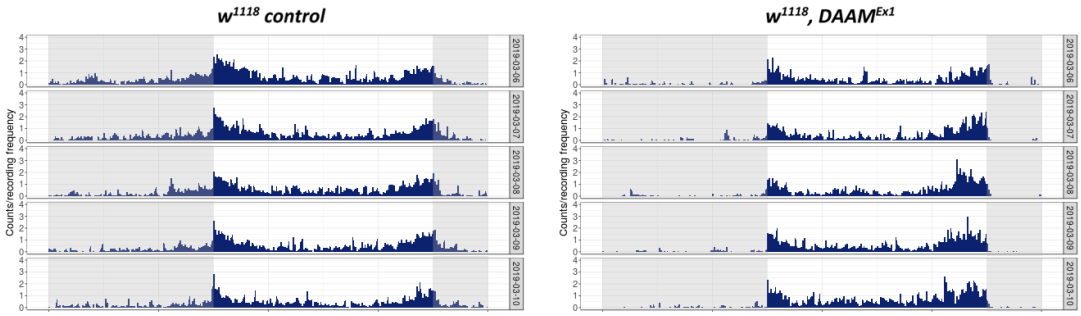

Figure 7. Actogram of the *DAAM*^{Ex1} mutant adult flies

Mean actograms of adult male flies in LD for 5 days (w^{1118}, n=11; w^{1118}, *DAAM*^{Ex1}, n=14), showing the circadian activity of the w^{1118} control and the *DAAM*^{Ex1} mutant flies. Horizontal rows display the 5 days of recording, in which blue vertical bars represent the mean of counts. The light periods are indicated by the white areas, whereas grey shaded areas show the dark periods.

8. References

1. Twelvetrees, A., A.G. Hendricks, and E.L. Holzbaur, *SnapShot: axonal transport.* Cell, 2012. **149**(4): p. 950-950.e1.
2. Xu, K., G. Zhong, and X. Zhuang, *Actin, spectrin, and associated proteins form a periodic cytoskeletal structure in axons.* Science, 2013. **339**(6118): p. 452-6.
3. Baas, P.W. and S. Lin, *Hooks and comets: The story of microtubule polarity orientation in the neuron.* Dev Neurobiol, 2011. **71**(6): p. 403-18.
4. Prokop, A., et al., *Using fly genetics to dissect the cytoskeletal machinery of neurons during axonal growth and maintenance.* J Cell Sci, 2013. **126**(Pt 11): p. 2331-41.
5. Dent, E.W. and F.B. Gertler, *Cytoskeletal dynamics and transport in growth cone motility and axon guidance.* Neuron, 2003. **40**(2): p. 209-27.
6. Dent, E.W., S.L. Gupton, and F.B. Gertler, *The growth cone cytoskeleton in axon outgrowth and guidance.* Cold Spring Harb Perspect Biol, 2011. **3**(3).
7. Goldberg, D.J. and D.W. Burmeister, *Stages in axon formation: observations of growth of Aplysia axons in culture using video-enhanced contrast-differential interference contrast microscopy.* J Cell Biol, 1986. **103**(5): p. 1921-31.
8. Kaufmann, N., Z.P. Wills, and D. Van Vactor, *Drosophila Rac1 controls motor axon guidance.* Development, 1998. **125**(3): p. 453-61.
9. Chien, C.B., et al., *Navigational errors made by growth cones without filopodia in the embryonic Xenopus brain.* Neuron, 1993. **11**(2): p. 237-51.
10. Bentley, D. and A. Toroian-Raymond, *Disoriented pathfinding by pioneer neurone growth cones deprived of filopodia by cytochalasin treatment.* Nature, 1986. **323**(6090): p. 712-5.
11. Marsh, L. and P.C. Letourneau, *Growth of neurites without filopodial or lamellipodial activity in the presence of cytochalasin B.* J Cell Biol, 1984. **99**(6): p. 2041-7.
12. Lafont, F., et al., *Specific responses of axons and dendrites to cytoskeleton perturbations: an in vitro study.* J Cell Sci, 1993. **104 (Pt 2)**: p. 433-43.
13. Dent, E.W. and K. Kalil, *Axon branching requires interactions between dynamic microtubules and actin filaments.* J Neurosci, 2001. **21**(24): p. 9757-69.
14. Sánchez-Soriano, N., et al., *Drosophila growth cones: a genetically tractable platform for the analysis of axonal growth dynamics.* Dev Neurobiol, 2010. **70**(1): p. 58-71.
15. Letourneau, P.C. and A.H. Ressler, *Inhibition of neurite initiation and growth by taxol.* J Cell Biol, 1984. **98**(4): p. 1355-62.
16. Tanaka, E. and M.W. Kirschner, *The role of microtubules in growth cone turning at substrate boundaries.* J Cell Biol, 1995. **128**(1-2): p. 127-37.
17. Lee, A.C. and D.M. Suter, *Quantitative analysis of microtubule dynamics during adhesion-mediated growth cone guidance.* Dev Neurobiol, 2008. **68**(12): p. 1363-77.
18. Schaefer, A.W., N. Kabir, and P. Forscher, *Filopodia and actin arcs guide the assembly and transport of two populations of microtubules with unique dynamic parameters in neuronal growth cones.* J Cell Biol, 2002. **158**(1): p. 139-52.
19. Lowery, L.A. and D. Van Vactor, *The trip of the tip: understanding the growth cone machinery.* Nat Rev Mol Cell Biol, 2009. **10**(5): p. 332-43.
20. Geraldo, S. and P.R. Gordon-Weeks, *Cytoskeletal dynamics in growth-cone steering.* J Cell Sci, 2009. **122**(Pt 20): p. 3595-604.
21. Hawkins, T., et al., *Mechanics of microtubules.* J Biomech, 2010. **43**(1): p. 23-30.
22. Howard, J. and A.A. Hyman, *Dynamics and mechanics of the microtubule plus end.* Nature, 2003. **422**(6933): p. 753-8.

23. Mitchison, T. and M. Kirschner, *Dynamic instability of microtubule growth.* Nature, 1984. **312**(5991): p. 237-42.
24. Stricker, J., T. Falzone, and M.L. Gardel, *Mechanics of the F-actin cytoskeleton.* J Biomech, 2010. **43**(1): p. 9-14.
25. Pak, C.W., K.C. Flynn, and J.R. Bamburg, *Actin-binding proteins take the reins in growth cones.* Nat Rev Neurosci, 2008. **9**(2): p. 136-47.
26. Voelzmann, A., et al., *A conceptual view at microtubule plus end dynamics in neuronal axons.* Brain Res Bull, 2016. **126**(Pt 3): p. 226-237.
27. Machesky, L.M., et al., *Purification of a cortical complex containing two unconventional actins from Acanthamoeba by affinity chromatography on profilin-agarose.* J Cell Biol, 1994. **127**(1): p. 107-15.
28. Mullins, R.D., J.A. Heuser, and T.D. Pollard, *The interaction of Arp2/3 complex with actin: nucleation, high affinity pointed end capping, and formation of branching networks of filaments.* Proc Natl Acad Sci U S A, 1998. **95**(11): p. 6181-6.
29. Rouiller, I., et al., *The structural basis of actin filament branching by the Arp2/3 complex.* J Cell Biol, 2008. **180**(5): p. 887-95.
30. Goley, E.D. and M.D. Welch, *The ARP2/3 complex: an actin nucleator comes of age.* Nat Rev Mol Cell Biol, 2006. **7**(10): p. 713-26.
31. Pollard, T.D. and C.C. Beltzner, *Structure and function of the Arp2/3 complex.* Curr Opin Struct Biol, 2002. **12**(6): p. 768-74.
32. Chereau, D., et al., *Actin-bound structures of Wiskott-Aldrich syndrome protein (WASP)-homology domain 2 and the implications for filament assembly.* Proc Natl Acad Sci U S A, 2005. **102**(46): p. 16644-9.
33. Hüfner, K., et al., *The verprolin-like central (vc) region of Wiskott-Aldrich syndrome protein induces Arp2/3 complex-dependent actin nucleation.* J Biol Chem, 2001. **276**(38): p. 35761-7.
34. Machesky, L.M. and R.H. Insall, *Scar1 and the related Wiskott-Aldrich syndrome protein, WASP, regulate the actin cytoskeleton through the Arp2/3 complex.* Curr Biol, 1998. **8**(25): p. 1347-56.
35. Padrick, S.B., et al., *Arp2/3 complex is bound and activated by two WASP proteins.* Proc Natl Acad Sci U S A, 2011. **108**(33): p. E472-9.
36. Buracco, S., S. Claydon, and R. Insall, *Control of actin dynamics during cell motility.* F1000Res, 2019. **8**.
37. Siton-Mendelson, O. and A. Bernheim-Groswasser, *Functional Actin Networks under Construction: The Cooperative Action of Actin Nucleation and Elongation Factors.* Trends Biochem Sci, 2017. **42**(6): p. 414-430.
38. Higgs, H.N. and K.J. Peterson, *Phylogenetic analysis of the formin homology 2 domain.* Mol Biol Cell, 2005. **16**(1): p. 1-13.
39. Rivero, F., et al., *A comparative sequence analysis reveals a common GBD/FH3-FH1-FH2-DAD architecture in formins from Dictyostelium, fungi and metazoa.* BMC Genomics, 2005. **6**: p. 28.
40. Castrillon, D.H. and S.A. Wasserman, *Diaphanous is required for cytokinesis in Drosophila and shares domains of similarity with the products of the limb deformity gene.* Development, 1994. **120**(12): p. 3367-77.
41. Higgs, H.N., *Formin proteins: a domain-based approach.* Trends Biochem Sci, 2005. **30**(6): p. 342-53.
42. Pruyne, D., *Revisiting the Phylogeny of the Animal Formins: Two New Subtypes, Relationships with Multiple Wing Hairs Proteins, and a Lost Human Formin.* PLoS One, 2016. **11**(10): p. e0164067.
43. Krebs, A., et al., *Characterization of functional domains of mDia1, a link between the small GTPase Rho and the actin cytoskeleton.* J Cell Sci, 2001. **114**(Pt 20): p. 3663-72.

44. Courtemanche, N., *Mechanisms of formin-mediated actin assembly and dynamics.* Biophys Rev, 2018. **10**(6): p. 1553-1569.
45. Chesarone, M.A., A.G. DuPage, and B.L. Goode, *Unleashing formins to remodel the actin and microtubule cytoskeletons.* Nat Rev Mol Cell Biol, 2010. **11**(1): p. 62-74.
46. Maiti, S., et al., *Structure and activity of full-length formin mDia1.* Cytoskeleton (Hoboken), 2012. **69**(6): p. 393-405.
47. Nezami, A.G., F. Poy, and M.J. Eck, *Structure of the autoinhibitory switch in formin mDia1.* Structure, 2006. **14**(2): p. 257-63.
48. Li, F. and H.N. Higgs, *The mouse Formin mDia1 is a potent actin nucleation factor regulated by autoinhibition.* Curr Biol, 2003. **13**(15): p. 1335-40.
49. Li, F. and H.N. Higgs, *Dissecting requirements for auto-inhibition of actin nucleation by the formin, mDia1.* J Biol Chem, 2005. **280**(8): p. 6986-92.
50. Lammers, M., et al., *The regulation of mDia1 by autoinhibition and its release by Rho*GTP.* EMBO J, 2005. **24**(23): p. 4176-87.
51. Pruyne, D., et al., *Role of formins in actin assembly: nucleation and barbed-end association.* Science, 2002. **297**(5581): p. 612-5.
52. Zigmond, S.H., et al., *Formin leaky cap allows elongation in the presence of tight capping proteins.* Curr Biol, 2003. **13**(20): p. 1820-3.
53. Otomo, T., et al., *Structural basis of actin filament nucleation and processive capping by a formin homology 2 domain.* Nature, 2005. **433**(7025): p. 488-94.
54. Vavylonis, D., et al., *Model of formin-associated actin filament elongation.* Mol Cell, 2006. **21**(4): p. 455-66.
55. Paul, A.S., et al., *The role of the FH1 domain and profilin in formin-mediated actin-filament elongation and nucleation.* Curr Biol, 2008. **18**(1): p. 9-19.
56. Foldi, I., S. Szikora, and J. Mihály, *Formin' bridges between microtubules and actin filaments in axonal growth cones.* Neural Regen Res, 2017. **12**(12): p. 1971-1973.
57. Quinlan, M.E., et al., *Drosophila Spire is an actin nucleation factor.* Nature, 2005. **433**(7024): p. 382-8.
58. Ahuja, R., et al., *Cordon-bleu is an actin nucleation factor and controls neuronal morphology.* Cell, 2007. **131**(2): p. 337-50.
59. Chereau, D., et al., *Leiomodin is an actin filament nucleator in muscle cells.* Science, 2008. **320**(5873): p. 239-43.
60. Zuchero, J.B., et al., *p53-cofactor JMY is a multifunctional actin nucleation factor.* Nat Cell Biol, 2009. **11**(4): p. 451-9.
61. Firat-Karalar, E.N. and M.D. Welch, *New mechanisms and functions of actin nucleation.* Curr Opin Cell Biol, 2011. **23**(1): p. 4-13.
62. Dominguez, R., *Actin filament nucleation and elongation factors--structure-function relationships.* Crit Rev Biochem Mol Biol, 2009. **44**(6): p. 351-66.
63. Chesarone, M.A. and B.L. Goode, *Actin nucleation and elongation factors: mechanisms and interplay.* Curr Opin Cell Biol, 2009. **21**(1): p. 28-37.
64. Gonçalves-Pimentel, C., et al., *Dissecting regulatory networks of filopodia formation in a Drosophila growth cone model.* PLoS One, 2011. **6**(3): p. e18340.
65. Dickson, B.J., *Molecular mechanisms of axon guidance.* Science, 2002. **298**(5600): p. 1959-64.
66. Tessier-Lavigne, M. and C.S. Goodman, *The molecular biology of axon guidance.* Science, 1996. **274**(5290): p. 1123-33.
67. Huber, A.B., et al., *Signaling at the growth cone: ligand-receptor complexes and the control of axon growth and guidance.* Annu Rev Neurosci, 2003. **26**: p. 509-63.
68. Culotti, J.G. and D.C. Merz, *DCC and netrins.* Curr Opin Cell Biol, 1998. **10**(5): p. 609-13.
69. Keleman, K. and B.J. Dickson, *Short- and long-range repulsion by the Drosophila Unc5 netrin receptor.* Neuron, 2001. **32**(4): p. 605-17.

70. Kidd, T., et al., *Roundabout controls axon crossing of the CNS midline and defines a novel subfamily of evolutionarily conserved guidance receptors.* Cell, 1998. **92**(2): p. 205-15.
71. Wilkinson, D.G., *Multiple roles of EPH receptors and ephrins in neural development.* Nat Rev Neurosci, 2001. **2**(3): p. 155-64.
72. Tamagnone, L., et al., *Plexins are a large family of receptors for transmembrane, secreted, and GPI-anchored semaphorins in vertebrates.* Cell, 1999. **99**(1): p. 71-80.
73. Kennedy, T.E., et al., *Netrins are diffusible chemotropic factors for commissural axons in the embryonic spinal cord.* Cell, 1994. **78**(3): p. 425-35.
74. Serafini, T., et al., *The netrins define a family of axon outgrowth-promoting proteins homologous to C. elegans UNC-6.* Cell, 1994. **78**(3): p. 409-24.
75. Charron, F. and M. Tessier-Lavigne, *Novel brain wiring functions for classical morphogens: a role as graded positional cues in axon guidance.* Development, 2005. **132**(10): p. 2251-62.
76. Araújo, S.J. and G. Tear, *Axon guidance mechanisms and molecules: lessons from invertebrates.* Nat Rev Neurosci, 2003. **4**(11): p. 910-22.
77. Koh, C.G., *Rho GTPases and their regulators in neuronal functions and development.* Neurosignals, 2006. **15**(5): p. 228-37.
78. Govek, E.E., S.E. Newey, and L. Van Aelst, *The role of the Rho GTPases in neuronal development.* Genes Dev, 2005. **19**(1): p. 1-49.
79. Watabe-Uchida, M., E.E. Govek, and L. Van Aelst, *Regulators of Rho GTPases in neuronal development.* J Neurosci, 2006. **26**(42): p. 10633-5.
80. Kurokawa, K., et al., *Mechanism and role of localized activation of Rho-family GTPases in growth factor-stimulated fibroblasts and neuronal cells.* Biochem Soc Trans, 2005. **33**(Pt 4): p. 631-4.
81. Pertz, O.C., et al., *Spatial mapping of the neurite and soma proteomes reveals a functional Cdc42/Rac regulatory network.* Proc Natl Acad Sci U S A, 2008. **105**(6): p. 1931-6.
82. Charron, F., et al., *The morphogen sonic hedgehog is an axonal chemoattractant that collaborates with netrin-1 in midline axon guidance.* Cell, 2003. **113**(1): p. 11-23.
83. Trousse, F., et al., *Control of retinal ganglion cell axon growth: a new role for Sonic hedgehog.* Development, 2001. **128**(20): p. 3927-36.
84. Augsburger, A., et al., *BMPs as mediators of roof plate repulsion of commissural neurons.* Neuron, 1999. **24**(1): p. 127-41.
85. Butler, S.J. and J. Dodd, *A role for BMP heterodimers in roof plate-mediated repulsion of commissural axons.* Neuron, 2003. **38**(3): p. 389-401.
86. Colavita, A., et al., *Pioneer axon guidance by UNC-129, a C. elegans TGF-beta.* Science, 1998. **281**(5377): p. 706-9.
87. Lyuksyutova, A.I., et al., *Anterior-posterior guidance of commissural axons by Wnt-frizzled signaling.* Science, 2003. **302**(5652): p. 1984-8.
88. Bourikas, D., et al., *Sonic hedgehog guides commissural axons along the longitudinal axis of the spinal cord.* Nat Neurosci, 2005. **8**(3): p. 297-304.
89. Wodarz, A. and R. Nusse, *Mechanisms of Wnt signaling in development.* Annu Rev Cell Dev Biol, 1998. **14**: p. 59-88.
90. Logan, C.Y. and R. Nusse, *The Wnt signaling pathway in development and disease.* Annu Rev Cell Dev Biol, 2004. **20**: p. 781-810.
91. Nusse, R. and H. Varmus, *Three decades of Wnts: a personal perspective on how a scientific field developed.* EMBO J, 2012. **31**(12): p. 2670-84.
92. He, C.W., C.P. Liao, and C.L. Pan, *Wnt signalling in the development of axon, dendrites and synapses.* Open Biol, 2018. **8**(10).
93. Huang, H.C. and P.S. Klein, *The Frizzled family: receptors for multiple signal transduction pathways.* Genome Biol, 2004. **5**(7): p. 234.

94. Gordon, M.D. and R. Nusse, *Wnt signaling: multiple pathways, multiple receptors, and multiple transcription factors.* J Biol Chem, 2006. **281**(32): p. 22429-33.
95. Nusse, R. and H. Clevers, *Wnt/β-Catenin Signaling, Disease, and Emerging Therapeutic Modalities.* Cell, 2017. **169**(6): p. 985-999.
96. Veeman, M.T., J.D. Axelrod, and R.T. Moon, *A second canon. Functions and mechanisms of beta-catenin-independent Wnt signaling.* Dev Cell, 2003. **5**(3): p. 367-77.
97. Kohn, A.D. and R.T. Moon, *Wnt and calcium signaling: beta-catenin-independent pathways.* Cell Calcium, 2005. **38**(3-4): p. 439-46.
98. Yang, Y. and M. Mlodzik, *Wnt-Frizzled/planar cell polarity signaling: cellular orientation by facing the wind (Wnt).* Annu Rev Cell Dev Biol, 2015. **31**: p. 623-46.
99. Cadigan, K.M. and Y.I. Liu, *Wnt signaling: complexity at the surface.* J Cell Sci, 2006. **119**(Pt 3): p. 395-402.
100. Tamai, K., et al., *LDL-receptor-related proteins in Wnt signal transduction.* Nature, 2000. **407**(6803): p. 530-5.
101. Pinson, K.I., et al., *An LDL-receptor-related protein mediates Wnt signalling in mice.* Nature, 2000. **407**(6803): p. 535-8.
102. Lee, J.S., A. Ishimoto, and S. Yanagawa, *Characterization of mouse dishevelled (Dvl) proteins in Wnt/Wingless signaling pathway.* J Biol Chem, 1999. **274**(30): p. 21464-70.
103. Willert, K., et al., *Casein kinase 2 associates with and phosphorylates dishevelled.* EMBO J, 1997. **16**(11): p. 3089-96.
104. Yanagawa, S., et al., *The dishevelled protein is modified by wingless signaling in Drosophila.* Genes Dev, 1995. **9**(9): p. 1087-97.
105. Rothbächer, U., et al., *Dishevelled phosphorylation, subcellular localization and multimerization regulate its role in early embryogenesis.* EMBO J, 2000. **19**(5): p. 1010-22.
106. Wallingford, J.B. and R. Habas, *The developmental biology of Dishevelled: an enigmatic protein governing cell fate and cell polarity.* Development, 2005. **132**(20): p. 4421-36.
107. Habas, R. and I.B. Dawid, *Dishevelled and Wnt signaling: is the nucleus the final frontier?* J Biol, 2005. **4**(1): p. 2.
108. Wehrli, M., et al., *arrow encodes an LDL-receptor-related protein essential for Wingless signalling.* Nature, 2000. **407**(6803): p. 527-30.
109. Hart, M., et al., *The F-box protein beta-TrCP associates with phosphorylated beta-catenin and regulates its activity in the cell.* Curr Biol, 1999. **9**(4): p. 207-10.
110. Liu, C., et al., *Control of beta-catenin phosphorylation/degradation by a dual-kinase mechanism.* Cell, 2002. **108**(6): p. 837-47.
111. Clevers, H. and R. Nusse, *Wnt/β-catenin signaling and disease.* Cell, 2012. **149**(6): p. 1192-205.
112. Montcouquiol, M., E.B. Crenshaw, and M.W. Kelley, *Noncanonical Wnt signaling and neural polarity.* Annu Rev Neurosci, 2006. **29**: p. 363-86.
113. Miller, J.R., et al., *Mechanism and function of signal transduction by the Wnt/beta-catenin and Wnt/Ca2+ pathways.* Oncogene, 1999. **18**(55): p. 7860-72.
114. Kühl, M., *Non-canonical Wnt signaling in Xenopus: regulation of axis formation and gastrulation.* Semin Cell Dev Biol, 2002. **13**(3): p. 243-9.
115. Inestrosa, N.C. and L. Varela-Nallar, *Wnt signalling in neuronal differentiation and development.* Cell Tissue Res, 2015. **359**(1): p. 215-23.
116. Habas, R., Y. Kato, and X. He, *Wnt/Frizzled activation of Rho regulates vertebrate gastrulation and requires a novel Formin homology protein Daam1.* Cell, 2001. **107**(7): p. 843-54.

117. Marlow, F., et al., *Zebrafish Rho kinase 2 acts downstream of Wnt11 to mediate cell polarity and effective convergence and extension movements.* Curr Biol, 2002. **12**(11): p. 876-84.
118. Habas, R., I.B. Dawid, and X. He, *Coactivation of Rac and Rho by Wnt/Frizzled signaling is required for vertebrate gastrulation.* Genes Dev, 2003. **17**(2): p. 295-309.
119. Boutros, M., et al., *Dishevelled activates JNK and discriminates between JNK pathways in planar polarity and wingless signaling.* Cell, 1998. **94**(1): p. 109-18.
120. Rosso, S.B., et al., *Wnt signaling through Dishevelled, Rac and JNK regulates dendritic development.* Nat Neurosci, 2005. **8**(1): p. 34-42.
121. Park, T.J., et al., *Dishevelled controls apical docking and planar polarization of basal bodies in ciliated epithelial cells.* Nat Genet, 2008. **40**(7): p. 871-9.
122. Vladar, E.K., et al., *Microtubules enable the planar cell polarity of airway cilia.* Curr Biol, 2012. **22**(23): p. 2203-12.
123. Turner, C.M. and P.N. Adler, *Distinct roles for the actin and microtubule cytoskeletons in the morphogenesis of epidermal hairs during wing development in Drosophila.* Mech Dev, 1998. **70**(1-2): p. 181-92.
124. Wong, L.L. and P.N. Adler, *Tissue polarity genes of Drosophila regulate the subcellular location for prehair initiation in pupal wing cells.* J Cell Biol, 1993. **123**(1): p. 209-21.
125. Adler, P.N., *Planar signaling and morphogenesis in Drosophila.* Dev Cell, 2002. **2**(5): p. 525-35.
126. Lawrence, P.A., G. Struhl, and J. Casal, *Planar cell polarity: one or two pathways?* Nat Rev Genet, 2007. **8**(7): p. 555-63.
127. Wang, Y. and J. Nathans, *Tissue/planar cell polarity in vertebrates: new insights and new questions.* Development, 2007. **134**(4): p. 647-58.
128. Maung, S.M. and A. Jenny, *Planar cell polarity in Drosophila.* Organogenesis, 2011. **7**(3): p. 165-79.
129. Le Borgne, R., Y. Bellaïche, and F. Schweisguth, *Drosophila E-cadherin regulates the orientation of asymmetric cell division in the sensory organ lineage.* Curr Biol, 2002. **12**(2): p. 95-104.
130. Roegiers, F., et al., *Two types of asymmetric divisions in the Drosophila sensory organ precursor cell lineage.* Nat Cell Biol, 2001. **3**(1): p. 58-67.
131. Bellaïche, Y., et al., *The planar cell polarity protein Strabismus promotes Pins anterior localization during asymmetric division of sensory organ precursor cells in Drosophila.* Development, 2004. **131**(2): p. 469-78.
132. Bellaïche, Y., et al., *Frizzled regulates localization of cell-fate determinants and mitotic spindle rotation during asymmetric cell division.* Nat Cell Biol, 2001. **3**(1): p. 50-7.
133. Tomlinson, A. and G. Struhl, *Decoding vectorial information from a gradient: sequential roles of the receptors Frizzled and Notch in establishing planar polarity in the Drosophila eye.* Development, 1999. **126**(24): p. 5725-38.
134. Zheng, L., J. Zhang, and R.W. Carthew, *frizzled regulates mirror-symmetric pattern formation in the Drosophila eye.* Development, 1995. **121**(9): p. 3045-55.
135. Jenny, A., *Planar cell polarity signaling in the Drosophila eye.* Curr Top Dev Biol, 2010. **93**: p. 189-227.
136. Bhanot, P., et al., *A new member of the frizzled family from Drosophila functions as a Wingless receptor.* Nature, 1996. **382**(6588): p. 225-30.
137. Chen, C.M. and G. Struhl, *Wingless transduction by the Frizzled and Frizzled2 proteins of Drosophila.* Development, 1999. **126**(23): p. 5441-52.
138. Usui, T., et al., *Flamingo, a seven-pass transmembrane cadherin, regulates planar cell polarity under the control of Frizzled.* Cell, 1999. **98**(5): p. 585-95.
139. Taylor, J., et al., *Van Gogh: a new Drosophila tissue polarity gene.* Genetics, 1998. **150**(1): p. 199-210.

140. Wolff, T. and G.M. Rubin, *Strabismus, a novel gene that regulates tissue polarity and cell fate decisions in Drosophila.* Development, 1998. **125**(6): p. 1149-59.
141. Axelrod, J.D., et al., *Differential recruitment of Dishevelled provides signaling specificity in the planar cell polarity and Wingless signaling pathways.* Genes Dev, 1998. **12**(16): p. 2610-22.
142. Gubb, D., et al., *The balance between isoforms of the prickle LIM domain protein is critical for planar polarity in Drosophila imaginal discs.* Genes Dev, 1999. **13**(17): p. 2315-27.
143. Feiguin, F., et al., *The ankyrin repeat protein Diego mediates Frizzled-dependent planar polarization.* Dev Cell, 2001. **1**(1): p. 93-101.
144. Strutt, H. and D. Strutt, *Nonautonomous planar polarity patterning in Drosophila: dishevelled-independent functions of frizzled.* Dev Cell, 2002. **3**(6): p. 851-63.
145. Strutt, H. and D. Strutt, *Long-range coordination of planar polarity in Drosophila.* Bioessays, 2005. **27**(12): p. 1218-27.
146. Wu, J., T.J. Klein, and M. Mlodzik, *Subcellular localization of frizzled receptors, mediated by their cytoplasmic tails, regulates signaling pathway specificity.* PLoS Biol, 2004. **2**(7): p. E158.
147. Strutt, D. and S.J. Warrington, *Planar polarity genes in the Drosophila wing regulate the localisation of the FH3-domain protein Multiple Wing Hairs to control the site of hair production.* Development, 2008. **135**(18): p. 3103-11.
148. Strutt, D. and H. Strutt, *Differential activities of the core planar polarity proteins during Drosophila wing patterning.* Dev Biol, 2007. **302**(1): p. 181-94.
149. Mihály, J., T. Matusek, and C. Pataki, *Diego and friends play again.* FEBS J, 2005. **272**(13): p. 3241-52.
150. Strutt, D.I., *The asymmetric subcellular localisation of components of the planar polarity pathway.* Semin Cell Dev Biol, 2002. **13**(3): p. 225-31.
151. Hale, R. and D. Strutt, *Conservation of Planar Polarity Pathway Function Across the Animal Kingdom.* Annu Rev Genet, 2015. **49**: p. 529-51.
152. Wang, J., et al., *Dishevelled genes mediate a conserved mammalian PCP pathway to regulate convergent extension during neurulation.* Development, 2006. **133**(9): p. 1767-78.
153. Ybot-Gonzalez, P., et al., *Convergent extension, planar-cell-polarity signalling and initiation of mouse neural tube closure.* Development, 2007. **134**(4): p. 789-99.
154. Jessen, J.R., et al., *Zebrafish trilobite identifies new roles for Strabismus in gastrulation and neuronal movements.* Nat Cell Biol, 2002. **4**(8): p. 610-5.
155. Wallingford, J.B. and R.M. Harland, *Neural tube closure requires Dishevelled-dependent convergent extension of the midline.* Development, 2002. **129**(24): p. 5815-25.
156. Kibar, Z., et al., *Ltap, a mammalian homolog of Drosophila Strabismus/Van Gogh, is altered in the mouse neural tube mutant Loop-tail.* Nat Genet, 2001. **28**(3): p. 251-5.
157. Wang, Y., N. Guo, and J. Nathans, *The role of Frizzled3 and Frizzled6 in neural tube closure and in the planar polarity of inner-ear sensory hair cells.* J Neurosci, 2006. **26**(8): p. 2147-56.
158. Hamblet, N.S., et al., *Dishevelled 2 is essential for cardiac outflow tract development, somite segmentation and neural tube closure.* Development, 2002. **129**(24): p. 5827-38.
159. Curtin, J.A., et al., *Mutation of Celsr1 disrupts planar polarity of inner ear hair cells and causes severe neural tube defects in the mouse.* Curr Biol, 2003. **13**(13): p. 1129-33.
160. Juriloff, D.M. and M.J. Harris, *A consideration of the evidence that genetic defects in planar cell polarity contribute to the etiology of human neural tube defects.* Birth Defects Res A Clin Mol Teratol, 2012. **94**(10): p. 824-40.

161. Greene, N.D. and A.J. Copp, *Development of the vertebrate central nervous system: formation of the neural tube.* Prenat Diagn, 2009. **29**(4): p. 303-11.
162. Tissir, F. and A.M. Goffinet, *Shaping the nervous system: role of the core planar cell polarity genes.* Nat Rev Neurosci, 2013. **14**(8): p. 525-35.
163. Chandrasekhar, A., *Turning heads: development of vertebrate branchiomotor neurons.* Dev Dyn, 2004. **229**(1): p. 143-61.
164. Garel, S., M. Garcia-Dominguez, and P. Charnay, *Control of the migratory pathway of facial branchiomotor neurones.* Development, 2000. **127**(24): p. 5297-307.
165. Gilland, E. and R. Baker, *Evolutionary patterns of cranial nerve efferent nuclei in vertebrates.* Brain Behav Evol, 2005. **66**(4): p. 234-54.
166. Bingham, S., et al., *The Zebrafish trilobite gene is essential for tangential migration of branchiomotor neurons.* Dev Biol, 2002. **242**(2): p. 149-60.
167. Carreira-Barbosa, F., et al., *Prickle 1 regulates cell movements during gastrulation and neuronal migration in zebrafish.* Development, 2003. **130**(17): p. 4037-46.
168. Wada, H., et al., *Frizzled3a and Celsr2 function in the neuroepithelium to regulate migration of facial motor neurons in the developing zebrafish hindbrain.* Development, 2006. **133**(23): p. 4749-59.
169. Qu, Y., et al., *Atypical cadherins Celsr1-3 differentially regulate migration of facial branchiomotor neurons in mice.* J Neurosci, 2010. **30**(28): p. 9392-401.
170. Mapp, O.M., et al., *Prickle1b mediates interpretation of migratory cues during zebrafish facial branchiomotor neuron migration.* Dev Dyn, 2010. **239**(6): p. 1596-608.
171. Lee, R.C., et al., *The protocadherin Flamingo is required for axon target selection in the Drosophila visual system.* Nat Neurosci, 2003. **6**(6): p. 557-63.
172. Senti, K.A., et al., *Flamingo regulates R8 axon-axon and axon-target interactions in the Drosophila visual system.* Curr Biol, 2003. **13**(10): p. 828-32.
173. Steinel, M.C. and P.M. Whitington, *The atypical cadherin Flamingo is required for sensory axon advance beyond intermediate target cells.* Dev Biol, 2009. **327**(2): p. 447-57.
174. Mrkusich, E.M., D.J. Flanagan, and P.M. Whitington, *The core planar cell polarity gene prickle interacts with flamingo to promote sensory axon advance in the Drosophila embryo.* Dev Biol, 2011. **358**(1): p. 224-30.
175. Shimizu, K., M. Sato, and T. Tabata, *The Wnt5/planar cell polarity pathway regulates axonal development of the Drosophila mushroom body neuron.* J Neurosci, 2011. **31**(13): p. 4944-54.
176. Ng, J., *Wnt/PCP proteins regulate stereotyped axon branch extension in Drosophila.* Development, 2012. **139**(1): p. 165-77.
177. Gombos, R., et al., *The Formin DAAM Functions as Molecular Effector of the Planar Cell Polarity Pathway during Axonal Development in Drosophila.* J Neurosci, 2015. **35**(28): p. 10154-67.
178. Tissir, F., et al., *Protocadherin Celsr3 is crucial in axonal tract development.* Nat Neurosci, 2005. **8**(4): p. 451-7.
179. Wang, Y., et al., *Frizzled-3 is required for the development of major fiber tracts in the rostral CNS.* J Neurosci, 2002. **22**(19): p. 8563-73.
180. Price, D.J., et al., *The development of cortical connections.* Eur J Neurosci, 2006. **23**(4): p. 910-20.
181. Shafer, B., et al., *Vangl2 promotes Wnt/planar cell polarity-like signaling by antagonizing Dvl1-mediated feedback inhibition in growth cone guidance.* Dev Cell, 2011. **20**(2): p. 177-91.
182. Sun, S.D., A.M. Purdy, and G.S. Walsh, *Planar cell polarity genes Frizzled3a, Vangl2, and Scribble are required for spinal commissural axon guidance.* BMC Neurosci, 2016. **17**(1): p. 83.

183. Gao, F.B., et al., *Control of dendritic field formation in Drosophila: the roles of flamingo and competition between homologous neurons.* Neuron, 2000. **28**(1): p. 91-101.
184. Kimura, H., et al., *Potential dual molecular interaction of the Drosophila 7-pass transmembrane cadherin Flamingo in dendritic morphogenesis.* J Cell Sci, 2006. **119**(Pt 6): p. 1118-29.
185. Matsubara, D., et al., *The seven-pass transmembrane cadherin Flamingo controls dendritic self-avoidance via its binding to a LIM domain protein, Espinas, in Drosophila sensory neurons.* Genes Dev, 2011. **25**(18): p. 1982-96.
186. Shima, Y., et al., *Regulation of dendritic maintenance and growth by a mammalian 7-pass transmembrane cadherin.* Dev Cell, 2004. **7**(2): p. 205-16.
187. Adams, M.D., et al., *The genome sequence of Drosophila melanogaster.* Science, 2000. **287**(5461): p. 2185-95.
188. Reiter, L.T., et al., *A systematic analysis of human disease-associated gene sequences in Drosophila melanogaster.* Genome Res, 2001. **11**(6): p. 1114-25.
189. Prokop, A., *A rough guide to Drosophila mating schemes*.
190. Brand, A.H. and N. Perrimon, *Targeted gene expression as a means of altering cell fates and generating dominant phenotypes.* Development, 1993. **118**(2): p. 401-15.
191. Duffy, J.B., *GAL4 system in Drosophila: a fly geneticist's Swiss army knife.* Genesis, 2002. **34**(1-2): p. 1-15.
192. McGuire, S.E., et al., *Spatiotemporal rescue of memory dysfunction in Drosophila.* Science, 2003. **302**(5651): p. 1765-8.
193. McGuire, S.E., G. Roman, and R.L. Davis, *Gene expression systems in Drosophila: a synthesis of time and space.* Trends Genet, 2004. **20**(8): p. 384-91.
194. Cho, K.S., S.M. Bang, and A. Toh, *Chapter 26 - Lipids and Lipid Signaling in Drosophila Models of Neurodegenerative Diseases*. 2014, Academic Press: Omega-3 Fatty Acids in Brain and Neurological Health. p. 327-336.
195. Sánchez-Soriano, N., et al., *Are dendrites in Drosophila homologous to vertebrate dendrites?* Dev Biol, 2005. **288**(1): p. 126-38.
196. Truman, J., B. Taylor, and T. Awad, *Formation of the adult nervous system*. 1993, Cold Spring Harbor, New York: Cold Spring Harbor Laboratory Press: *The Development of Drosophila melanogaster Volume 2*. p. 1245-1275.
197. Sánchez-Soriano, N., et al., *Drosophila as a genetic and cellular model for studies on axonal growth.* Neural Dev, 2007. **2**: p. 9.
198. Bossing, T., et al., *The embryonic central nervous system lineages of Drosophila melanogaster. I. Neuroblast lineages derived from the ventral half of the neuroectoderm.* Dev Biol, 1996. **179**(1): p. 41-64.
199. Schmidt, H., et al., *The embryonic central nervous system lineages of Drosophila melanogaster. II. Neuroblast lineages derived from the dorsal part of the neuroectoderm.* Dev Biol, 1997. **189**(2): p. 186-204.
200. Landgraf, M., et al., *The origin, location, and projections of the embryonic abdominal motorneurons of Drosophila.* J Neurosci, 1997. **17**(24): p. 9642-55.
201. Prokop, A., *Organization of the efferent system and structure of neuromuscular junctions in Drosophila.* Int Rev Neurobiol, 2006. **75**: p. 71-90.
202. Merritt, D.J. and P.M. Whitington, *Central projections of sensory neurons in the Drosophila embryo correlate with sensory modality, soma position, and proneural gene function.* J Neurosci, 1995. **15**(3 Pt 1): p. 1755-67.
203. Matusek, T., et al., *Formin proteins of the DAAM subfamily play a role during axon growth.* J Neurosci, 2008. **28**(49): p. 13310-9.
204. Jeong, S., *Visualization of the Axonal Projection Pattern of Embryonic Motor Neurons in Drosophila.* J Vis Exp, 2017(124).

205. Löhr, R., et al., *Compartmentalization of central neurons in Drosophila: a new strategy of mosaic analysis reveals localization of presynaptic sites to specific segments of neurites.* J Neurosci, 2002. **22**(23): p. 10357-67.
206. Vactor, D.V., et al., *Genes that control neuromuscular specificity in Drosophila.* Cell, 1993. **73**(6): p. 1137-53.
207. Hoang, B. and A. Chiba, *Single-cell analysis of Drosophila larval neuromuscular synapses.* Dev Biol, 2001. **229**(1): p. 55-70.
208. Kaneko, M., C. Helfrich-Förster, and J.C. Hall, *Spatial and temporal expression of the period and timeless genes in the developing nervous system of Drosophila: newly identified pacemaker candidates and novel features of clock gene product cycling.* J Neurosci, 1997. **17**(17): p. 6745-60.
209. Helfrich-Förster, C. and U. Homberg, *Pigment-dispersing hormone-immunoreactive neurons in the nervous system of wild-type Drosophila melanogaster and of several mutants with altered circadian rhythmicity.* J Comp Neurol, 1993. **337**(2): p. 177-90.
210. Helfrich-Förster, C., *Robust circadian rhythmicity of Drosophila melanogaster requires the presence of lateral neurons: a brain-behavioral study of disconnected mutants.* J Comp Physiol A, 1998. **182**(4): p. 435-53.
211. Renn, S.C., et al., *A pdf neuropeptide gene mutation and ablation of PDF neurons each cause severe abnormalities of behavioral circadian rhythms in Drosophila.* Cell, 1999. **99**(7): p. 791-802.
212. Blanchardon, E., et al., *Defining the role of Drosophila lateral neurons in the control of circadian rhythms in motor activity and eclosion by targeted genetic ablation and PERIOD protein overexpression.* Eur J Neurosci, 2001. **13**(5): p. 871-88.
213. Sheeba, V., et al., *Large ventral lateral neurons modulate arousal and sleep in Drosophila.* Curr Biol, 2008. **18**(20): p. 1537-45.
214. Helfrich-Förster, C., *Development of pigment-dispersing hormone-immunoreactive neurons in the nervous system of Drosophila melanogaster.* J Comp Neurol, 1997. **380**(3): p. 335-54.
215. Helfrich-Förster, C., et al., *Development and morphology of the clock-gene-expressing lateral neurons of Drosophila melanogaster.* J Comp Neurol, 2007. **500**(1): p. 47-70.
216. Helfrich-Förster, C., *The neuroarchitecture of the circadian clock in the brain of Drosophila melanogaster.* Microsc Res Tech, 2003. **62**(2): p. 94-102.
217. Sánchez-Soriano, N. and A. Prokop, *The influence of pioneer neurons on a growing motor nerve in Drosophila requires the neural cell adhesion molecule homolog FasciclinII.* J Neurosci, 2005. **25**(1): p. 78-87.
218. Rieger, D., et al., *Functional analysis of circadian pacemaker neurons in Drosophila melanogaster.* J Neurosci, 2006. **26**(9): p. 2531-43.
219. Grima, B., et al., *Morning and evening peaks of activity rely on different clock neurons of the Drosophila brain.* Nature, 2004. **431**(7010): p. 869-73.
220. Parisky, K.M., et al., *PDF cells are a GABA-responsive wake-promoting component of the Drosophila sleep circuit.* Neuron, 2008. **60**(4): p. 672-82.
221. Shang, Y., L.C. Griffith, and M. Rosbash, *Light-arousal and circadian photoreception circuits intersect at the large PDF cells of the Drosophila brain.* Proc Natl Acad Sci U S A, 2008. **105**(50): p. 19587-94.
222. Strutt, H., J. Gamage, and D. Strutt, *Robust Asymmetric Localization of Planar Polarity Proteins Is Associated with Organization into Signalosome-like Domains of Variable Stoichiometry.* Cell Rep, 2016. **17**(10): p. 2660-2671.
223. Adler, P.N., et al., *Molecular structure of frizzled, a Drosophila tissue polarity gene.* Genetics, 1990. **126**(2): p. 401-16.
224. Jones, K.H., J. Liu, and P.N. Adler, *Molecular analysis of EMS-induced frizzled mutations in Drosophila melanogaster.* Genetics, 1996. **142**(1): p. 205-15.

225. Lin, Y.Y. and D. Gubb, *Molecular dissection of Drosophila Prickle isoforms distinguishes their essential and overlapping roles in planar cell polarity.* Dev Biol, 2009. **325**(2): p. 386-99.
226. Rawls, A.S. and T. Wolff, *Strabismus requires Flamingo and Prickle function to regulate tissue polarity in the Drosophila eye.* Development, 2003. **130**(9): p. 1877-87.
227. Cichewicz, K. and J. Hirsh, *ShinyR-DAM: a program analyzing Drosophila activity, sleep and circadian rhythms.* Commun Biol, 2018. **1**.
228. Chiu, J.C., et al., *Assaying locomotor activity to study circadian rhythms and sleep parameters in Drosophila.* J Vis Exp, 2010(43).
229. Prokop, A.-M., BarbaraSánchez-Soriano, Natalia, *Using Primary Neuron Cultures of Drosophila to Analyze Neuronal Circuit Formation and Function*, in *The Making and Un-Making of Neuronal Circuits in Drosophila*. 2012, Humana Press: Springer Protocols, Neuromethods. p. 225-247.
230. Spillane, M., et al., *The actin nucleating Arp2/3 complex contributes to the formation of axonal filopodia and branches through the regulation of actin patch precursors to filopodia.* Dev Neurobiol, 2011. **71**(9): p. 747-58.
231. Higashida, C., et al., *Actin polymerization-driven molecular movement of mDia1 in living cells.* Science, 2004. **303**(5666): p. 2007-10.
232. Watanabe, N. and C. Higashida, *Formins: processive cappers of growing actin filaments.* Exp Cell Res, 2004. **301**(1): p. 16-22.
233. Kovar, D.R. and T.D. Pollard, *Insertional assembly of actin filament barbed ends in association with formins produces piconewton forces.* Proc Natl Acad Sci U S A, 2004. **101**(41): p. 14725-30.
234. Sagot, I., et al., *An actin nucleation mechanism mediated by Bni1 and profilin.* Nat Cell Biol, 2002. **4**(8): p. 626-31.
235. Liu, W., et al., *Mechanism of activation of the Formin protein Daam1.* Proc Natl Acad Sci U S A, 2008. **105**(1): p. 210-5.
236. Sato, A., et al., *Profilin is an effector for Daam1 in non-canonical Wnt signaling and is required for vertebrate gastrulation.* Development, 2006. **133**(21): p. 4219-31.
237. Kim, G.H. and J.K. Han, *Essential role for beta-arrestin 2 in the regulation of Xenopus convergent extension movements.* EMBO J, 2007. **26**(10): p. 2513-26.
238. Matusek, T., et al., *The Drosophila formin DAAM regulates the tracheal cuticle pattern through organizing the actin cytoskeleton.* Development, 2006. **133**(5): p. 957-66.
239. Bartolini, F. and G.G. Gundersen, *Formins and microtubules.* Biochim Biophys Acta, 2010. **1803**(2): p. 164-73.
240. Migh, E., et al., *Microtubule organization in presynaptic boutons relies on the formin DAAM.* Development, 2018. **145**(6).
241. Prokop, A., et al., *DAAM family members leading a novel path into formin research.* Commun Integr Biol, 2011. **4**(5): p. 538-42.
242. Bartolini, F., et al., *The formin mDia2 stabilizes microtubules independently of its actin nucleation activity.* J Cell Biol, 2008. **181**(3): p. 523-36.
243. Gaillard, J., et al., *Differential interactions of the formins INF2, mDia1, and mDia2 with microtubules.* Mol Biol Cell, 2011. **22**(23): p. 4575-87.
244. Rosales-Nieves, A.E., et al., *Coordination of microtubule and microfilament dynamics by Drosophila Rho1, Spire and Cappuccino.* Nat Cell Biol, 2006. **8**(4): p. 367-76.
245. Roth-Johnson, E.A., et al., *Interaction between microtubules and the Drosophila formin Cappuccino and its effect on actin assembly.* J Biol Chem, 2014. **289**(7): p. 4395-404.
246. Young, K.G., et al., *INF1 is a novel microtubule-associated formin.* Mol Biol Cell, 2008. **19**(12): p. 5168-80.

247. Zhou, F., P. Leder, and S.S. Martin, *Formin-1 protein associates with microtubules through a peptide domain encoded by exon-2.* Exp Cell Res, 2006. **312**(7): p. 1119-26.
248. Shafer, O.T. and P.H. Taghert, *RNA-interference knockdown of Drosophila pigment dispersing factor in neuronal subsets: the anatomical basis of a neuropeptide's circadian functions.* PLoS One, 2009. **4**(12): p. e8298.
249. Potdar, S. and V. Sheeba, *Wakefulness Is Promoted during Day Time by PDFR Signalling to Dopaminergic Neurons in Drosophila melanogaster.* eNeuro, 2018. **5**(4).
250. Oh, Y., et al., *A homeostatic sleep-stabilizing pathway in Drosophila composed of the sex peptide receptor and its ligand, the myoinhibitory peptide.* PLoS Biol, 2014. **12**(10): p. e1001974.
251. Wen, Y., et al., *EB1 and APC bind to mDia to stabilize microtubules downstream of Rho and promote cell migration.* Nat Cell Biol, 2004. **6**(9): p. 820-30.
252. Vig, A.T., et al., *The activities of the C-terminal regions of the formin protein disheveled-associated activator of morphogenesis (DAAM) in actin dynamics.* J Biol Chem, 2017. **292**(33): p. 13566-13583.